

+

Effects of a Niobium-Boron Grain Refiner on Undercooling and Microstructural Evolution of Aluminium Silicon Alloys

A thesis submitted for the degree of Master of Philosophy
(MPhil)

by

Samuel Jordan Lloyd
Samuel.Lloyd@Brunel.ac.uk

Brunel Centre for Advanced Solidification Technology
(BCAST)

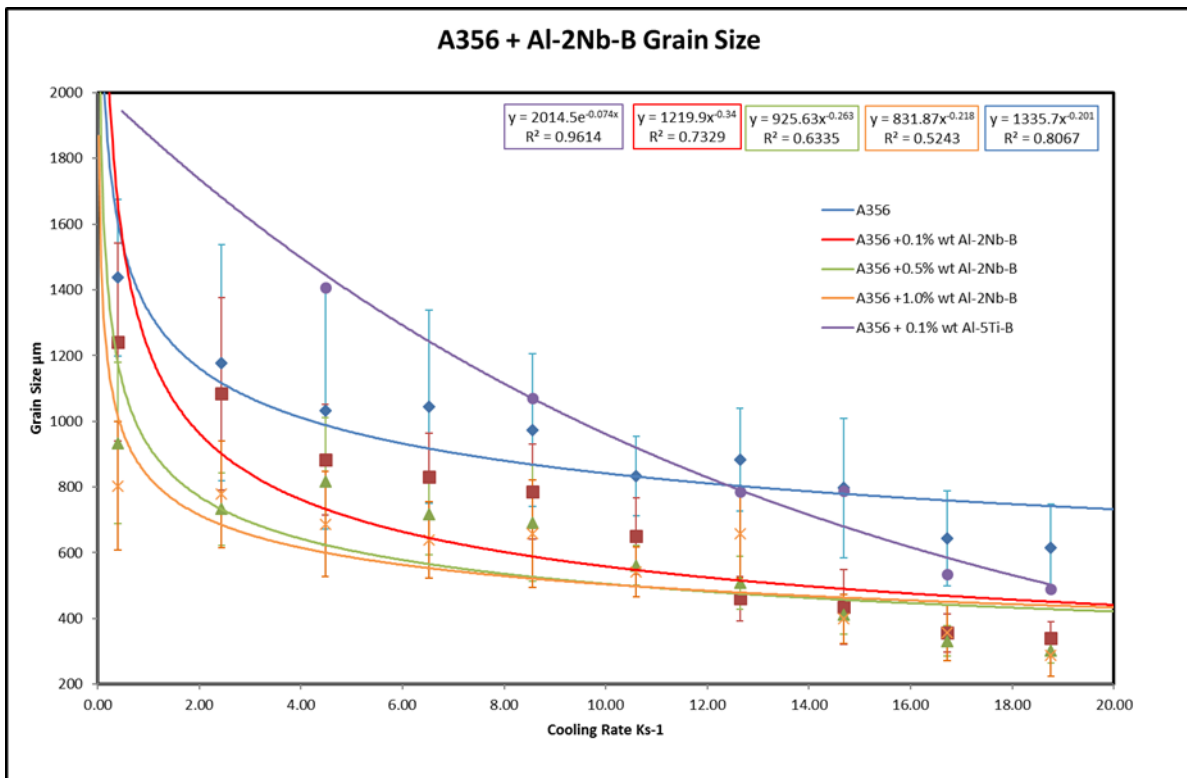
Brunel University

Abstract

The effectiveness of two novel niobium boron grain refiners, Al-2Nb-2B and Al-2Nb-B, in reducing undercooling and grain size, were evaluated in A354 (Al-9Si-2Cu-0.5Mg) and A356 (Al-7Si-0.3Mg), through practical experimentation.

The grain refiners were found to influence eutectic undercooling in both alloys, whereas primary aluminium undercooling reduction was only seen in A354.

The key finding was the effectiveness of the reduction in grain size of A356 at addition rates as low as 0.1% weight, as shown in graph below. This is significant as at these addition rates, the grain refiner may be an economical alternative to the commercially available Al-5Ti-B.



It was also found, through spectrographic analysis, that the grain refiners cause sedimentation of titanium from the alloys, which increased with higher boron systems. This suggests that the excess boron is affecting the alloying of the materials, which may be a concern.

Alloy compositions are expressed in weight percentages throughout the thesis.

Acknowledgements

Firstly, I would like to thank the Directors of Grainger & Worrall Ltd, Edward Grainger, James Grainger & Matthew Grainger, for their financial support of this project, and allowing me the opportunity for further learning and development. Without their support, this project would not have been possible.

I would like to thank Keith Denholm, Grainger & Worrall Ltd, for continuing to provide me with further opportunities for learning and development, and for giving me a fantastic start to my career.

I also wish to thank Steve Roberts, Grainger & Worrall Ltd, for his continued support and mentoring, on this project and many others. He has been a great help and support over the past few years, and has kept me motivated to complete my studies.

My thanks also to Dr Hari-Babu Nadendla, Brunel University, for the opportunity to carry out my research at BCAST Brunel University, and his support and mentoring during that period.

I also wish to thank Tom Greenwood, for introducing me to BCAST's research activities, and supporting my learning of aluminium metallurgy.

My Mom, Dad, Nan and Girlfriend Fern have been a constant source of support during this project, to which I owe them my thanks.

Contents

Abstract.....	i
Acknowledgements.....	ii
List of figures.....	v
List of tables.....	vii
References.....	viii
1.0 Introduction	1
2.0 Background.....	2
2.1 Aluminium alloys	2
2.2 Wrought alloys.....	2
2.3 Cast alloys.....	2
2.4 Typical sand casting alloys and their properties.....	4
2.5 Roles of elements in alloying.....	5
2.6 Comparison of sand casting and die casting.....	6
2.6.1 Sand casting	6
2.6.2 Die casting	6
2.7 Grain size and cooling rate.....	7
2.8 Grain size and mechanical properties	7
2.9 Undercooling	8
2.9.1 Homogeneous nucleation	8
2.9.2 Heterogeneous nucleation.....	8
2.10 Grain refinement in aluminium-silicon casting alloys.....	10
2.10.1 Nucleant effects	10
2.10.2 Poisoning effects of silicon on titanium.....	11
2.11 Grain refinement systems	11
2.11.1 Hypoperitectic.....	11
2.11.2 Hyperperitectic.....	11
2.11.3 Phase diagram.....	11
2.11.4 Peritectic Hulk.....	12
2.11.5 Hypernucleation.....	12
2.10.7 Solute effects	12
2.11.8 Growth restriction factor.....	13
2.11.9 Niobium-boron grain refiners	14
2.12 Aluminium silicon alloy microstructures.....	15
3.0 Experimental design	17
3.1 Undercooling	17
3.1.1 Experiment development.....	17

3.1.2 Procedure	18
3.2 Grain Size.....	19
3.2.1 Procedure	19
3.2.2 Mould preparation.....	20
3.3 Die-casting 40mm diameter bar mould	20
3.3.1 Mould preparation.....	20
3.4 Sand casting 40mm diameter bar mould.....	20
3.4.1 Mould preparation.....	20
3.4.2 Casting procedures.....	21
3.5 Sample preparation	21
3.5.1 Optical microscopy sample.....	21
3.5.2 SEM sample	21
3.5.3 Grain size.....	21
4.0 Results	23
4.1 A354	23
4.1.1 Undercooling.....	23
4.1.2 Spectrographic analysis of titanium levels.....	29
4.2 A356	30
4.2.1 Undercooling.....	30
4.2.2 Grain Size	33
4.2.3 SEM Data	36
4.3 Measurement error	40
5.0 Discussions	41
5.1 A356	41
5.1.1 Undercooling.....	41
5.1.2 Grain size.....	42
5.1.3 SEM analysis	44
5.2 A354	45
5.2.1 Undercooling.....	45
5.2.2 Spectrographic analysis.....	47
6.0 Conclusions.....	48
6.1 Effectiveness as a grain refiner in A356.....	48
6.2 Effectiveness as a grain refiner in A354.....	48
6.3 Recommendations for future work	48

List of figures

Figure 1 - Time temperature tracer, showing how undercooling is measured during solidification. (14)	8
Figure 2 - Difference in energy barriers of homogeneous and heterogeneous nucleation. (18)	9
Figure 3 Contact angle between substrate and solid / liquid interface. (19)	9
Figure 4 A schematic cooling curve showing the basis of the Maxwell-Hellawell model (37).	13
Figure 5 Low magnification microstructure of Al-12Si, showing typical Al-Si microstructure (41).	15
Figure 6 Microstructure of Al-Si12, with eutectic silicon regions modified with sodium (41).	16
Figure 7 Microstructure of Al-Si12 showing the dendritic nature of the aluminium grains (41).	16
Figure 8 Final design of the undercooling mould assembly. A thermally insulating sleeve in positioned within a sand mould support. A K type thermocouple is positioned 75mm above the bottom of the sand mould base, with the tip positioned centrally to the sleeve (A-A plane).	18
Figure 9 Wedge mould assembly, as used to determine cooling rate function. The same mould was used, without thermocouples, to produce the wedge samples.	20
Figure 10 Time temperature tracer for A354 alloy, with no grain refiners added, recorded in the undercooling mould. This curve clearly shows both the primary aluminium undercooling and the eutectic undercooling of the material.	23
Figure 11 Time temperature tracer for A354 alloy, with 0.1% wt Al-5Ti-B grain refiner addition, recorded in the undercooling mould.	24
Figure 12 Time temperature tracer for A354 alloy, with 2.0% wt Al-5Ti-B grain refiner addition, recorded in the undercooling mould.	24
Figure 13 Time temperature tracer for A354 alloy, with 0.1% wt Al-2Nb-2B grain refiner addition, recorded in the undercooling mould.	25
Figure 14 Time temperature tracer for A354 alloy, with 1.0% wt Al-2Nb-2B grain refiner addition, recorded in the undercooling mould.	25
Figure 15 Time temperature tracer for A354 alloy, with 5.0% wt Al-2Nb-2B grain refiner addition, recorded in the undercooling mould.	26
Figure 16 Time temperature tracer for A354 alloy, with 0.5% wt Al-2Nb-B grain refiner addition, recorded in the undercooling mould.	26
Figure 17 Time temperature tracer for A354 alloy, with 1.0% wt Al-2Nb-B grain refiner addition, recorded in the undercooling mould.	27
Figure 18 Time temperature tracer for A354 alloy, with 5.0% wt Al-2Nb-B grain refiner addition, recorded in the undercooling mould.	27
Figure 19 Spectrograph results, taken from die cast samples, for titanium levels in A354 after holding the melt with addition of Al-2Nb-0.5B (MA2,0.5), Al-2Nb-B (MA2,1) & Al-2Nb-2B (MA2,2).	29
Figure 20 Chart showing the temperature-time tracer, and cooling rate, during solidification of A356, in the undercooling mould.	30
Figure 21 Chart showing the temperature-time tracer, and cooling rate, during solidification of A356 with 0.1% wt Al-2Nb-B, in the undercooling mould.	30
Figure 22 Chart showing the temperature-time tracer, and cooling rate, during solidification of A356 with 0.5% wt Al-2Nb-B, in the undercooling mould.	31
Figure 23 Chart showing the temperature-time tracer, and cooling rate, during solidification of A356 with 1.0% wt. Al-2Nb-B, in the undercooling mould.	31

Figure 24 - Cooling rates along the sand-cast wedge samples, at 10, 30 and 90mm from the wedge tip.....	33
Figure 25 Variations in grain size, at different locations along the wedge sample, with different addition of the niobium boron grain refiner, and an existing titanium boron grain refiner.....	35
Figure 26 SEM phase map of a 40mm sand cast A356 with 5.0% wt. addition of Al-2Nb-B sample, at a magnification of x4240. Phases containing niobium are visible within the eutectic silicon regions. These are shown as yellow and green areas.	36
Figure 27 SEM phase map of a 40mm sand cast A356 with 5.0% wt. addition of Al-2Nb-B sample, at a magnification of x4240. Phases containing niobium are visible within the eutectic silicon regions. These are shown as orange and blue areas.	36
Figure 28 SEM phase map of a 40mm sand cast A356 with 5.0% wt. addition of Al-2Nb-B sample, at a magnification of x38383. Phases containing niobium are visible within the eutectic silicon regions. These are shown as yellow and blue areas.....	37
Figure 29 SEM image of a 40mm sand cast A356 with 5.0% wt. addition of Al-2Nb-B sample, at a magnification of x38383. Niobium phases are seen to be very angular in characteristics.	37
Figure 30 Average chemical analysis of the blue region in figure 23.....	38
Figure 31 Average chemical analysis of the yellow region in figure 23.	39
Figure 32 Grain size measurement error, from the line intercept method.....	40
Figure 33 Micrograph showing eutectic region in A356 wedge sample at 50mm from the tip.	41
Figure 34 Micrograph showing eutectic region in A356, with 0.5% wt addition of Al-2Nb-B, wedge sample at 50mm from the tip.....	42
Figure 35 Anodised microstructure of A356, taken at 40mm from the tip of the wedge mould, showing grain size.	43
Figure 36 Anodised microstructure of A356, with 0.1% wt. Al-2Nb-B addition, taken at 40mm from the tip of the wedge mould, showing grain size.....	43
Figure 37 Anodised microstructure of A356, with 0.5% wt. Al-2Nb-B addition, taken at 40mm from the tip of the wedge mould, showing grain size.	44
Figure 38 Micrograph showing eutectic region in A354 wedge sample at 50mm from the tip.	45
Figure 39 Micrograph showing eutectic region in A354, with 1.0% wt addition of Al-2Nb-B, wedge sample at 50mm from the tip.....	46
Figure 40 Microstructure of A354, taken at 40mm from the tip of the wedge mould, showing grain size.....	46
Figure 41 microstructure of A354, with 0.5% wt. Al-2Nb-B addition, taken at 40mm from the tip of the wedge mould, showing grain size.	47

List of tables

Table 1 Chemistry and typical properties of common Al-Si casting alloys.....	4
Table 2 The role of elements in the alloying of Al-Si alloys.	5
Table 3 The undercooling values found from analysis of the cooling curves of A354 alloy with various grain refiner additions.....	28
Table 4 Temperatures at the onset of primary aluminium, and eutectic solidification, in A354 alloy with various grain refiner additions.	28
Table 5 Undercooling values found from analysis of the cooling curves of A356 alloy with various grain refiner additions.....	32
Table 6 Temperatures at the onset of primary aluminium, and eutectic solidification, in A356 alloy with various grain refiner additions.	33
Table 7 Average grain sizes, based on 10 results, measured from wedge samples, using the line intercept method, at various cooling rates.....	34

References

1. Properties of Aluminium. *Aluminium Design*. [Online] 2 May 2016.
<http://www.aluminiumdesign.net/why-aluminium/properties-of-aluminium/>.
2. Wrought Aluminium Alloys. *Aluminium Matter*. [Online] 2 May 2016.
<http://www.aluminium.matter.org.uk/content/html/eng/default.asp?catid=214&pageid=2144417044>.
3. Aluminium - Aluminium Foil Production. *AZO Materials*. [Online]
<http://www.azom.com/article.aspx?ArticleID=1434>.
4. Castings. *The Aluminium Association*. [Online] 2 May 2016.
<http://www.aluminum.org/industries/processing/castings>.
5. Aluminium Casting Alloys. *Mid-Atlantic Casting*. [Online] 2 May 2016.
http://www.mid-atlanticcasting.com/alum-casting-alloys_FEB05.pdf.
6. Qiu, D, et al. *A mechanism for the poisoning effect of silicon on the grain*. Queensland : The University of Queensland, 2006.
7. LM6 (EN 1706 AC-44100) - Aluminium Casting Alloy. *Norton Aluminium*. [Online]
<http://www.nortal.co.uk/LM6/>.
8. LM9 (EN 1706 AC-43100) - Aluminium Casting Alloy. *Norton Aluminium*. [Online]
<http://www.nortal.co.uk/LM9/>.
9. 356 Aluminum Sand Castings. *Leitelt Bro's Inc*. [Online]
<http://www.lbfoundry.com/356-aluminum-sand-casting.html>.
10. Aluminum-Silicon Alloys. *Total Materia*. [Online] August 2003.
<http://www.totalmateria.com/Article80.htm>.
11. Smith, William F and Hashemi, Javad. *Foundations of Materials Science and Engineering (4th ed.)*. s.l. : McGraw-Hill, 2006.
12. Hall, E O. *The Deformation and Ageing of Mild Steel: III Discussion of Results*. London : Proc. Phys. Soc., 1951. pp. 747-753.
13. Petch, N J. *The Cleavage Strength of Polycrystals*. London : J. Iron Steel Inst., 1953.
14. Prasad, Hari. Solidification of Metals. [Online] [Cited: 2 August 2017.]
<https://www.slideshare.net/SachinHariprasad/solidification-of-metals-by-hari-prasad>.
15. Crystallization. *Subs Tech*. [Online]
<http://www.substech.com/dokuwiki/doku.php?id=crystallization>.
16. *Supercooled and Glassy Water*. Debenedetti, Pablo G and Stanley, H Eugene. 2003, Physics Today, p. 42.
17. Lecture 10: Homogeneous Nucleation. *The University of Utah*. [Online]
<http://www.eng.utah.edu/~lzung/images/lecture-10.pdf>.
18. Lecture 12: Heterogeneous Nucleation. *The University of Utah*. [Online]
<http://www.eng.utah.edu/~lzung/images/lecture-12.pdf>.
19. Dantzig, J A and Rappaz, M. *Solidification*. s.l. : EPFL Press, 2009. pp. 261-262.

20. Cibula, A. 1949, *Inst. Met.* 76, p. 321.
21. Crossley, F A and Mondolfo, L F. 1951, *Trans. AIME* 191, p. 1143.
22. Arnberg, L, Backerud, L and Klang, H. 9, 1982, *Materials Technology*, p. 7.
23. Influence of titanium to boron ratio on the ability to grain refine aluminium–silicon alloys. Srithran, T and Li, H. 1997, *Journal of Materials Processing Technology*, Vol. III, pp. 585-589.
24. Johnsson, M, Backerud, L and Sigworth, G K. 1993, *Metall. Trans. A24*, p. 481.
25. Mohanty, P S, Samuel, F H and Gruzleski, J E. 1995, *Metall. Mater. Trans. B26*, p. 103.
26. *Solidification processing*. Mondolfo, L F, Farooq, S and Tsc, C. 1988, (London: The Inst. of Metals), p. 133.
27. Macantonio, J A and Mondolfo, L F. 1971, *Metall. Trans. 2*, p. 465.
28. Jones, G P and Pearson, J. 1976, *Metall. Trans. B7* , p. 223.
29. Sigworth, G K. 1984, *Metall. Trans. A15* , p. 277.
30. Sigworth, G K. 1986, *Metall. Trans. A22* , p. 349.
31. Guzowski, M M, Sigworth, G K and Sentner, D A. 1987, *Metall. Trans. A18*, p. 603.
32. Vader, M and Noordegraaf, J. 1990, *Light metals* (ed.) C M Bickert (Warrendale, PA: TMS), p. 851.
33. Backerud, L, Gustafson, P and Johnsson, M. 1991, *Aluminium* 67 , p. 910.
34. Jones, G P. 1985. *Int. sem. on refining and alloying of liquid Al and ferro-alloys*. p. 213.
35. Jones, G P. (London: The Institute of Metals) : s.n., 1988. *Proc. conf. solidification processing*.
36. Tondel, P A. *Grain refinement of hypoeutectic Al–Si foundry alloys*. Trondheim : The University of Trondheim, 1994.
37. *Acta Metall.* Maxwell, I and Hellawell, A. 23, 1975, p. 229.
38. Cantor, B and O'Reilly, K. *Solidification and Casting*. 2003.
39. *The Utilization of Niobium as Aluminium Grain Refiner*. Robert, M H. Montreal : s.n., 1988. *Proceedings of the International Symposium on Reduction and Casting of Aluminum*. pp. 45-54.
40. Bolzoni, L, Nowak, M and Hari Babu, N. *Influence of a Novel Grain Refiner Addition on the Microstructural Features and Properties of Various Al-Si Alloys*. London : Brunel University.
41. Cornell, R. *Aluminium Silicon Casting Alloys*. University of Cambridge. [Online] [Cited: 19 August 2017.] <https://www.phase-trans.msm.cam.ac.uk/abstracts/M7-8.html>.

1.0 Introduction

Grain refiners are widely used in aluminium alloys to promote nucleation. Currently titanium-boron grain refiners are the most commonly used in industry. The effectiveness of these grain refiners in aluminium-silicon casting alloys is less effective than in wrought aluminium alloys. The higher silicon content of casting alloys leads to poisoning of the titanium-boron grain refiner, by the formation of aluminium silicides.

New research has suggested that niobium-boron grain refiners may be more effective in reducing undercooling, and promoting favourable microstructures, than titan-boron grain refiners, in aluminium-silicon alloys. The objective of this thesis was to identify whether Al-2Nb-2B, and Al-2Nb-B, were effective in grain refining A356 (Al-7Si-0.3Mg) & A354 (Al-9Si-2Cu-0.5Mg) aluminium alloys, compared with industry standard Al-5Ti-B, by studying the effects on:

- Undercooling
- Grain size
- Microstructure

The effects on grain size and undercooling, of two niobium based grain refiners, have been identified through practical experimentation, in small lab scale experiments, across a range of cooling rates. Comparisons are made between current commercially available grain refinement systems, and the novel niobium system.

Al-2Nb-2B and Al-2Nb-B were chosen, so as that the effect of varying boron concentrations with niobium could be characterised. Boron is known to form grain refining particles with other elements, which would be present, in A354 and A356.

2.0 Background

2.1 Aluminium alloys

Aluminium and its alloys are widely used for a vast range of different applications, from structural and engineering, to electrical and lithography. Its low density, high specific strength, excellent conductivity, and recyclability make it an ever increasingly important material in modern engineering (1).

Alloys can generally be divided into two different categories, wrought and cast (2).

2.2 Wrought alloys

Wrought alloys commonly start life as a large cast slab, which is milled, hot and cold rolled (or drawn if cast as a bar) to give the finished material. Generally strengthening mechanisms depend on the material microstructure undergoing work-hardening. (3)

Mechanical grade wrought alloys have superior and homogeneous mechanical properties, compared with their cast counter parts. They typically have fewer defects and can be rolled into foils just a few microns in thickness (3).

Depending on the final thickness which the slabs are hot and cold rolled to, wrought materials can be manufactured into billets or foils. Billets may undergo further processing via machining, to generate the net shape of more complex components. Heat treatment is also common to gain desired mechanical properties.

Extrusion can also be used to generate bar type initial castings, which are further reduced in diameter through hot and cold rolling.

Excellent mechanical properties, which are homogenous, make wrought alloys favourable where component performance is critical, such as aerospace applications.

High productivity, which can be achieved, through the manufacture of wrought sheet aluminium, makes it favourable for pressings such as automotive body panels. Lower material thicknesses can be achieved through this process than would be achievable through casting methods. (2)

2.3 Cast alloys

Cast alloys do not undergo work hardening after casting, although many alloys require heat treatment in order to attain desirable mechanical properties. Cast alloys are used in processes where the castings are much closer to the net shape of the final component, with much less machining required than machining from billet. Commonly used casting methods include high & low pressure die, sand and investment. (4)

As with their wrought counterparts, casting alloys come in a range of chemical compositions, to give a different balance of properties. Some alloys have superior mechanical properties, such as 2xx series alloys, whereas others offer greater corrosion resistance and easier recyclability, such as LM6.

Most alloys contain high levels of silicon, which gives a smaller freezing range near the eutectic. This helps the liquid metal to completely fill mould cavities, prior to solidification. Magnesium and copper are commonly used to improve the mechanical strength of aluminium alloys, through precipitation hardening mechanisms. (5)

Casting alloys do not respond as well to commercially available grain refiners as well as wrought alloys. The relatively high levels of silicon in cast alloys cause poisoning of the titanium in Al-5Ti-B, thus reducing its effectiveness in grain refinement. (6)

2.4 Typical sand casting alloys and their properties

There are a wide range of aluminium alloys commonly used for the production of sand casting. The table below lists some of the most common, and their particular applications.

Table 1 Chemistry and typical properties of common Al-Si casting alloys.

Alloy	Chemistry	Properties
LM6	Al-Si12	Very low alloying elements gives this material excellent corrosion resistance, and recyclability. As there is very little Mg or Cu, this alloy is not heat treated. This material has low UTS and PS (160MPa & 60MPa respectively), compared with other alloys, but has reasonable elongation, typically 5%. Typical applications are covers and casings. (7)
LM9	Al-Si12Mg0.5Mn0.5	High silicon content gives this alloy excellent castability, but increased tool wear when being machined. As with LM6 this alloy has very good corrosion resistance. The presence of Mg means this alloy has reasonable mechanical properties (UTS 170Mpa, PS 110MPa, EI 1.5%). This alloy is typically used in the same applications as LM6, but where higher mechanical strength is required. (8)
A354	Al-Si9Cu1.8Mg0.5	This alloy contains copper, which improves the strength of the alloy at higher temperatures. Typical applications therefore include cylinder heads for internal combustion engines, which see high temperatures in operation.
A356	Al-Si7Mg0.3	Excellent mechanical properties in the T6 heat treated condition. This alloy is typically used where high strength is required, such as flywheel housings, transmission cases, structural frames. (9)
A357	Al-Si7Mg0.6	Similar applications to A356, but with high mechanical strength, due to higher magnesium levels. (9)

2.5 Roles of elements in alloying

The table below details the role of each element in the alloying of aluminium.

Table 2 The role of elements in the alloying of Al-Si alloys.

Element	Role
Silicon (Si)	Silicon aids with the castability of the aluminium alloy.
Magnesium (Mg)	Magnesium additions increase the strength of the alloy, when heat treatment to achieve precipitation hardening is applied. Addition rates are typically 0.3 to 1.0%.
Copper (Cu)	Copper additions, like magnesium, increase the strength of the alloy. They also give some improvements to the strength of the material at elevated temperatures. Addition rates are typically up to 3.0%, depending on the alloy.
Iron (Fe)	Iron is deliberately added to die-casting alloys, above the solubility limit in aluminium, to prevent castings from soldering to the permanent moulds. Iron in sand castings is typically a contaminant which is minimised as best as is practically possible. Iron forms needle-like intermetallic phases which reduce the ductility of the alloys.
Manganese (Mn)	Manganese is used to prevent iron forming the needle-like intermetallic phases discussed above. Manganese is added in 1:2 ratios to iron, to modify the intermetallic phases, to more rounded morphologies, minimising their detrimental effects.
Titanium (Ti)	Titanium is added, along with boron or carbon, to promote grain refinement in aluminium alloys. It is typically added via rods in the final stages of alloy preparation. Addition rates are typically very low, 0.1 to 0.2%
Strontium (Sr)	Strontium is another element added as a modifier. It is used to make the eutectic silicon phases more rounded, so as to minimise reductions in ductility caused by those phases. This is added in the form of rods, in the final stages of alloy preparation.

(10)

2.6 Comparison of sand casting and die casting

2.6.1 Sand casting

Sand moulds are commonly employed for casting complex geometry components in a wide range of metallic alloys. The use of cores allows geometry, not possible with permanent die moulds, such as water jackets and oil passages.

Tooling is relatively cheap for low volume production, with small leads times, and resin board tooling is easily modified. These characteristics are perfect for prototyping, where customers require parts quickly, with minimal tooling costs and the flexibility to change their designs.

Modern technology even allows the rapid prototyping of sand moulds and cores, through 3D printing, giving even shorter lead times and lower tooling costs, although this process may be at the expense of other casting characteristics, such as surface finish.

The draw backs of sand moulding are that piece prices are relatively high in comparison to permanent mould casting, productivity is lower, and the difference in solidification rate gives a variation in material performance. This is covered in more detail later.

2.6.2 Die casting

Die casting is more favourable for high volume production of castings. Due to the reusable nature of the moulds, a much higher productivity is possible, at a reduced piece price, and greater repeatability between parts is possible.

Drawbacks to the use of die-casting include a higher initial cost of investment, due to the higher cost of producing die-moulds, compared with sand mould tooling. The lead time for this tooling is greater than that of sand casting, and is much less easily modified, in terms of both time, and cost.

Due to the nature of die-moulds, an amount of design for manufacture is required. All geometry must be able to draw from the moulds. Complex internal geometries are only possible with the use of single use cores, in low pressure die systems. It is not possible to utilise these in high pressure systems, as the cores would be destroyed under the injection pressure.

Higher cooling rates give superior mechanical properties, compared with sand casting. High pressure systems benefit from a higher runner system pressure, helping to vastly improve casting integrity.

2.7 Grain size and cooling rate

It is generally accepted that an increased cooling rate, decreases the grain size formed during solidification. The higher cooling rates of low/high pressure die casting, give smaller grain structures than those seen in precision sand castings.

Research has suggested that the reason for the decrease in grain size, is due to the increased number of substrates, which become viable nuclei, under high cooling rates. Given enough time, all substrates become nuclei, however if the solidification rate is slow, the first nuclei will have more time to grow, and deplete the available aluminium available for the later formed nuclei to grow, thus given fewer, but larger grains.

2.8 Grain size and mechanical properties

Research suggests a correlation between decreased grain size and increased mechanical properties.

Grain size influences the yield strength of a given metal. As stress is applied dislocations are pinned at grain boundaries. With fewer grain boundaries in materials with larger grain sizes, more dislocations build up at any given boundary, thus the average stress is higher. Smaller grain structures therefore give improved yield strength. This is known as the Hall-Petch strengthening, or grain boundary strengthening (11).

Hall's research showed that a relationship existed between crack lengths and grain sizes. His research was based around the yield strength of mild steels (12).

Petch derived the same relationship from research into the cleavage strength of varying ferritic grain sizes, at low temperature (13).

It is accepted as an accurate model for systems where the grain size is between 1mm and 1 μ m.

As previously discussed sand casting is often used as an economical means of prototyping components intended to be die-cast. Hall-Petch strengthening means that sand castings will often have inferior yield strength, and therefore behave differently to die-castings. This can be a major concern for engineers during their design phases, particularly with components under substantial stresses, such as brackets.

The relationship between yield stress and grain size is described by the following equation:

$$\sigma_y = \sigma_0 + \frac{k_y}{\sqrt{d}}$$

Where k_y is the strengthening coefficient of a given material, σ_0 is a materials constant for the starting stress for dislocation movement, d is the grain diameter and σ_y is the yield stress.

2.9 Undercooling

Undercooling is the phenomena of liquid being cooled below the material's freezing temperature, in order to drive solidification. The temperature difference between the freezing point of the material, and the temperature at which solidification begins, is the undercooling value of the material, as shown in figure 1.

Undercooling (or) Supercooling in pure metals

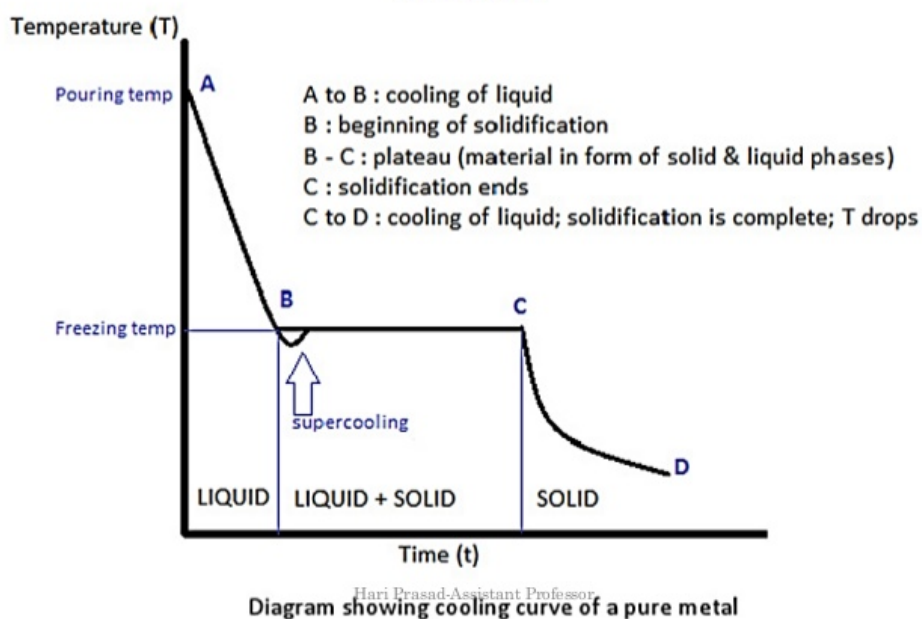


Figure 1 - Time temperature tracer, showing how undercooling is measured during solidification. (14)

2.9.1 Homogeneous nucleation

Homogeneous nucleation occurs in the absence of any impurities or other drivers of solidification, such as a mould wall. Homogeneous nucleation requires a large undercooling in order to create stable nuclei for solidification (15). Pure liquid water, has been known to be cooled to below -40°C , in conditions which prevent heterogeneous nucleation (16) (17).

2.9.2 Heterogeneous nucleation

Heterogeneous nucleation occurs in the presence of a foreign particle or substrate, which provides nucleation points, allowing solidification to occur at lower undercooling values (15), as shown in figure 2. These may take the form of a mould wall, a grain refiner, or another melt contaminant. They can be considered surface catalysts, offering a smaller contact angle θ , meaning a lower free energy change ΔG , or barrier to nucleation (18), as shown in figures 2 and 3.

$$\Delta G_{\text{Heterogeneous}} = \Delta G_{\text{Homogeneous}} \times f(\theta)$$

Where

$$f(\theta) = \frac{2 - 3 \cos \theta + \cos^3 \theta}{4}$$

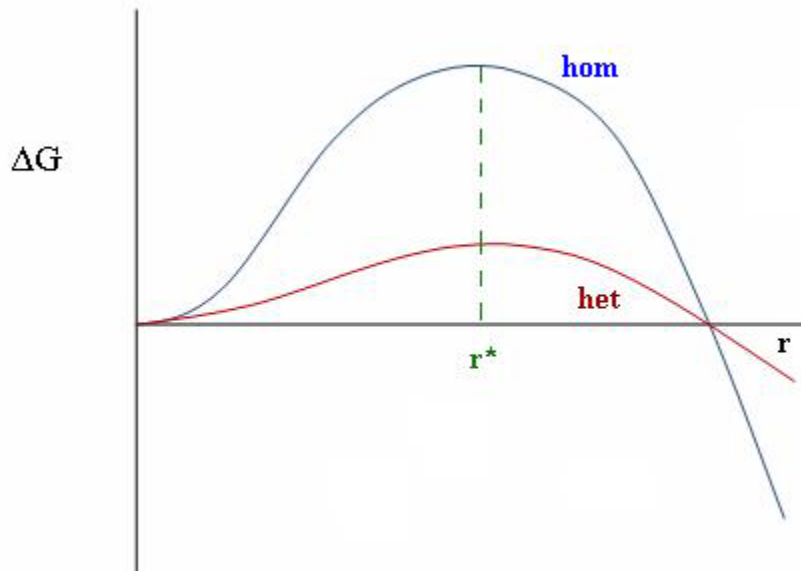


Figure 2 - Difference in energy barriers of homogeneous and heterogeneous nucleation. (18)

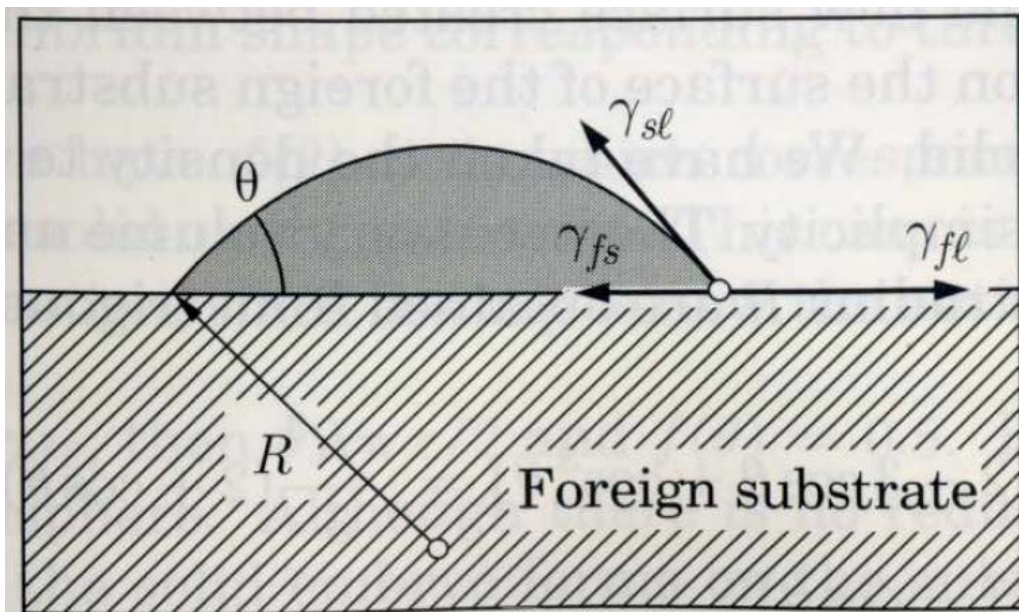


Figure 3 Contact angle between substrate and solid / liquid interface. (19)

Figure 3 shows schematically the physics of heterogeneous nucleation. When a foreign body or substrate has a structure and chemistry that match sufficiently well those of the solid, it is

energetically favourable to form a solid nucleus on the surface, as shown. It is assumed in the analysis that the embryo takes the form of a spherical cap. This implies that the surface energies are all isotropic, and that gravitational effects can be neglected.

Summation of the forces parallel to the surface in figure 3 relates the various surface energies to θ , the equilibrium contact angle (also called the wetting angle) in the Laplace-Young equation

$$\gamma_{fl} = \gamma_{fs} + \gamma_{sl} \cos \theta$$

where the two subscripts on the surface energies indicate the two substances in contact, and the index “f” represents the foreign substrate. There are two cases where there is no value for θ that satisfies the equation.

- When $\gamma_{fl} > \gamma_{fs} + \gamma_{sl}$, it is energetically favourable for the solid layer to completely cover the substrate, effectively separating the liquid from the substrate.
- Similarly, when $\gamma_{fs} > \gamma_{fl} + \gamma_{sl}$, there is no possible gain of energy by forming a solid layer on the foreign particle surface. Such particles do not participate in the heterogeneous nucleation process and might even be pushed away from a solid-liquid front coming from other nucleation centres due to this very unfavourable wetting condition. (19)

2.10 Grain refinement in aluminium-silicon casting alloys

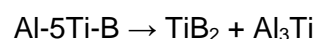
In order to increase the number of grain boundaries in a given system, grain refiners are used to promote heterogeneous nucleation of grains. Effective grain refiners lower the energy barrier to nucleation, and provide substrates which can form nuclei. They are also able to resist fading, meaning that they are able to produce castings with a refined grain structure, an appreciable amount of time after being added to the alloy melt.

The most commonly available grain refiners for aluminium casting alloys are aluminium-titanium-boron systems. These are readily available, and used throughout the aluminium casting industry, in a variety of casting manufacturing systems.

The exact mechanism by which aluminium-titanium-boron systems refine the grain structure of aluminium alloys is much debated.

2.10.1 Nucleant effects

In the 1940's, research by Cibula, suggested that aluminium could be nucleated by TiC or TiB₂ particles. Currently Al-5Ti-B master alloy is most commonly used grain refiner and it has TiB₂ phase and Al₃Ti particles.



(20)

An opposing theory was put forward by Crossley and Mondolfo, in 1951, suggesting that Al_3Ti particles nucleate aluminium via a peritectic reaction.



(21)

Al_3Ti layer is seen on TiB_2 particles, suggesting that they both contribute to heterogeneous nucleation of $\alpha\text{-Al}$ grains.

Al-Ti-B master alloys are very potent grain refiners where Si < 2%wt, (i.e. wrought alloys).

TiB_2 & AlB_2 are very similar. They are both isomorphous, and have hexagonal lattice parameters of $a=0.30311\text{nm}$ $c=0.32291\text{nm}$ & $a=0.3009\text{nm}$, $c=0.3262\text{nm}$ (22).

$(\text{Al}, \text{Ti})\text{B}_2$ is formed by the replacement of Ti by Al atoms in the lattice.

2.10.2 Poisoning effects of silicon on titanium

Al-Ti-B master alloys are poor grain refiners where Si > 4%wt, due to the formation of titanium silicides such as TiSi , TiSi_2 & Ti_3Si_3 , with only a limited number of TiB_2 particles forming. These deplete the available titanium in the melt (23). This is a major limitation of the traditional titanium based grain refiners.

2.11 Grain refinement systems

2.11.1 Hypoperitectic

In hypoperitectic systems ($\text{Ti} < 0.15\%$ wt.) boride particles or agglomerates are found in the centre of grains, with Ti enriched dendrites growing out of them. This suggests borides nucleate $\alpha\text{-Al}$ (24).

Research has shown borides are pushed to grain boundaries and no grain refinement is observed, where there is no solute Ti. This shows a lattice disregistry between borides and $\alpha\text{-Al}$, meaning borides are poor nuclei. Borides require undercooling, whereas aluminides do not. AlTi_3 is known to be a potent nucleant (25).

2.11.2 Hyperperitectic

Hyperperitectic systems have shown excellent grain refinement (21), and Al_3Ti particles have been found at the centre of grains, in multiple orientations.

2.11.3 Phase diagram

TiAl_3 assumed to be nucleation particle.

Theory suggests that boron shifts the peritectic composition in Al-Ti system from 0.15%wt Ti to 0.05%wt (26) (27). This allows $TiAl_3$ to be stable at low Ti concentrations in the melt.

Various researchers have performed theoretical calculations which showed that boron does not alter the Al-Ti phase diagram (28) (29) (30).

It has been argued that $TiAl_3$ particles from master alloys are stable at low Ti concentrations in the melt. Guzowski et al showed that these aluminides take 30 minutes to dissolve in the melt, at a temperature of 700°C (31). This dissolution leads to a phenomenon known as fade, meaning that during holding the effectiveness of the grain refiner reduces. This means that at low Ti concentrations $TiAl_3$ does not act as a nucleation site for aluminium.

2.11.4 Peritectic Hulk

The peritectic hulk theory assumes that $TiAl_3$ is a more powerful nucleant than TiB_2 . This theory suggests that boride particles slow down the dissolution rate of the aluminides, allowing them to remain active for longer.

Borides form a shell around the aluminide particles. Diffusion has to take place across this shell in order for the aluminides to dissolve. Once the aluminides are finally dissolved a cell of liquid, of roughly peritectic composition, remains within the boride shell. The peritectic reaction then occurs, and growth occurs from there (32) (33).

2.11.5 Hypernucleation

It has been theorised that melt solutes segregate stably to the melt-inoculant interface. Under the right conditions stable pseudo crystals are created above the principle liquidus of the melt and immediately below. These allow α -Al to grow without undercooling. There is no experimental evidence to support this theory (34) (35).

2.10.7 Solute effects

Solute elements, such as titanium, segregate to the inoculant-melt interface and affect the growth of dendrites and the constitutional undercooling at the solid-liquid interface.

Nucleants are important but solutes also play a role in grain refinement.

Solute titanium allows TiB_2 particles to act as effective grain refiners.

AlB_2 particles are known to grain refine aluminium above the Al-B eutectic (0.022% B). AlB_2 particles have been found in the centre of α -Al grains in hypoeutectic Al-Si alloys (36).

2.11.8 Growth restriction factor

Modelling of grain refinement, specifically addressing the issue of why it is so inefficient, was first attempted by Maxwell and Hellawell. They considered the cooling of an aluminium melt containing a population of refining particles, and noted that crystal growth on an increasing number of particles would give an accelerating rate of heat release, eventually surpassing the rate of external heat extraction and giving recalescence as shown in figure 4.

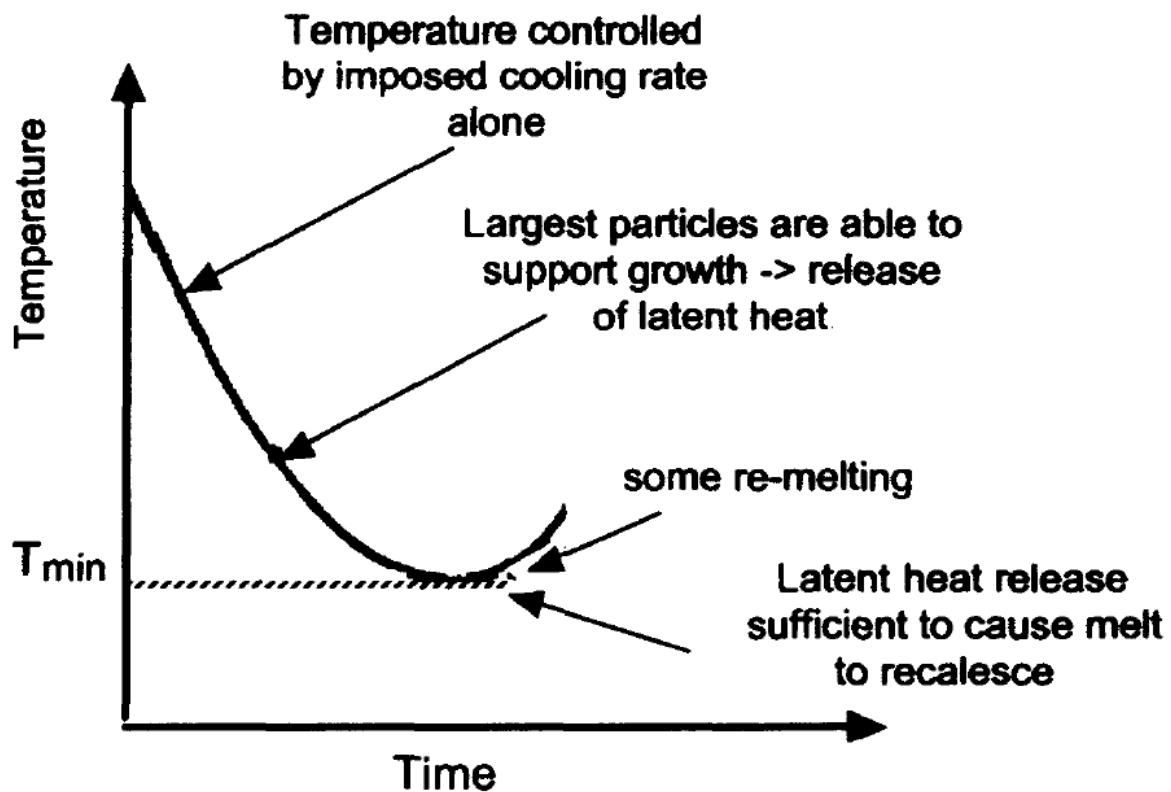


Figure 4 A schematic cooling curve showing the basis of the Maxwell-Hellawell model (37).

The recalescence limits the number of nucleation events and therefore restricts the degree of grain refinement which can be achieved. This could explain why refinement efficiencies are so low.

The classic spherical-cap model was used to calculate a heterogeneous nucleation frequency on the particles in the melt. For ease of computation, the particles were taken to all have the same size. Maxwell and Hellawell computed the shape of the cooling curve (figure 4) and the consequent number of grain nucleation events under various conditions, but did not make any comparison with experiment. They did note, however, that the important factors controlling the grain size are the number and potency of nucleant particles, the cooling rate, and the solute content in the melt. The solute content is important because it restricts the rate of growth of the crystals. Maxwell and Hellawell used a diffusion model

based on the invariant-size approximation. They showed that the dominant effect of solute content can be described by the quantity Q , defined as:

$$Q = m(k - 1)C_0$$

where m is the liquidus slope, k is the equilibrium partition coefficient and C_0 is the solute content in the alloy melt. Here, we term Q the growth-restriction parameter (38) (37).

2.11.9 Niobium-boron grain refiners

Niobium, as a potential aluminium grain refiner, has been previously researched by M H Robert in 1988 (39). His work researched the viability of niobium as an effective grain refiner, based on the peritectic reaction theory of aluminium grain refinement using Al-Ti-B grain refiners. Niobium was added to aluminium via both a salt of formulation K_2NbF_7 , and as a master alloy Al-5Nb. Robert found both of these methods of introducing grain refinement particles to be effective, with reduction in grain size to 10%. He concludes that Nb at peritectic concentration is most effective, with any additional Nb showing no further reduction in grain size.

Research has been conducted at Brunel University into the application of niobium boron grain refiners in aluminium castings. This research employed relatively high addition rates of master alloys, in a range of casting alloys. The research demonstrated that at addition rates of 5%, Al-2Nb-2B was an effective grain refiner in terms of grain size, with good fade performance (40). The addition rates employed would be far too costly for a mass production foundry to employ, as the cost per kilo of material would significantly increase. This would likely outweigh any advantages in its application.

2.12 Aluminium silicon alloy microstructures

The microstructure of aluminium silicon alloys is predominately dark grey silicon plates within a lighter aluminium rich matrix, due to silicon's low solubility in aluminium. Primary aluminium grains typically have a dendritic structure, as shown in figure 7.

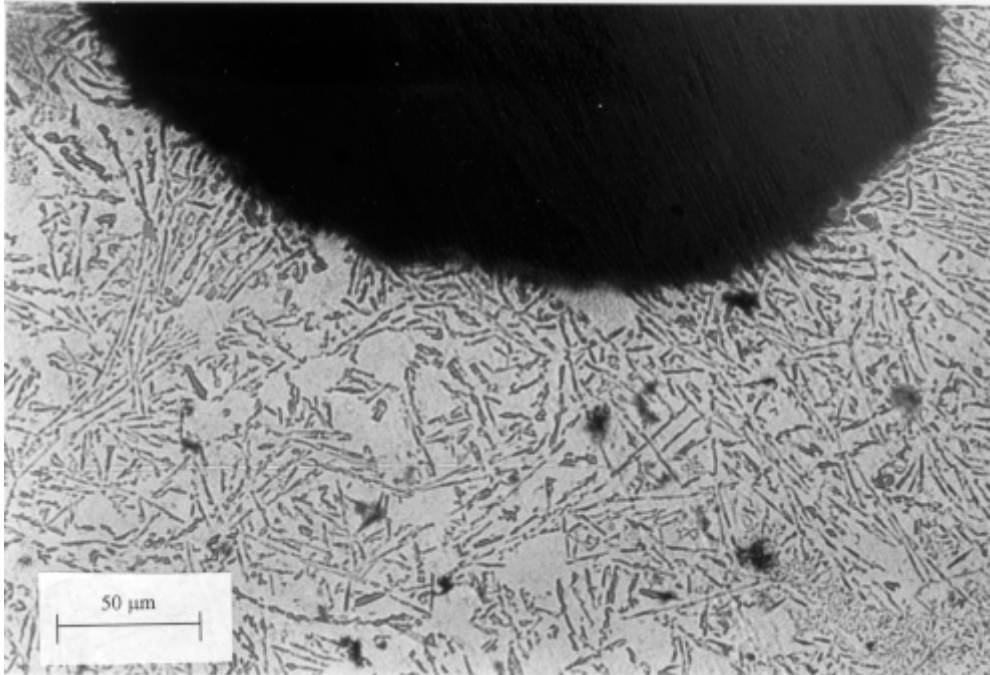


Figure 5 Low magnification microstructure of Al-12Si, showing typical Al-Si microstructure (41).

Figure 5 shows unmodified eutectic silicon phase, which are coarse. This is detrimental to the mechanical properties of the material (41). Sodium can be used to modify the eutectic phases to finer particles, and in turn improve the mechanical properties (41). The dark region is a porosity void, caused either by the presence of gas or through solidification shrinkage.

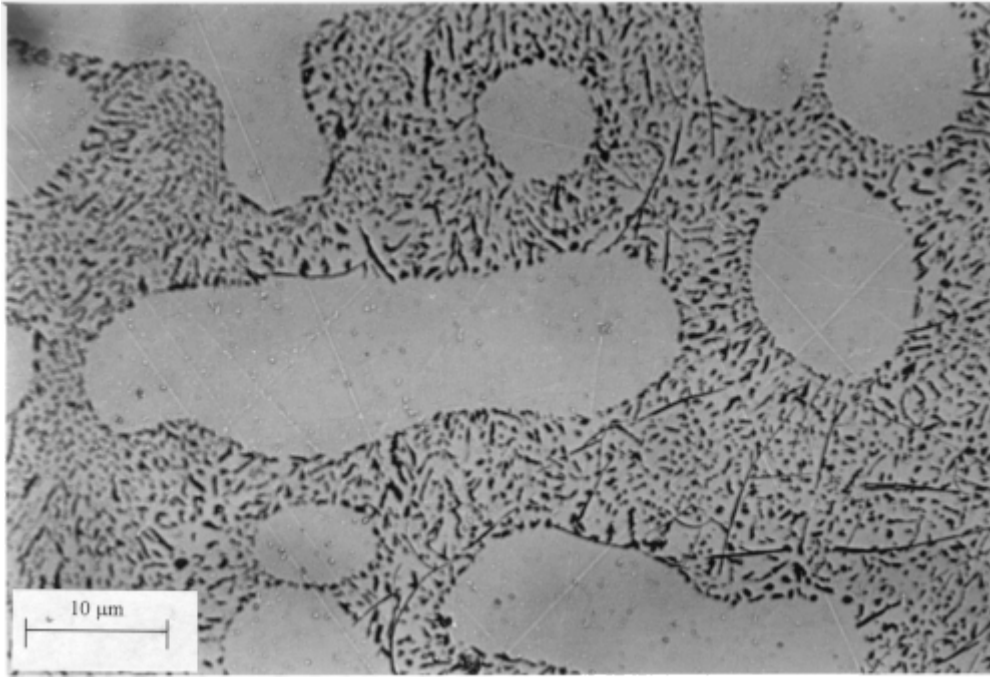


Figure 6 Microstructure of Al-Si12, with eutectic silicon regions modified with sodium (41).

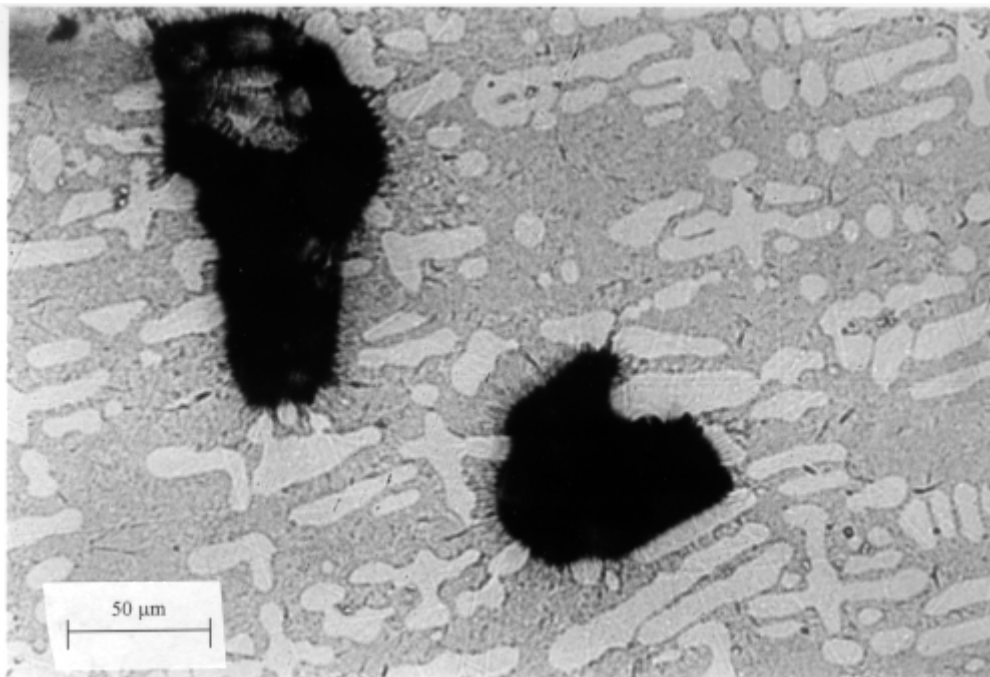


Figure 7 Microstructure of Al-Si12 showing the dendritic nature of the aluminium grains (41).

Figure 6 shows the effects of sodium on modifying the microstructure of aluminium silicon alloys. The silicon phases are much finer and evenly distributed, than those seen in figure 5.

Figure 7, as a low magnification, shows the dendritic nature of the primary aluminium grains (the lighter regions). Again, porosity defects are seen in the black regions.

3.0 Experimental design

Two niobium grain refiners were evaluated in A356 and A354. These were Al-2Nb-2B and Al-2Nb-B. Al-2Nb-2B was manufactured by Brunel University, whereas Al-2Nb-B was produced by AMG metals.

A number of different moulds were used, to cast samples for different types of analysis. Sand-cast wedge moulds, were used to cast samples for grain size vs cooling rate analysis. Moulds which were insulated with feeder sleeves and thermal wool were used to deliberately slow down heat loss, to more accurately measure undercooling of the difference grain refiner addition rates.

Die cast 40mm dia bar samples were cast for both very high cooling rate conditions and spectrographic analysis. Thermocouple experiments showed that the cooling rate had a very high variability, and as such the samples were used solely for spectrographic analysis.

Sand cast 40mm dia bar samples were cast to be used as SEM samples.

All moulds were cast from the sample prepared melt for each alloy-grain refiner addition system.

All sand moulds were silica sand with Novathane binder resin.

3.1 Undercooling

3.1.1 Experiment development

Much work was undertaken to develop a procedure, to accurately measure the cooling curves of the alloy systems. The main issues were accurate and repeatable location of the thermocouple within a mould, and the cooling rate was too high for the thermocouple to sense the rapid change in temperature and the data logging equipment to record the temperature changes during solidification, and in turn the undercooling curves.

3.1.1.1 Undercooling mould design 1

The initial mould design was a permanent steel mould, with a thermocouple positioned using wires. The wires gave poor repeatability, in terms of the thermocouple positioning, and the mould was prone to leaking material, which invalidated results.

The main issue with the steel mould was that the cooling rate was too high for the data logging equipment to record the temperature changes during solidification, and in turn the undercooling curves.

3.1.1.2 Undercooling mould design 2

A second mould was created, using a sand mould, with a 40mm cylindrical void.

Thermocouple positioning was much improved. The sand moulds were only used to cast a

single sample, so it was possible to drill a hole in each one, to accurately and repeatedly position the thermocouple within the sample.

Whilst the cooling rate was slowed in the sand system, it was still too high to record both primary aluminium and eutectic undercooling. For this reason, further development was undertaken to further slowdown the cooling rate.

3.1.1.3 Undercooling mould design 3 (final design)

Figure 3 shows the final design of the undercooling mould. A thermally insulating sleeve was placed inside the sand mould support. This considerably slowed down the cooling rate, allowing the necessary time temperature curves to be recorded.

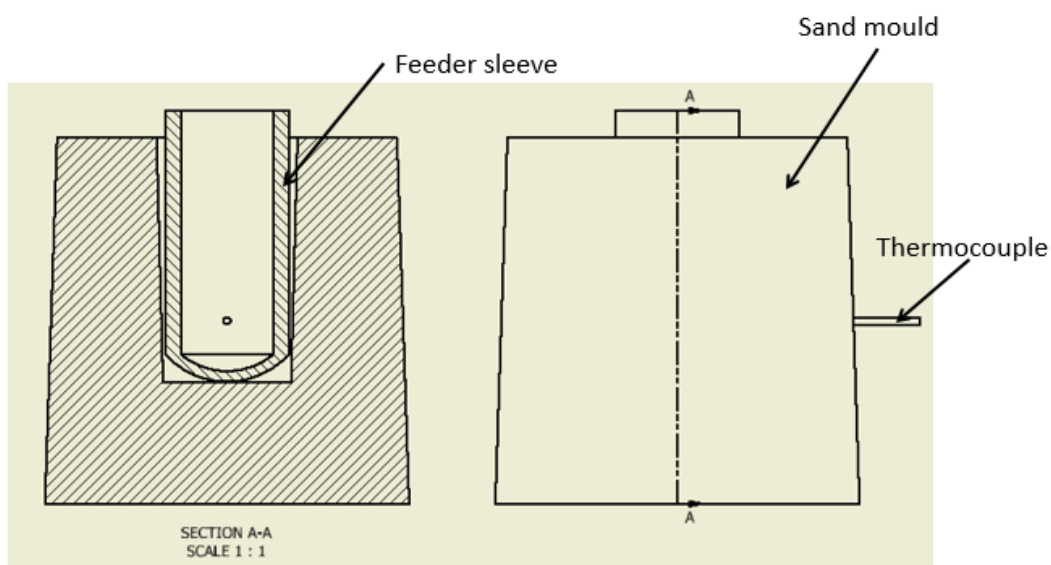


Figure 8 Final design of the undercooling mould assembly. A thermally insulating sleeve is positioned within a sand mould support. A K type thermocouple is positioned 75mm above the bottom of the sand mould base, with the tip positioned centrally to the sleeve (A-A plane).

3.1.2 Procedure

3.1.2.1 Alloy preparation

1. Approximately 2kg of aluminium alloy ingot was weighed to $\pm 0.5\text{g}$, prior to melting in a refractory coated crucible, at 780°C for 150 minutes, in an electric resistance furnace.
2. Grain refiner additions were prepared, and weighed to $\pm 0.005\text{g}$.
3. The dross from the top of the melted ingot was removed, using a ceramic spoon, so as not to contaminate the melt. Grain refiner additions were made to the melt, stirred through, and the melt was returned to the furnace, for a further 10 minutes.

3.1.2.2 Mould preparation

1. Type K thermocouples, were manufactured using 2.0mm diameter ceramic tubes, with wire of diameter 0.1mm.

2. A sand mould, of dimensions approximately 150x150x150mm, with a centre bore of 50mm diameter by 100mm deep, had a cardboard feeder sleeve insert into it, as shown below. A 2mm hole was drilled, centrally through the side of the mould, until it broke through into the centre bore.
3. The thermocouple was push fitted into this hole and a thermally resistant sealant was used on the outside of the mould, to prevent liquid alloy leaking.

3.1.2.3 Casting procedure

1. The thermocouple was connected to a data logger, with a recording frequency of 100Hz.
2. The prepared alloy was removed from the oven, and further surface dross was removed.
3. A separate type K thermocouple, was used to monitor the temperature of the alloy. Once the temperature dropped to 740°C, the liquid alloy was poured into the mould.
4. Thermal matting was used to seal the top of the mould, to create maximum insulation.
5. The temperature tracer was recorded, until the alloy had undergone eutectic solidification.

3.2 Grain Size

Grain size vs cooling rate vs grain refiner system was characterised through practical experimentation, involving the use of wedge shaped sand moulds. These were designed so as that the tip would see a fast cooling rate, which would decrease as the cross-section thickness increased. The wedge was designed so that these cooling rates would cover the typical cooling rates see in gravity sand casting.

3.2.1 Procedure

3.2.1.1 Alloy preparation

1. Approximately 2kg of aluminium alloy ingot was weighed to $\pm 0.5\text{g}$, prior to melting in a refractory coated crucible, at 780°C for 150 minutes, in an electric resistance furnace.
2. Grain refiner additions were prepared, and weighed to $\pm 0.005\text{g}$.
3. The dross from the top of the melted ingot was removed, using a ceramic spoon, so as not to contaminate the melt. Additions were added to the melt, stirred through, and the melt was returned to the furnace, for a further 10 minutes.

3.2.1.2 Mould preparation (cooling function calculation)

1. Drill locations were marked onto the wedge mould. These were calculated using a steel ruler. The locations are detailed in figure 4.
2. An electric drill was used to drill the holes into the moulds.

3. Thermocouples were push fitted into the holes, and aligned by eye to the Z-X plane of the mould.
4. Loose sand and debris was removed using a compressed airline.

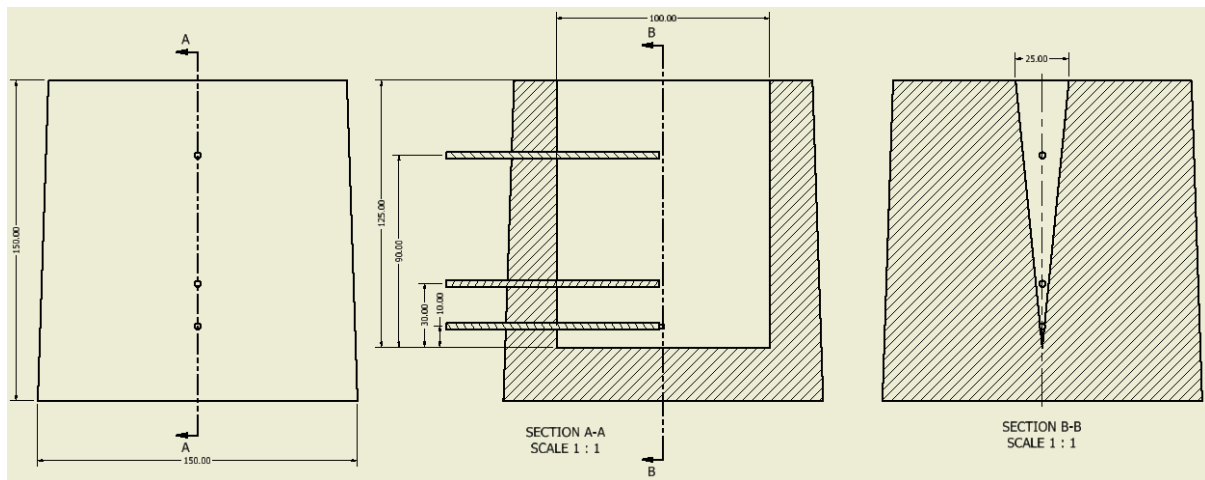


Figure 9 Wedge mould assembly, as used to determine cooling rate function. The same mould was used, without thermocouples, to produce the wedge samples.

3.2.1.3 Procedure (alloy system samples)

A sand wedge mould was used to create a test specimen which showed the influence of cooling rate on microstructure, for a given system. In these samples, thermocouples were not used.

3.2.2 Mould preparation

1. Moulds were cleaned from loose sand and debris using a compressed airline.

3.3 Die-casting 40mm diameter bar mould

A permanent die-mould was used to create a microstructure formed under fast solidification conditions. These were used for spectrographic analysis of the alloy chemistry in each experiment.

3.3.1 Mould preparation

1. Die mould is preheated in an oven to 200°C. Minimum oven time of 2 hours.
2. A ceramic board of approximately 150 x 150 mm is cleaned and used as a base for the mould.
3. Immediately before the casting procedure, the mould is removed from the oven, and clamped together, and sat onto the ceramic board.

3.4 Sand casting 40mm diameter bar mould

A 40mm diameter bar was sand cast for each system. A cross section of this was used for SEM analysis.

3.4.1 Mould preparation

1. Moulds were cleaned from loose sand and debris using a compressed air line.

3.4.2 Casting procedures

1. Once all four moulds are prepared, they are lined up, to allow them to be cast in quick succession. The 40mm diameter die-mould is only removed from the oven, immediately before the casting procedure. The cast order remains the same for all melts:
 - i. Wedge mould (grain size analysis)
 - ii. Insulated mould (undercooling analysis)
 - iii. 40mm diameter sand mould.
 - iv. 40mm diameter die-mould.
2. The prepared alloy is removed from the furnace, and transferred to the casting area.
3. Dross is removed from the melt, and a thermocouple is used to monitor the temperature.
4. Once the temperature of the melt drops to 740°C, the melt is immediately cast into the moulds.
5. Castings left for one hour before being removed from moulds.

3.5 Sample preparation

3.5.1 Optical microscopy sample

1. Sand cast bar samples were sectioned, 20mm from the bottom face (as cast) using a water cooled rotary saw.
2. The central regions of samples were mounted in 30mm Bakelite.
3. Grinding and polishing of samples was undertaken to a 1µm polish.

3.5.2 SEM sample

1. The sand cast samples were sectioned, 20mm from the bottom face (as cast) using a water cooled rotary saw.
2. The central regions of samples were mounted in 30mm diameter Bakelite.
3. The cross sections were ground using SiC papers of different granulometry, and polished with oxide polishing suspensions, undertaken up to 1µm polish.
4. Plasma cleaning was used, to clean the sample of any organic contaminants.
5. Samples were mounted using carbon tape.

3.5.3 Grain size

1. The wedge moulds were sectioned, 25mm from the left face (as cast) using a band saw.
2. The cross section was ground using SiC papers of different granulometry, and polished with oxide polishing suspensions. Finally, samples were etched using Tuckers' reactant, to best define grain boundaries.

3. Micrographs were taken at 10mm intervals, along the Z-axis of the sample. The line intercept method was used to calculate approximate grain size, with the aid of ImageJ software.

3.5.3.1 Line intercept method

This method of grain size analysis, involves plotting a grid over a micrograph, and counting the number of grain boundaries occur over a given line, and dividing the length of the line by this number. For example, if the line was 10mm long, and there were 2 grain boundaries, the grain size measurement would be recorded as 5mm. A number of repeats are taken for each micrograph, and the average result used.

4.0 Results

4.1 A354

4.1.1 Undercooling

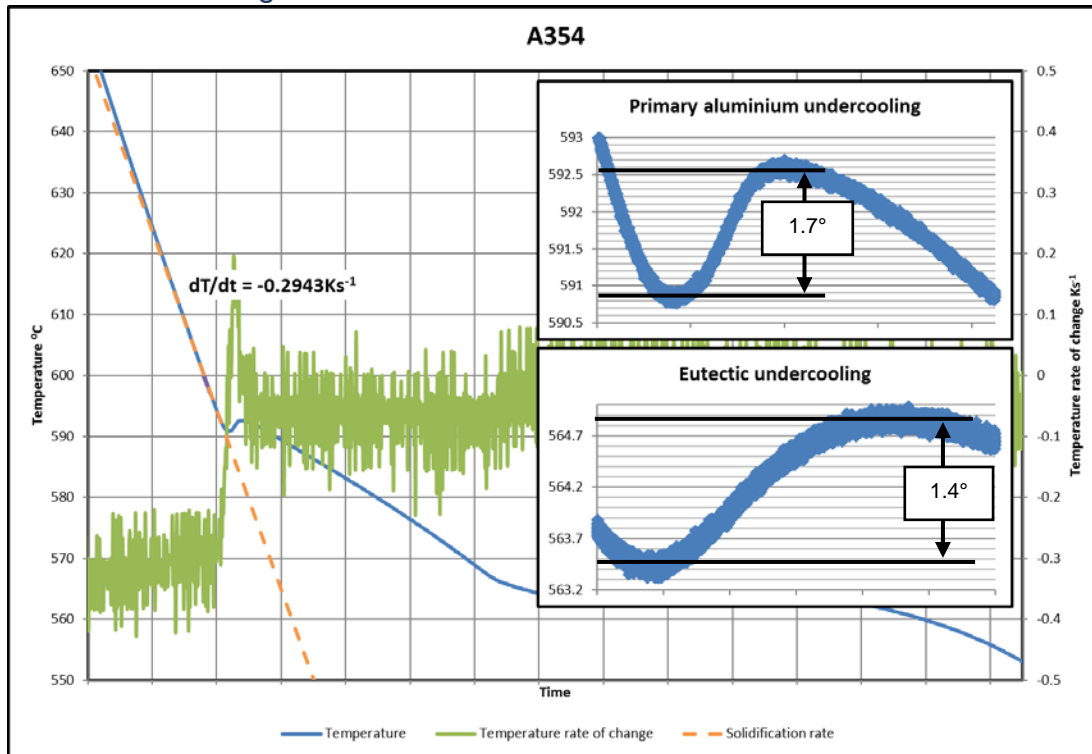


Figure 10 Time temperature tracer for A354 alloy, with no grain refiners added, recorded in the undercooling mould. This curve clearly shows both the primary aluminium undercooling and the eutectic undercooling of the material.

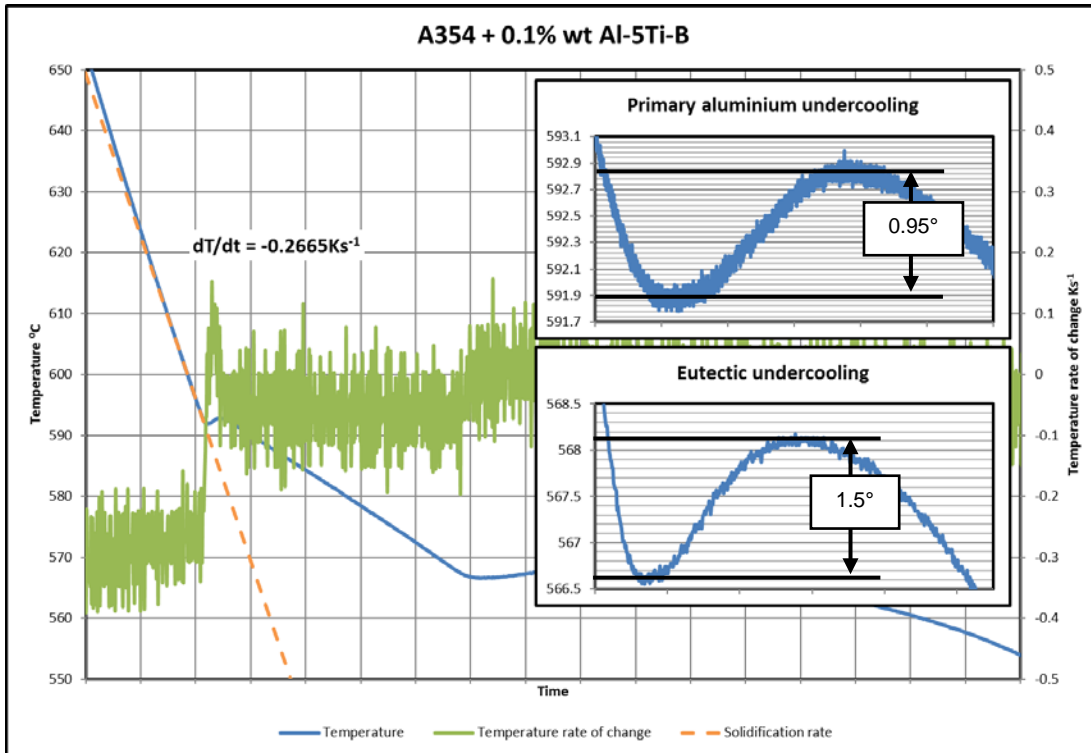


Figure 11 Time temperature tracer for A354 alloy, with 0.1% wt Al-5Ti-B grain refiner addition, recorded in the undercooling mould.

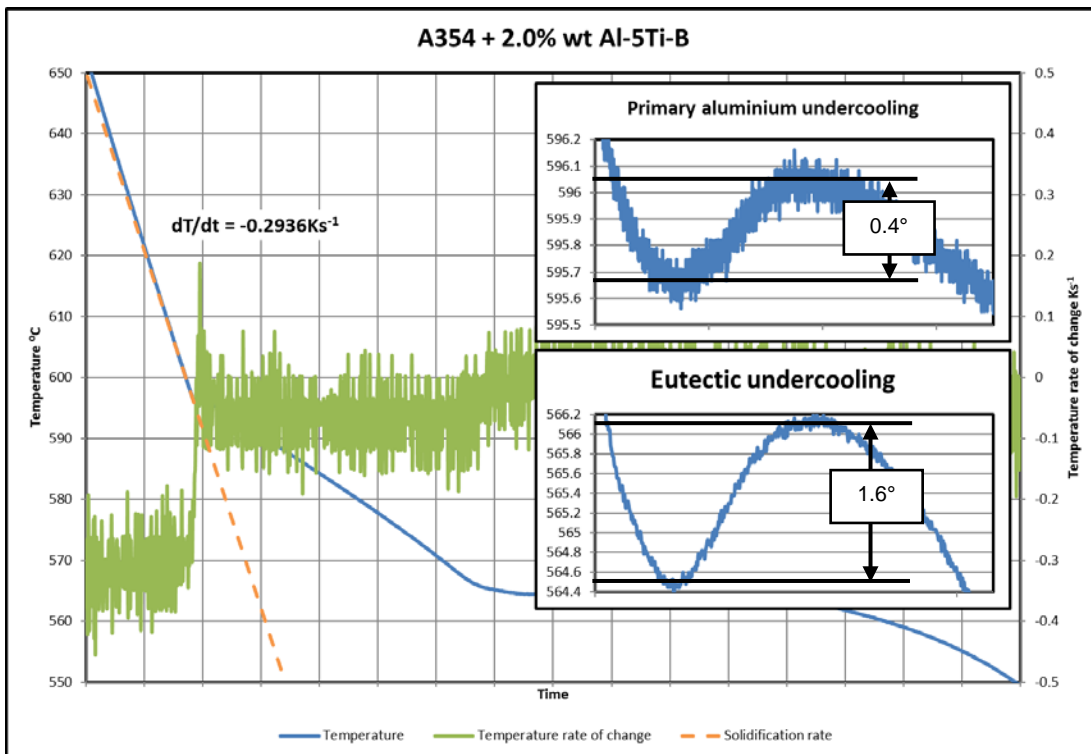


Figure 12 Time temperature tracer for A354 alloy, with 2.0% wt Al-5Ti-B grain refiner addition, recorded in the undercooling mould.

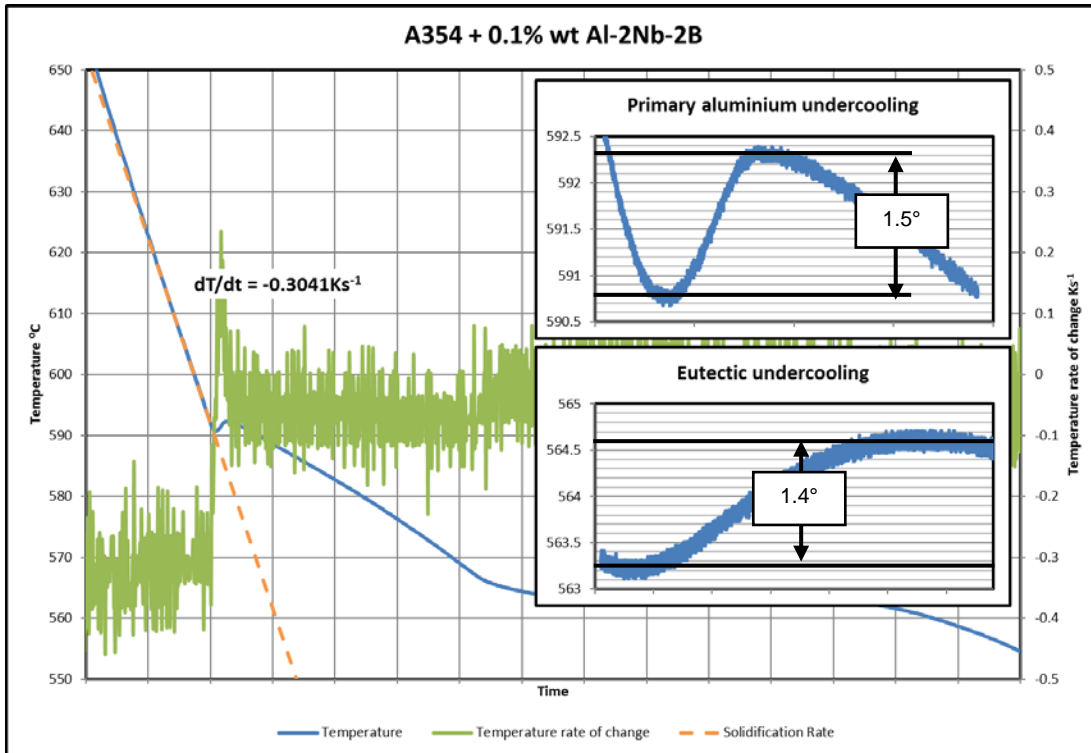


Figure 13 Time temperature tracer for A354 alloy, with 0.1% wt Al-2Nb-2B grain refiner addition, recorded in the undercooling mould.

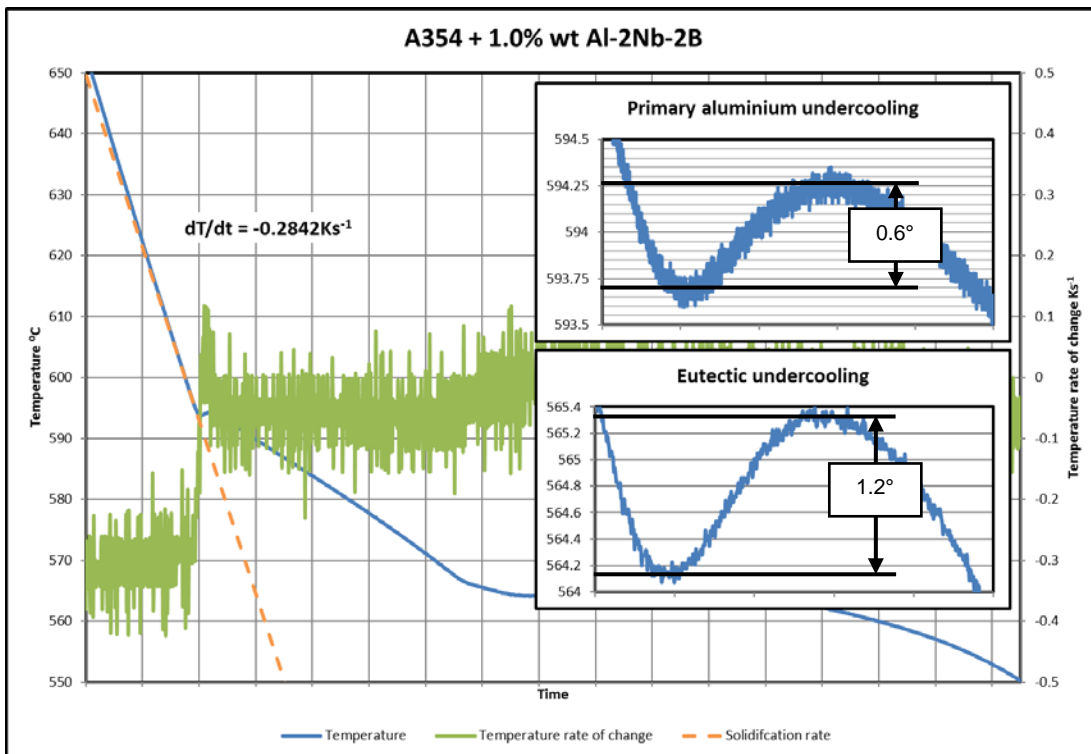


Figure 14 Time temperature tracer for A354 alloy, with 1.0% wt Al-2Nb-2B grain refiner addition, recorded in the undercooling mould.

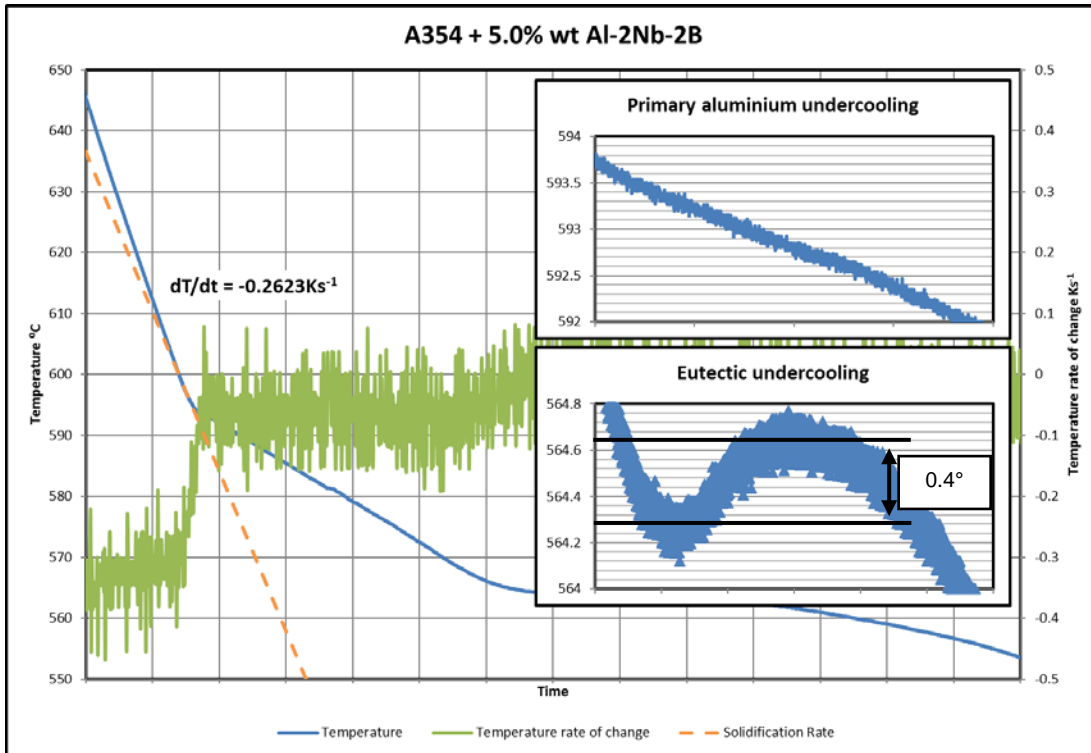


Figure 15 Time temperature tracer for A354 alloy, with 5.0% wt Al-2Nb-2B grain refiner addition, recorded in the undercooling mould.

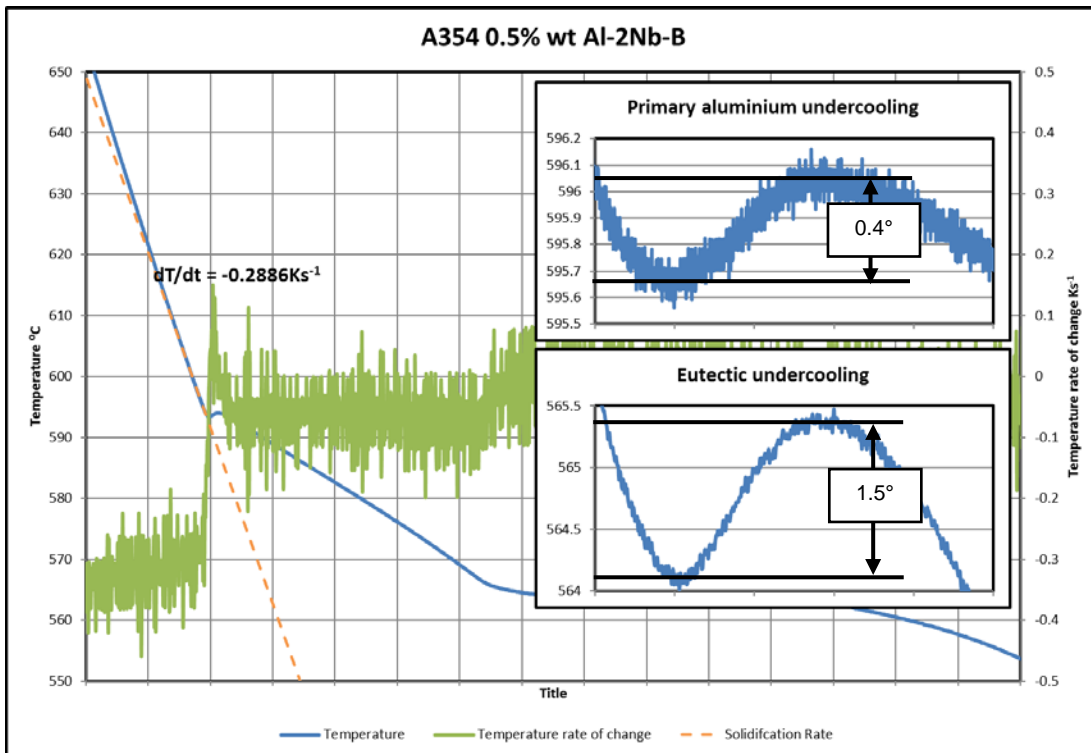


Figure 16 Time temperature tracer for A354 alloy, with 0.5% wt Al-2Nb-B grain refiner addition, recorded in the undercooling mould.

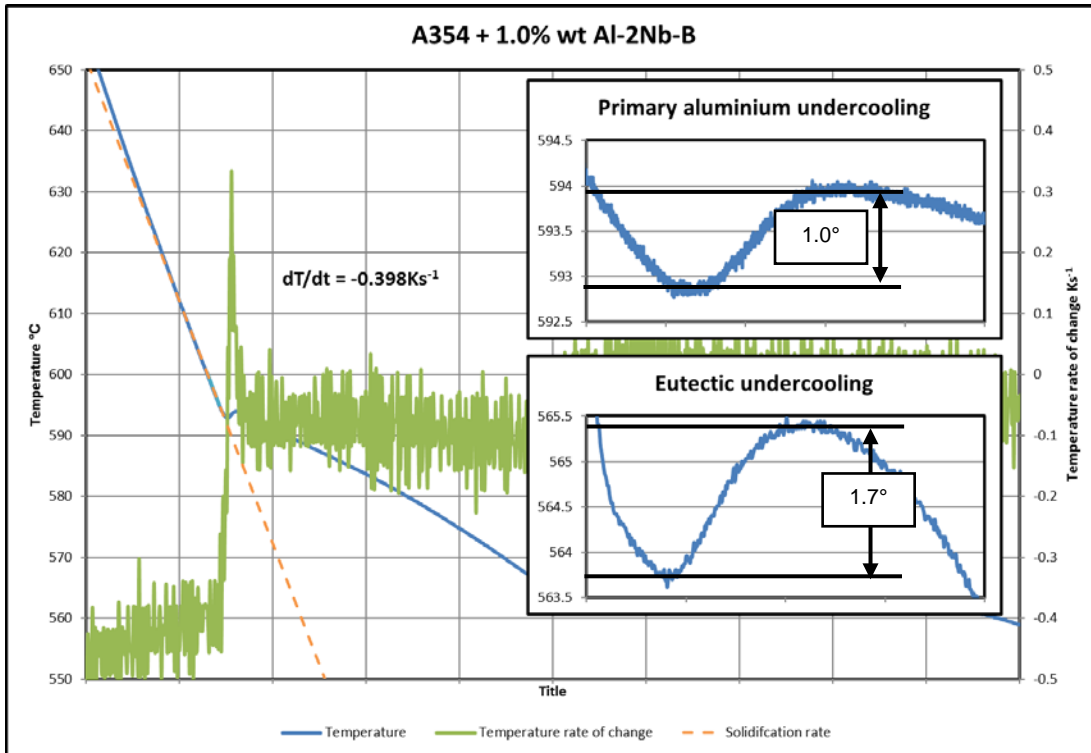


Figure 17 Time temperature tracer for A354 alloy, with 1.0% wt Al-2Nb-B grain refiner addition, recorded in the undercooling mould.

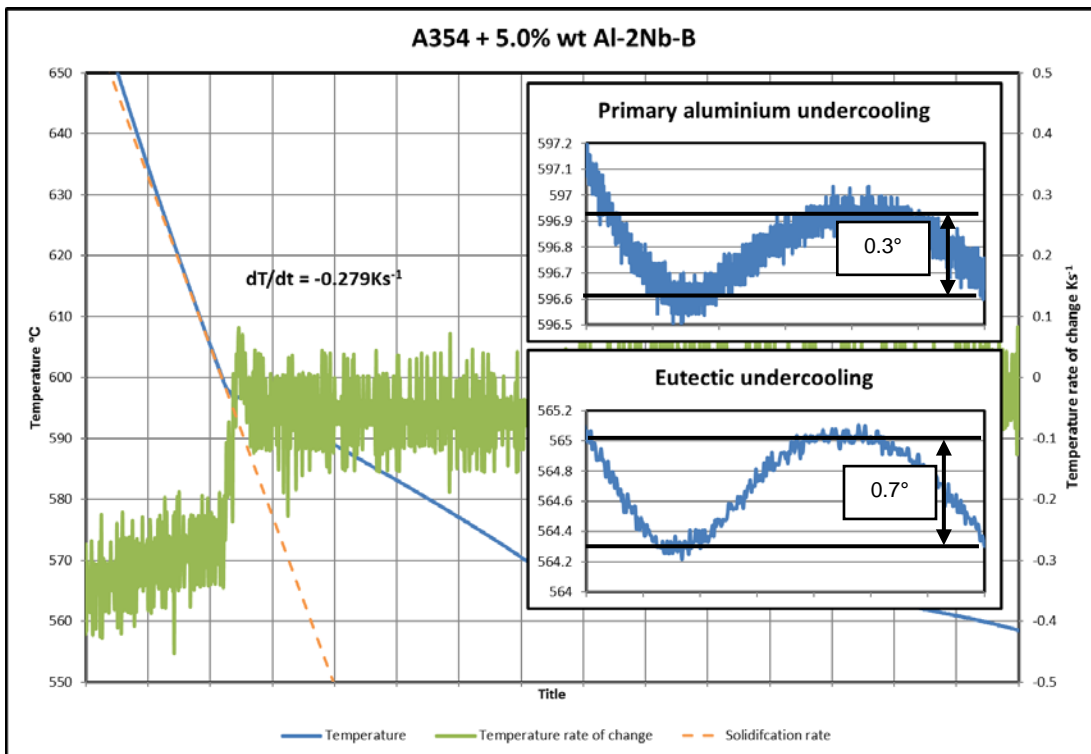


Figure 18 Time temperature tracer for A354 alloy, with 5.0% wt Al-2Nb-B grain refiner addition, recorded in the undercooling mould.

Table 3 The undercooling values found from analysis of the cooling curves of A354 alloy with various grain refiner additions.

Alloy system	Primary aluminium undercooling (K)	Eutectic undercooling (K)
A354	1.70	1.40
A354 +0.1% wt. Al-5Ti-B	0.95	1.50
A354 + 2.0% wt. Al-5Ti-B	0.40	1.60
A354 + 0.1% wt. Al-2Nb-2B	1.50	1.40
A354 + 1.0% wt. Al-2Nb-2B	0.60	1.20
A354 + 5.0% wt. Al-2Nb-2B	0.00	0.40
A354 + 0.5% wt. Al-2Nb-B	0.40	1.50
A354 + 1.0% wt. Al-2Nb-B	1.00	1.70
A354 + 5.0% wt. Al-2Nb-B	0.30	0.70

The results shown in table 3 suggest that Al-2Nb-2B reduces both the eutectic and primary aluminium grain undercooling more than Al-2Nb-B at an addition rate of 5.0% wt. The data above shows that at high enough addition rates, undercooling becomes negligible for primary aluminium, and reduced by around 70% for eutectic solidification, with Al-2Nb-2B.

Measurements are taken from the centre of the curves, as shown in figures 5, 6, 7, 8, 9, 10, 11, 12, 13, 15, 16, 17 & 18, due to the noise created by the high rate of data recording.

Table 4 Temperatures at the onset of primary aluminium, and eutectic solidification, in A354 alloy with various grain refiner additions.

Alloy system	Primary aluminium solidification temperature (°C)	Eutectic solidification temperature (°C)
A354	590.7	563.3
A354 +0.1% wt. Al-5Ti-B	591.9	566.6
A354 + 2.0% wt. Al-5Ti-B	595.7	564.5
A354 + 0.1% wt. Al-2Nb-2B	590.8	563.3
A354 + 1.0% wt. Al-2Nb-2B	593.7	564.1
A354 + 5.0% wt. Al-2Nb-2B	595.2	564.3
A354 + 0.5% wt. Al-2Nb-B	595.7	564.1
A354 + 1.0% wt. Al-2Nb-B	592.9	563.7
A354 + 5.0% wt. Al-2Nb-B	596.6	564.3

The data in table 4 suggests that there is a general trend of increased temperature at the onset of primary aluminium solidification with increased Al-2Nb-2B, Al-2Nb-B and Al-5Ti-B. This suggests that there may be some influence on the alloying of the material when these grain refiners are added at certain levels. Easier nucleation will also increase the onset of solidification. There is not enough data to derive a function to describe the relationship.

4.1.2 Spectrographic analysis of titanium levels

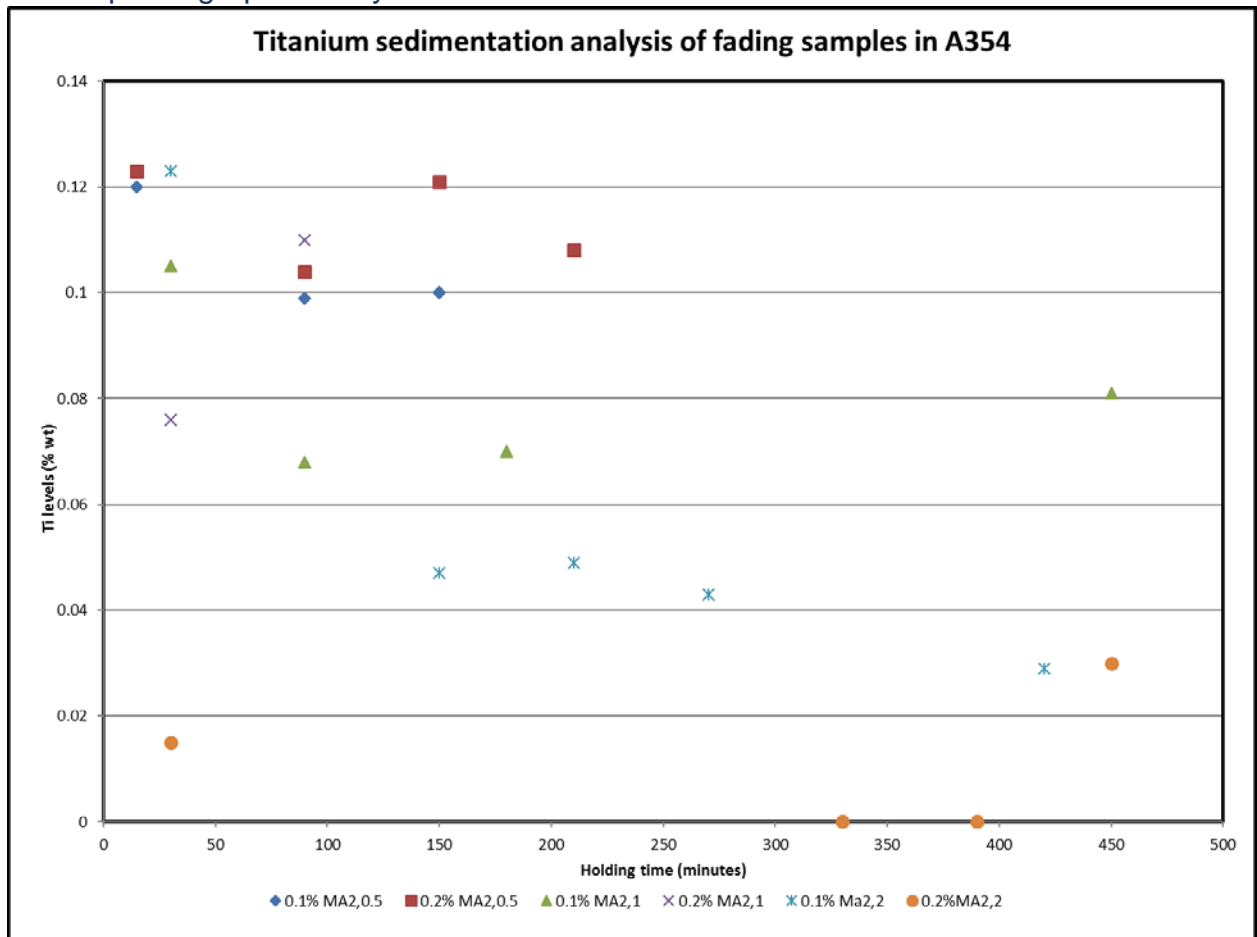


Figure 19 Spectrograph results, taken from die cast samples, for titanium levels in A354 after holding the melt with addition of Al-2Nb-0.5B (MA2,0.5), Al-2Nb-B (MA2,1) & Al-2Nb-2B (MA2,2).

Figure 19 displays data collected from spectrographic analysis of diecast samples, from previous work carried out by Hari-Babu Nadendla at Brunel University. Samples were cast after various periods of holding the molten alloy, after addition of the grain refiner. It can be seen that increased boron levels and holding times cause a decrease in the levels of titanium present in the alloy. This may suggest that excess boron is reacting with titanium to create "TiB₂, AlB₂ or MgB" particles. This may suggest that excess boron is reacting with titanium and possibly with other alloying elements to create TiB₂ and Mg₂B₂ particles. The excess boron may also form other particles such as MgB₂.

4.2 A356

4.2.1 Undercooling

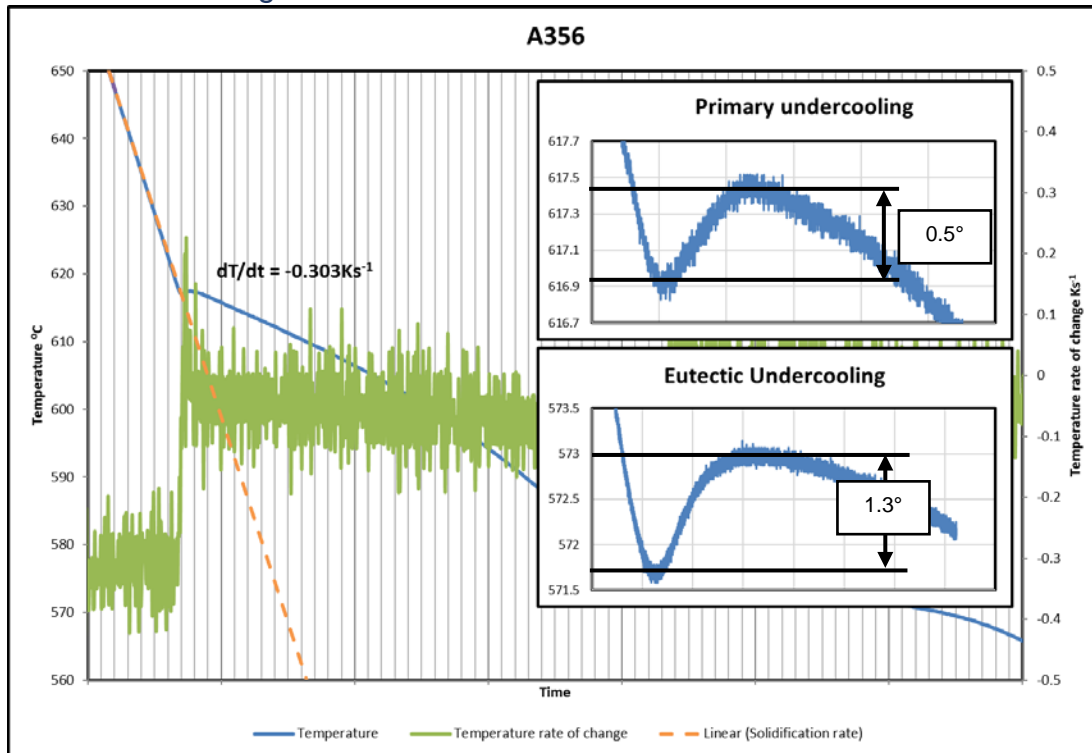


Figure 20 Chart showing the temperature-time tracer, and cooling rate, during solidification of A356, in the undercooling mould.

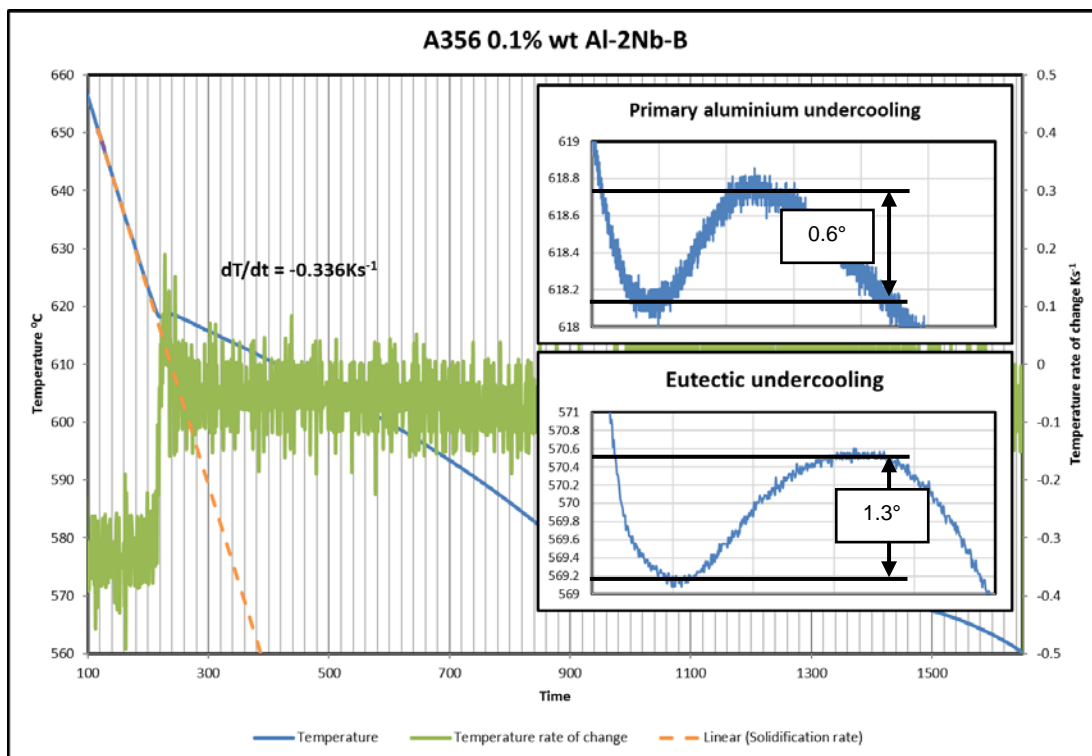


Figure 21 Chart showing the temperature-time tracer, and cooling rate, during solidification of A356 with 0.1% wt Al-2Nb-B, in the undercooling mould.

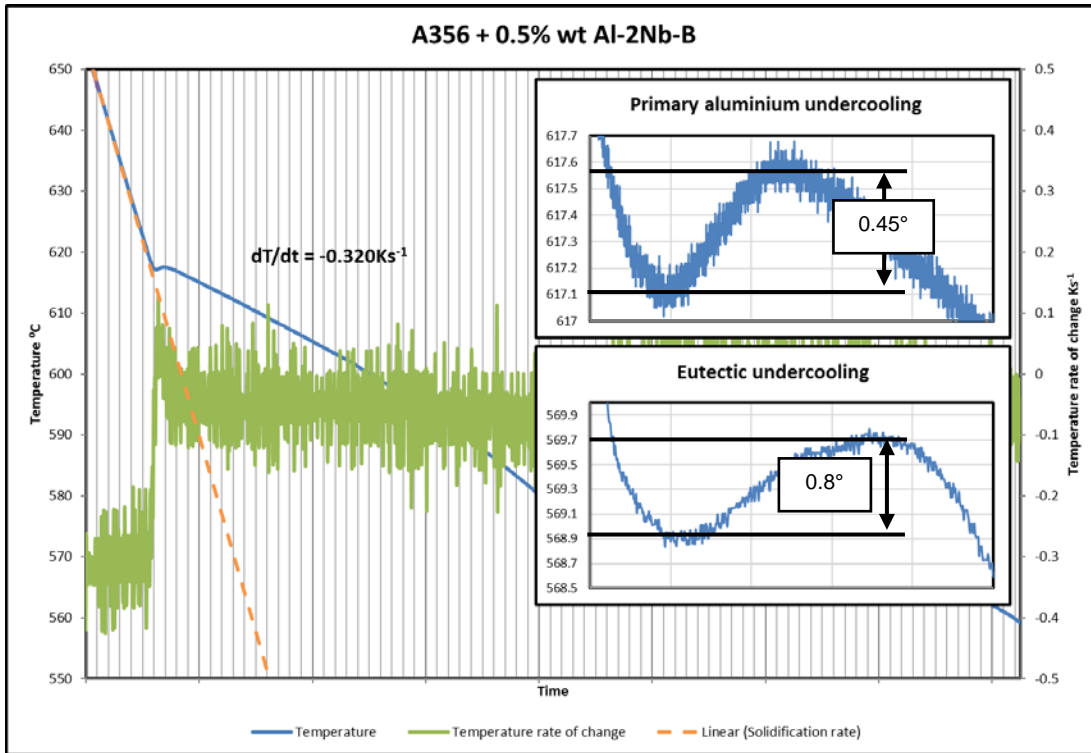


Figure 22 Chart showing the temperature-time tracer, and cooling rate, during solidification of A356 with 0.5% wt Al-2Nb-B, in the undercooling mould.

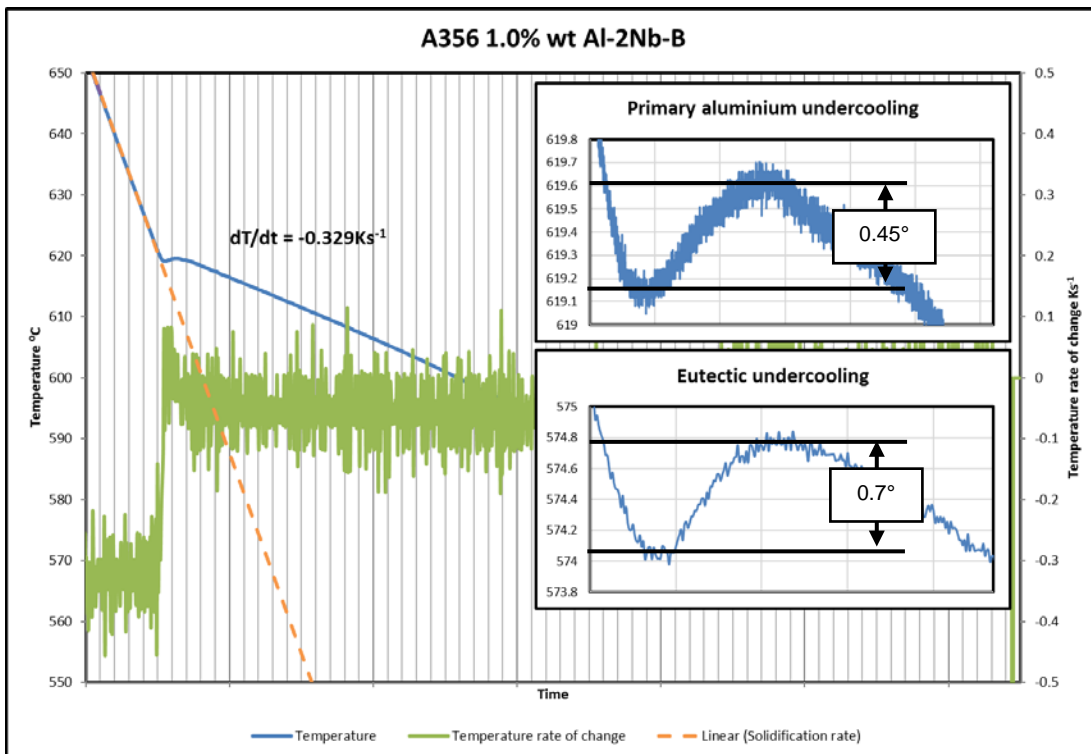


Figure 23 Chart showing the temperature-time tracer, and cooling rate, during solidification of A356 with 1.0% wt Al-2Nb-B, in the undercooling mould.

Table 5 Undercooling values found from analysis of the cooling curves of A356 alloy with various grain refiner additions.

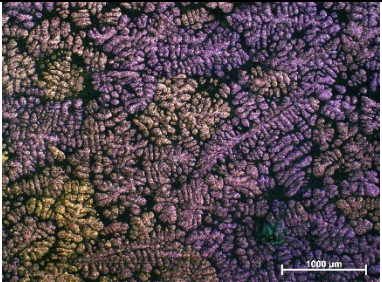

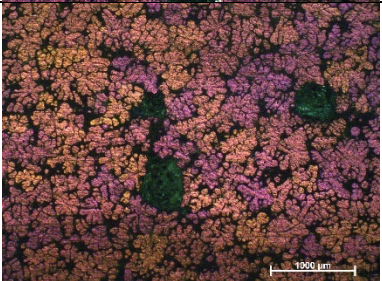

Alloy system	Primary aluminium undercooling (K)	Eutectic undercooling (K)	Microstructure at 90mm from tip of wedge sample
A356	0.50K	1.30K	
A356 + 0.1% wt. Al-2Nb-B	0.60K	1.30K	
A356 + 0.5% wt. Al-2Nb-B	0.45K	0.80K	
A356 + 1.0% wt. Al-2Nb-B	0.45K	0.70K	

Table 5 shows the recorded undercooling values, and resulting microstructures, taken from sand cast wedge samples, form in the wedge sand moulds, at 90mm from the tip, for A356 with various addition rates of Al-2Nb-B.

Table 6 Temperatures at the onset of primary aluminium, and eutectic solidification, in A356 alloy with various grain refiner additions.

Alloy system	Primary aluminium solidification temperature (°C)	Eutectic solidification temperature (°C)
A356	616.9	571.7
A356 + 0.1% wt. Al-2Nb-B	618.1	569.2
A356 + 0.5% wt. Al-2Nb-B	617.1	568.9
A356 + 1.0% wt. Al-2Nb-B	619.1	574.1

4.2.2 Grain Size

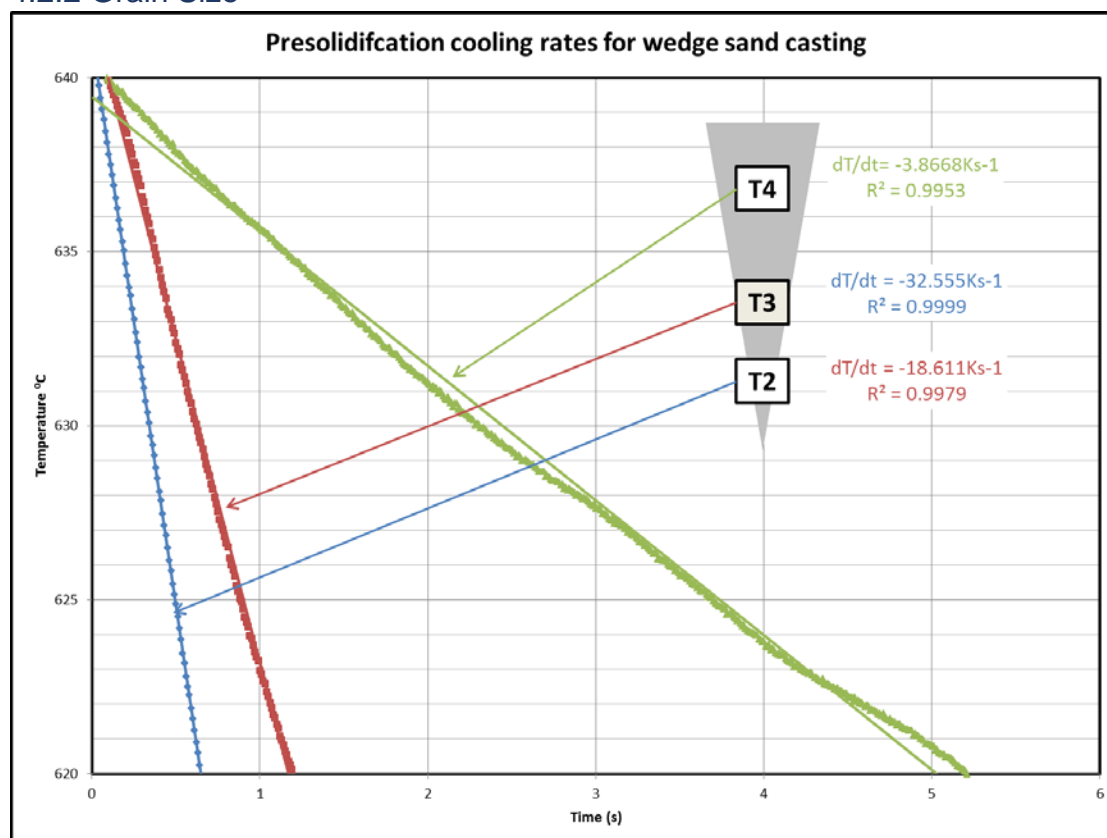


Figure 24 - Cooling rates along the sand-cast wedge samples, at 10, 30 and 90mm from the wedge tip.

Figure 24 shows the cooling rates obtained at three locations along the wedge sample. These were used to obtain a function which described the cooling rate at any particle location, from the tip of the wedge, along its axis of symmetry.

$$\text{Cooling rate} = (20.8 - 0.204X)Ks^{-1}$$

Where X is the distance from the tip of the wedge sample, in millimetres.

Table 7 Average grain sizes, based on 10 results, measured from wedge samples, using the line intercept method, at various cooling rates.

Alloy system	Cooling rate (Ks⁻¹)	18.8 (10mm)	16.7 (20mm)	14.7 (30mm)	12.6 (40mm)	10.6 (50mm)	8.6 (60mm)	6.5 (70mm)	4.5 (80mm)	2.4 (90mm)	0.4 (100mm)
A356	Average grain size (µm)	616	643	797	883	834	974	1044	1034	1178	1438
	StDev	132	144	213	157	121	233	294	360	359	238
A356 + 0.1% wt. Al-2Nb-B	Average grain size (µm)	339	356	435	460	650	785	832	883	1084	1241
	StDev	52	58	114	67	116	144	132	168	293	302
A356 + 0.5% wt. Al-2Nb-B	Average grain size (µm)	302	332	412	509	561	692	718	817	733	934
	StDev	37	47	61	80	60	177	123	194	109	246
A356 - 1.0% wt. Al-2Nb-B	Average grain size (µm)	288	356	399	658	542	658	639	688	779	804
	StDev	63	85	75	135	76	163	117	160	163	195
A356 + 0.1% wt. Al-5Ti-B	Average grain size (µm)	490	535	788	787		1070		1407		
	StDev	182	81	191	140		179		477		

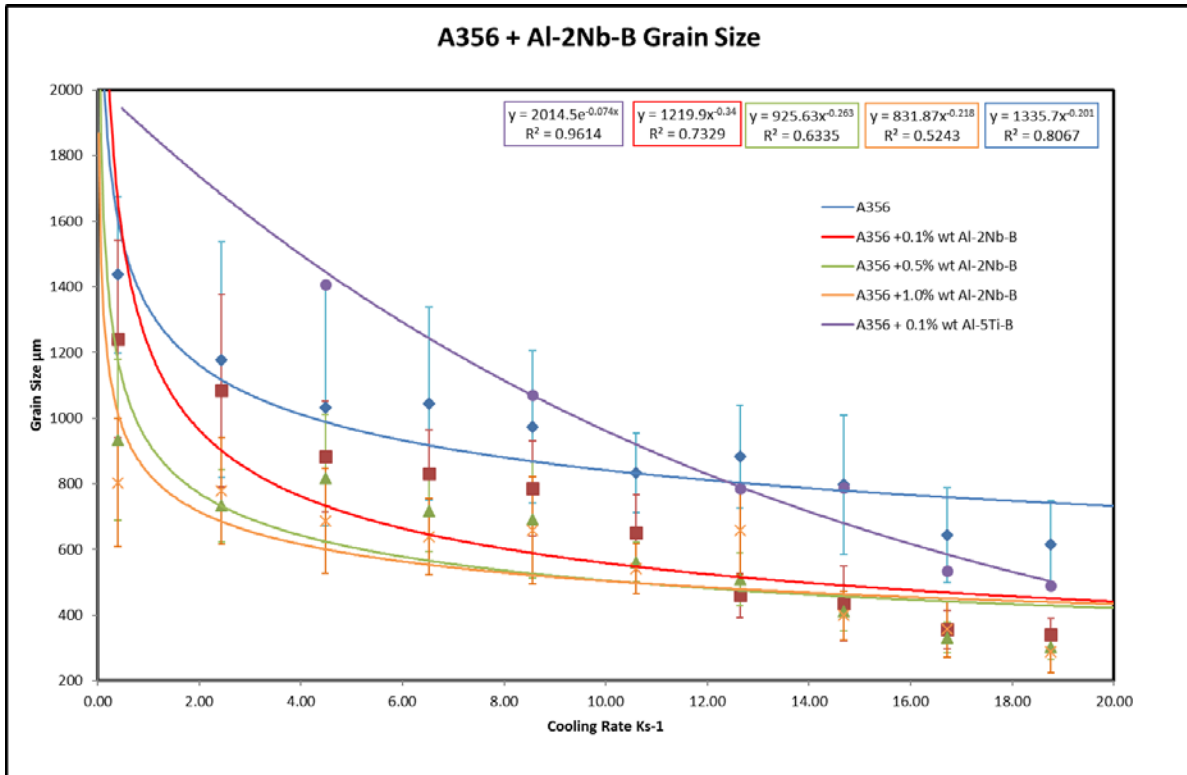


Figure 25 Variations in grain size, at different locations along the wedge sample, with different addition of the niobium boron grain refiner, and an existing titanium boron grain refiner.

The data in table 7 and figure 25 shows a grain size reduction of 30%, at an addition rate of just 0.1% wt., at cooling rates above 6Ks⁻¹. Addition rates of 0.5 – 1.0% can extend this to cooling down to 4Ks⁻¹. The data suggests that increased addition rates of Al-2Nb-B, show greater benefits at decreasing cooling rates. Above 12Ks⁻¹ there appears to be little benefit in addition rates greater than 0.1% wt. The data also suggests that Al-5Ti-B, a commercially available grain refiner, is ineffective at cooling rates below 12Ks⁻¹, and there appears to be an increase in grain size.

4.2.3 SEM Data

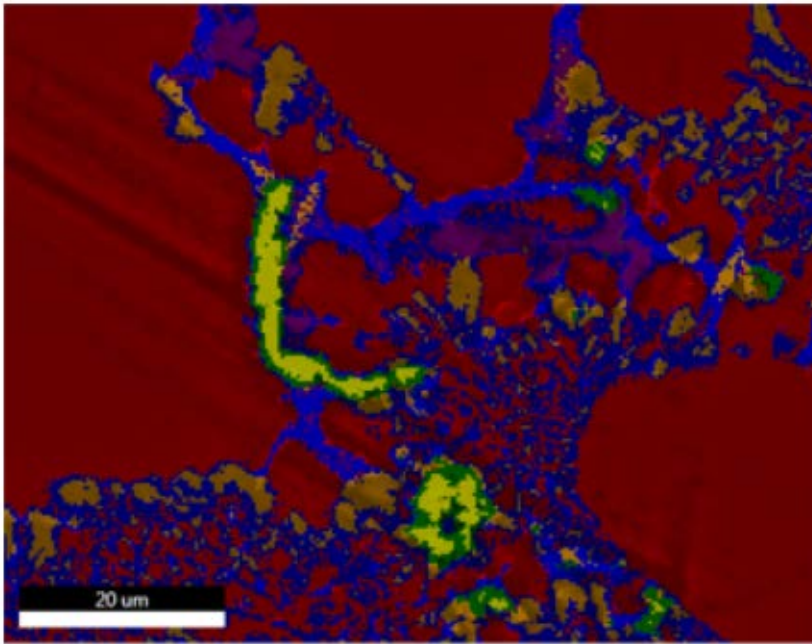


Figure 26 SEM phase map of a 40mm sand cast A356 with 5.0% wt. addition of Al-2Nb-B sample, at a magnification of x4240. Phases containing niobium are visible within the eutectic silicon regions. These are shown as yellow and green areas.

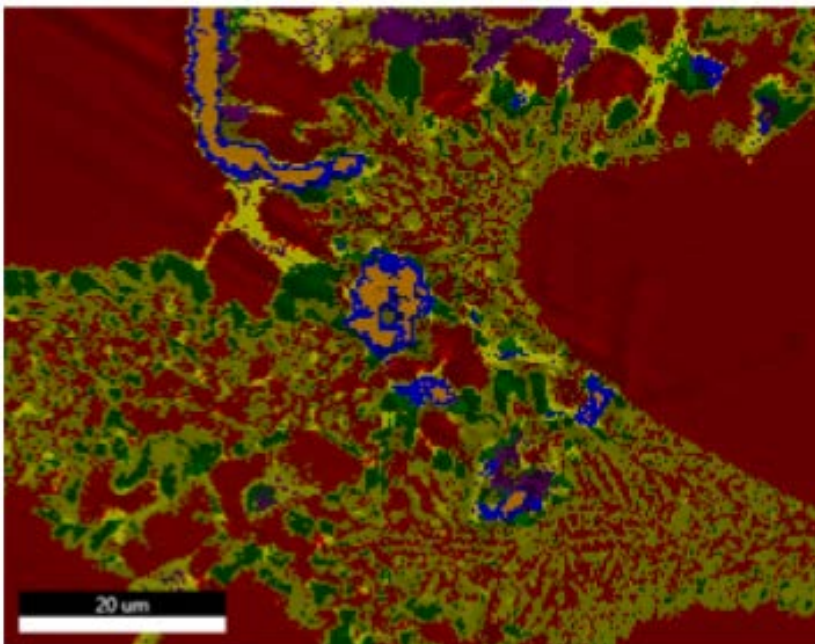


Figure 27 SEM phase map of a 40mm sand cast A356 with 5.0% wt. addition of Al-2Nb-B sample, at a magnification of x4240. Phases containing niobium are visible within the eutectic silicon regions. These are shown as orange and blue areas.

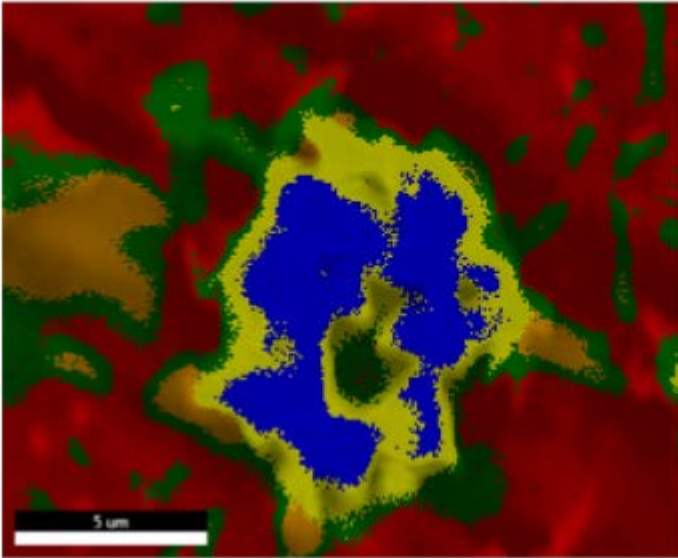


Figure 28 SEM phase map of a 40mm sand cast A356 with 5.0% wt. addition of Al-2Nb-B sample, at a magnification of x38383. Phases containing niobium are visible within the eutectic silicon regions. These are shown as yellow and blue areas.

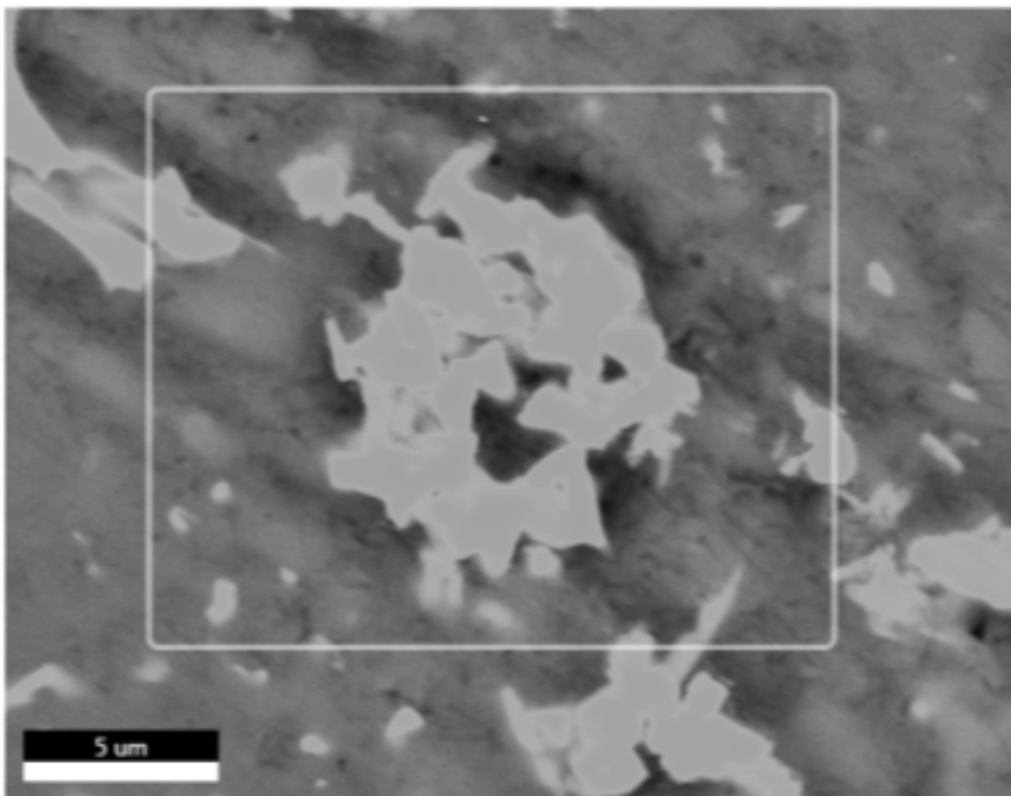
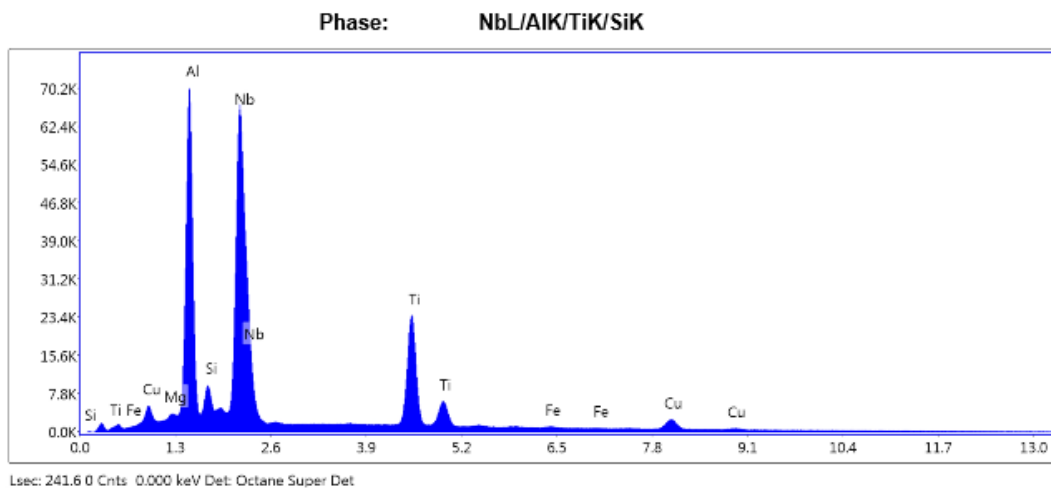


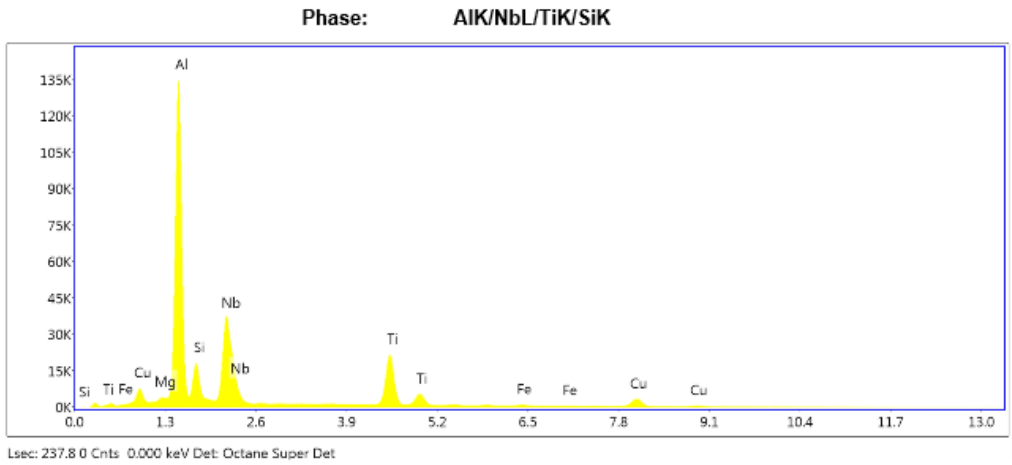
Figure 29 SEM image of a 40mm sand cast A356 with 5.0% wt. addition of Al-2Nb-B sample, at a magnification of x38383. Niobium phases are seen to be very angular in characteristics.



eZAF Smart Quant Results

Element	Weight %	Atomic %	Net Int.	Error %	Kratio	Z	R	A	F
MgK	0.04	0.09	4.20	60.05	0.0002	1.1928	0.8933	0.4460	1.0093
AlK	24.40	45.14	3035.90	5.31	0.1646	1.1507	0.9024	0.5813	1.0086
SiK	2.85	4.72	302.40	6.40	0.0168	1.1780	0.9112	0.5304	1.0135
NbL	48.48	26.05	2937.50	2.72	0.3785	0.9135	1.0915	0.8466	1.0096
TiK	18.41	19.18	1386.10	2.89	0.1657	1.0201	0.9710	0.8610	1.0248
FeK	0.90	0.81	42.60	7.01	0.0091	1.0107	0.9947	0.9321	1.0686
CuK	5.11	4.02	158.00	3.82	0.0534	0.9749	1.0086	0.9692	1.1053

Figure 30 Average chemical analysis of the blue region in figure 23.



eZAF Smart Quant Results

Element	Weight %	Atomic %	Net Int.	Error %	Kratio	Z	R	A	F
MgK	0.25	0.40	29.80	11.89	0.0014	1.1362	0.9287	0.5010	1.0120
AlK	41.35	60.36	6095.20	4.72	0.2901	1.0957	0.9375	0.6383	1.0084
SiK	7.01	9.82	762.00	6.67	0.0372	1.1212	0.9459	0.4693	1.0084
NbL	28.35	12.02	1857.70	3.74	0.1875	0.8689	1.1314	0.7538	1.0099
TiK	14.96	12.30	1264.20	2.62	0.1327	0.9677	1.0013	0.8913	1.0281
FeK	0.91	0.64	47.90	6.29	0.0090	0.9564	1.0216	0.9505	1.0794
CuK	7.17	4.45	240.20	3.21	0.0712	0.9200	1.0318	0.9797	1.1016

Figure 31 Average chemical analysis of the yellow region in figure 23.

SEM results show that niobium forms Al-Si-Ti-Nb system intermetallic phases. Figure 26, 27 & 28 appear to show that more niobium rich regions exist, surrounded by regions of lower niobium levels. Conversely, silicon appears to be higher in the outer regions, than the most niobium rich central regions. Titanium levels appear to be similar in both regions.

4.3 Measurement error

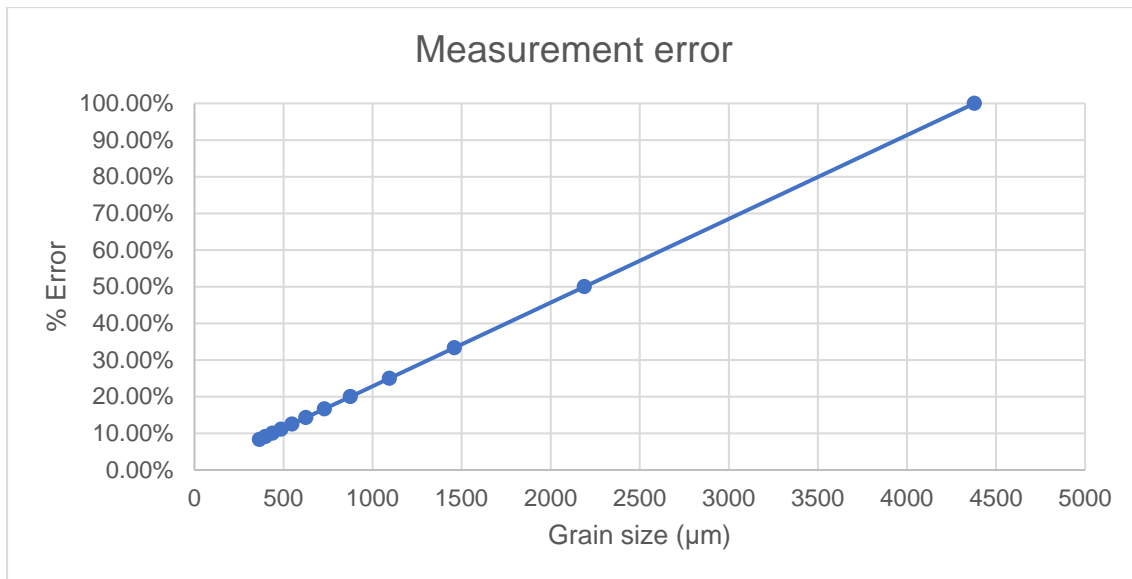


Figure 32 Grain size measurement error, from the line intercept method.

Figure 32 shows the percentage error vs grain size, for the line intercept method employed.

Type K thermocouples were used for temperature measurement of the furnace, the melt, and the undercooling of samples. The error for a type K thermocouple is $\pm 0.75\%$, or $\pm 2.2^{\circ}\text{C}$ (42).

5.0 Discussions

5.1 A356

5.1.1 Undercooling

Al-2Nb-B has been shown to reduce the undercooling temperature of A356 by around 10%. This was shown by a reduction in primary undercooling temperature of around 0.05K. Considering the error in the experimentation, it cannot be said with certainty that the grain refiner is influencing the primary aluminium undercooling, at these addition rates.

Eutectic undercooling was reduced by nearly 50%, from 1.3K to 0.7K, with an addition rate of 1.0% wt. Al-2Nb-B. Such small reductions in primary aluminium undercooling, suggest that lower barriers to nucleation may not be the reason for reduction in grain size, although they may have some level of influence. Figure 33 shows a finer, and more uniform structure, with 0.5% wt addition of Al-2Nb-B, compared with A354 without additions as shown in figure 34.

Different temperatures were recorded at the onset of primary aluminium, and eutectic solidification. Primary solidification temperatures appear to increase with increased addition of Al-2Nb-B, whilst it is not clear what the effect on eutectic solidification temperatures are. Further work would be need to more accurately characterise these relationships.

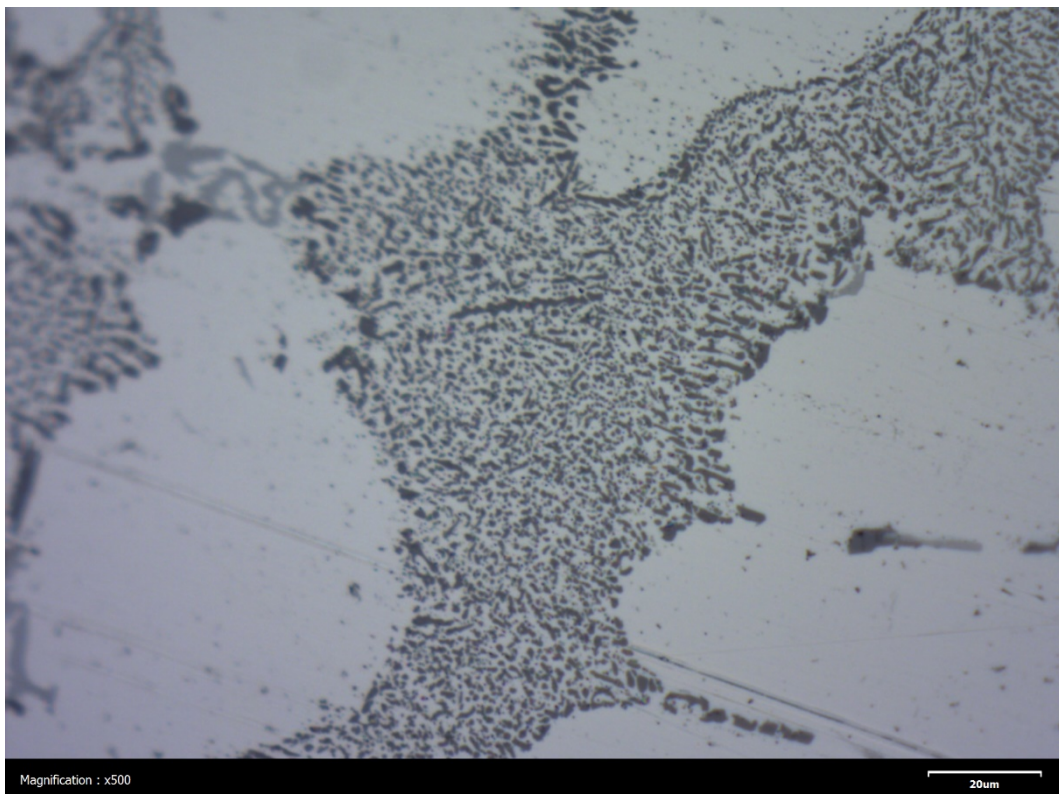


Figure 33 Micrograph showing eutectic region in A356 wedge sample at 50mm from the tip.

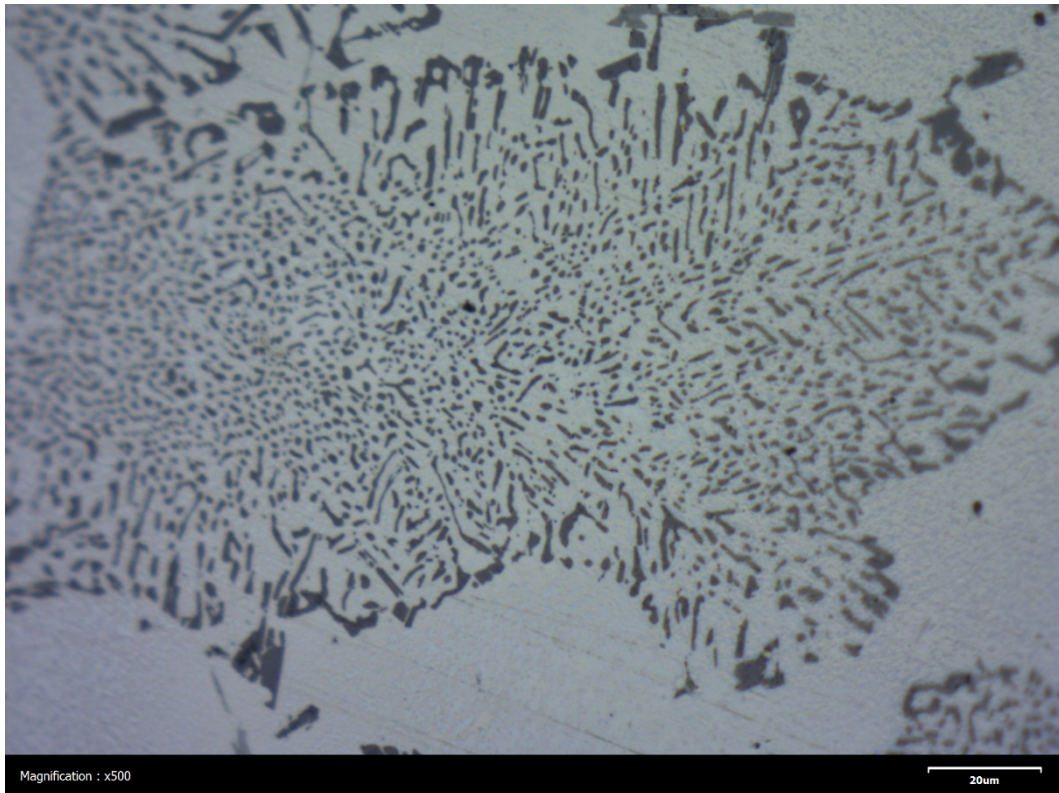


Figure 34 Micrograph showing eutectic region in A356, with 0.5% wt addition of Al-2Nb-B, wedge sample at 50mm from the tip.

5.1.2 Grain size

The results for grain size, in A356 alloy, show that by application of Al-2Nb-B, primary aluminium grain sizes can be reduced to 500-600 μm for cooling rates greater than 4Ks⁻¹. This is important, as cooling rates above 4Ks⁻¹ would be achievable through a majority of a sand casting during solidification. An addition rate of between 0.5% and 1.0% wt. is required to achieve this reduction in grain size. Data for a conventional grain refinement system (0.1% wt. Al-5Ti-B), suggests that there is little or no influence on grain size in A356.

Such an addition rate may prove too costly for a production foundry, where material costs because a major factor in the total production cost of the product, and where the end cost is also much more sensitive. In the case of prototyping, where material costs are a much lower percentage of the manufacturing cost, the additional cost of using a large amount of a more expensive grain refiner, is outweighed by the benefits seen in an improved product.

The results show that for continued reduction of grain size, to the 500-600 μm range, exponential increases in Al-2Nb-B additions are required. A more logical decision, in the casting method design, would be to employ chills to bring the solidification rates above the 4Ks⁻¹ to achieve the desired grain size.

The results suggest that in thin walled castings, which will by their nature have higher cooling rates, only a small addition rate would be required. A356 is more likely to be

employed in body structure thin wall castings as there is much focus from automotive manufacturers to use as purer alloys as possible, due to recycling.

Even at addition rates of just 0.1% wt. there is a reduction in grain size, at cooling rates above 1Ks^{-1} , as seen in figure 20. This means that the grain refiner may be an economical alternative for production castings. Figures 35 & 36 show the grains sizes, at cooling rates of circa 6.5Ks^{-1} , with and without an addition of 0.1% Al-2Nb-B. The reduction in grain size is very clear. Little benefit is seen in higher addition rates as shown in figure 37.

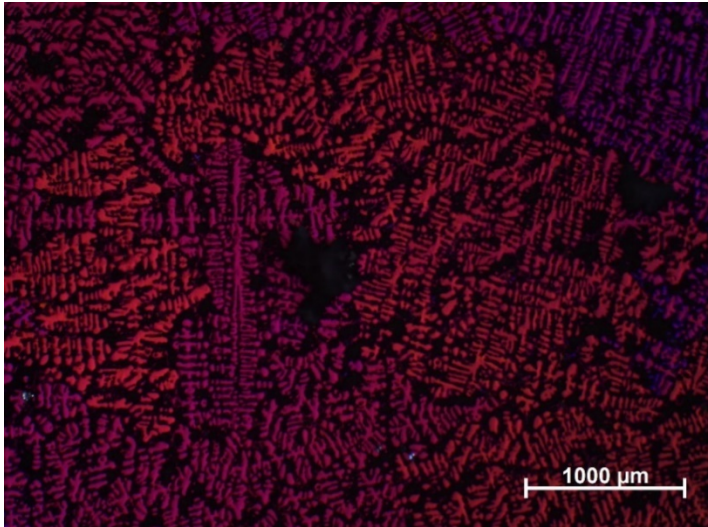


Figure 35 Anodised microstructure of A356, taken at 40mm from the tip of the wedge mould, showing grain size.

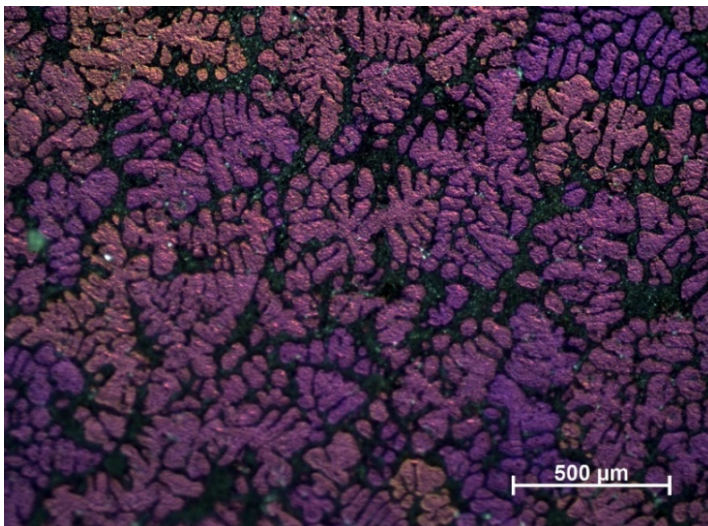


Figure 36 Anodised microstructure of A356, with 0.1% wt. Al-2Nb-B addition, taken at 40mm from the tip of the wedge mould, showing grain size.

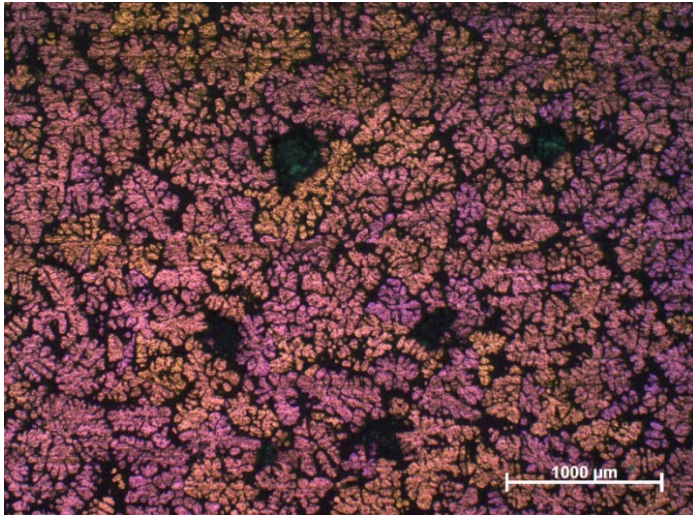


Figure 37 Anodised microstructure of A356, with 0.5% wt. Al-2Nb-B addition, taken at 40mm from the tip of the wedge mould, showing grain size.

5.1.3 SEM analysis

SEM analysis found niobium rich regions around the eutectic regions of the microstructure. The typical characteristics were a rich niobium region (circa >40%), surrounded by a lower niobium containing region (circa >25%). These areas were mostly formed from aluminium, silicon, niobium and titanium. Titanium levels in both of the regions was around 15 to 20%. Silicon content was lower in the centre of the niobium regions, at around 3%. It was much higher, at around 7% in the outer region.

These niobium rich regions may be decreasing the overall number of available niobium containing particles for nucleation.

The SEM analysis undertaken did not quantify the particles or phases which were being formed. Further research could be undertaken to identify these particles, and analysis their theoretical suitability for grain refining aluminium alloys.

5.2 A354

5.2.1 Undercooling

Both Al-2Nb-2B and Al-2Nb-B have been shown to reduce both primary aluminium and eutectic undercooling in A354. At an addition rate of 1.0% wt., Al-2Nb-B was able to reduce the undercooling value by around 40%. This is more than was achieved in A356. A possible reason for the higher effectiveness in A354 than A356, is that it has a higher silicon content, which can poison titanium from forming TiB_2 particles. If niobium particles do not suffer the same poisoning effects, Al-2Nb-B may be a very effective grain refiner for high silicon alloys.

Al-2Nb-2B has been shown to be the more effective of the two in reducing undercooling. The reason for this may be that the excess boron is forming other potential nucleation particles, such as TiB_2 , AlB_2 and MgB particles.

Conventional Al-5Ti-B appears to influence primary aluminium undercooling, but has little effect on eutectic undercooling. Little effect is seen on the microstructure of the eutectic regions, as shown in figures 38 & 39. Both show coarser silicon along grain boundaries, with a similar, finer structure, in the middle of the eutectic regions. Little difference is seen in the primary aluminium grain size, in the same conditions, as shown in figures 40 & 41.

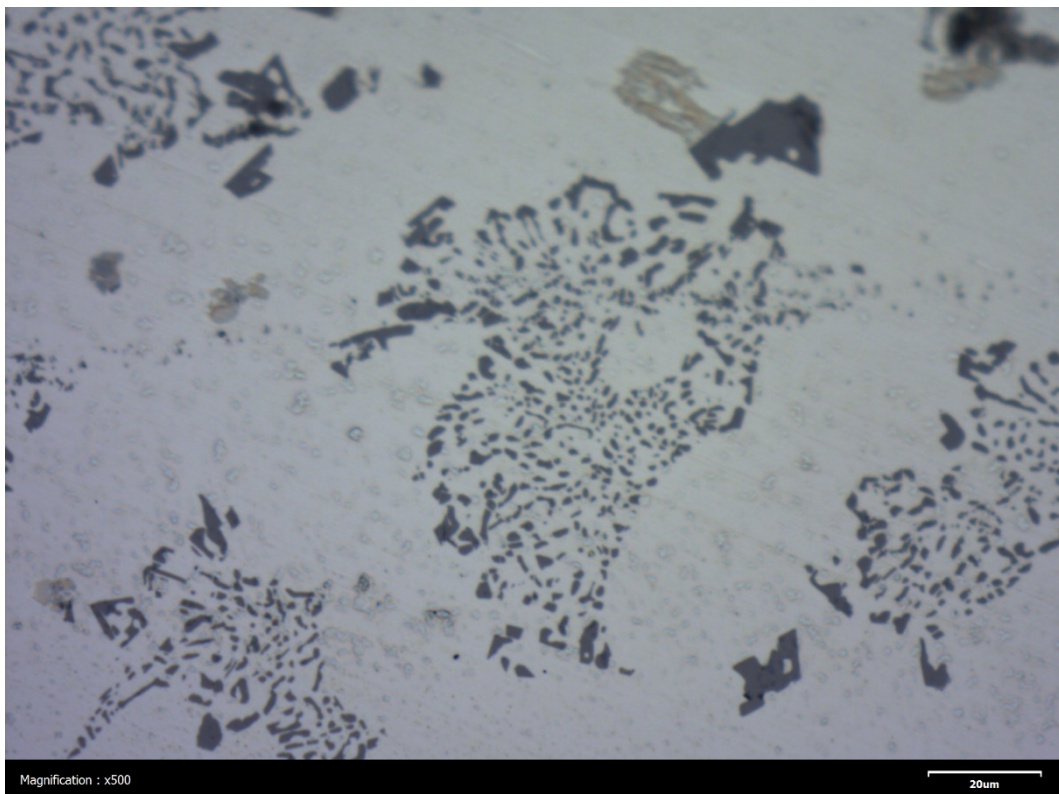


Figure 38 Micrograph showing eutectic region in A354 wedge sample at 50mm from the tip.

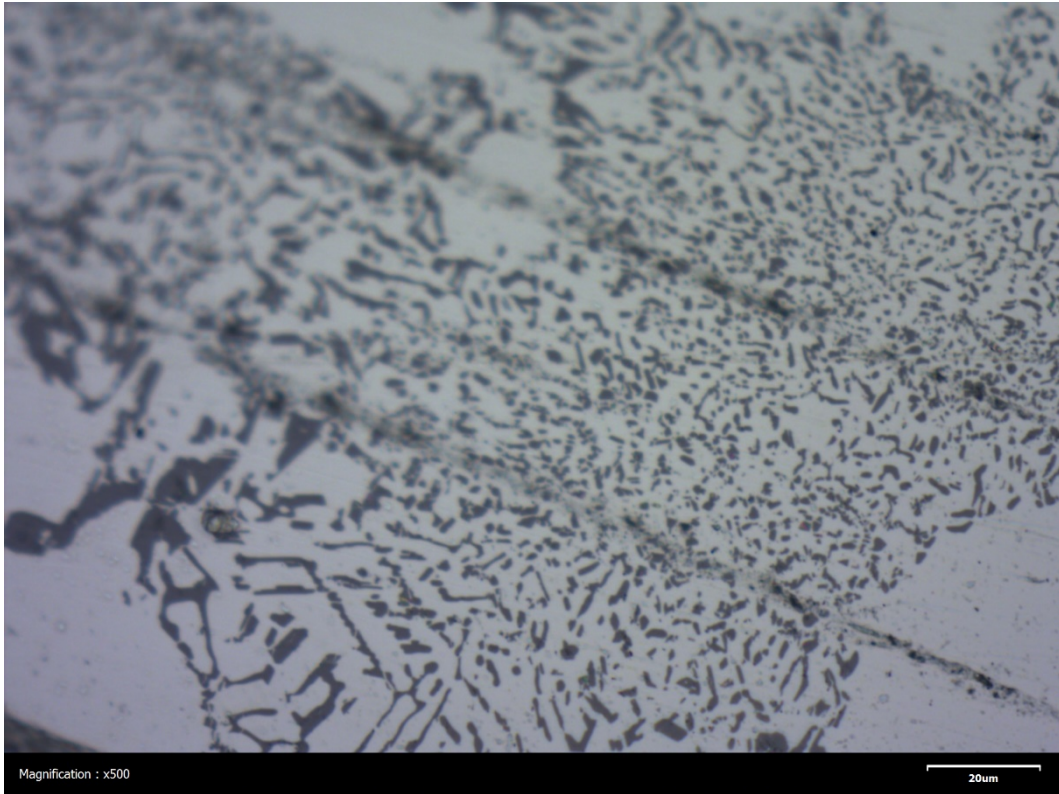


Figure 39 Micrograph showing eutectic region in A354, with 1.0% wt addition of Al-2Nb-B, wedge sample at 50mm from the tip.

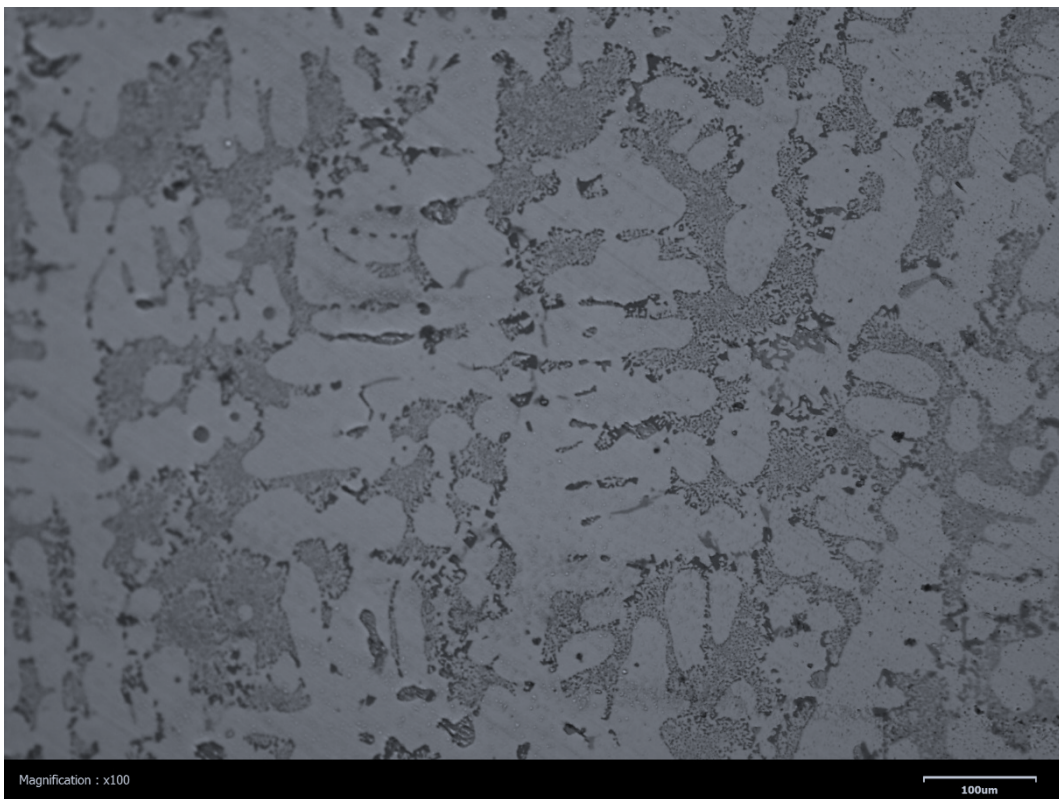


Figure 40 Microstructure of A354, taken at 40mm from the tip of the wedge mould, showing grain size.

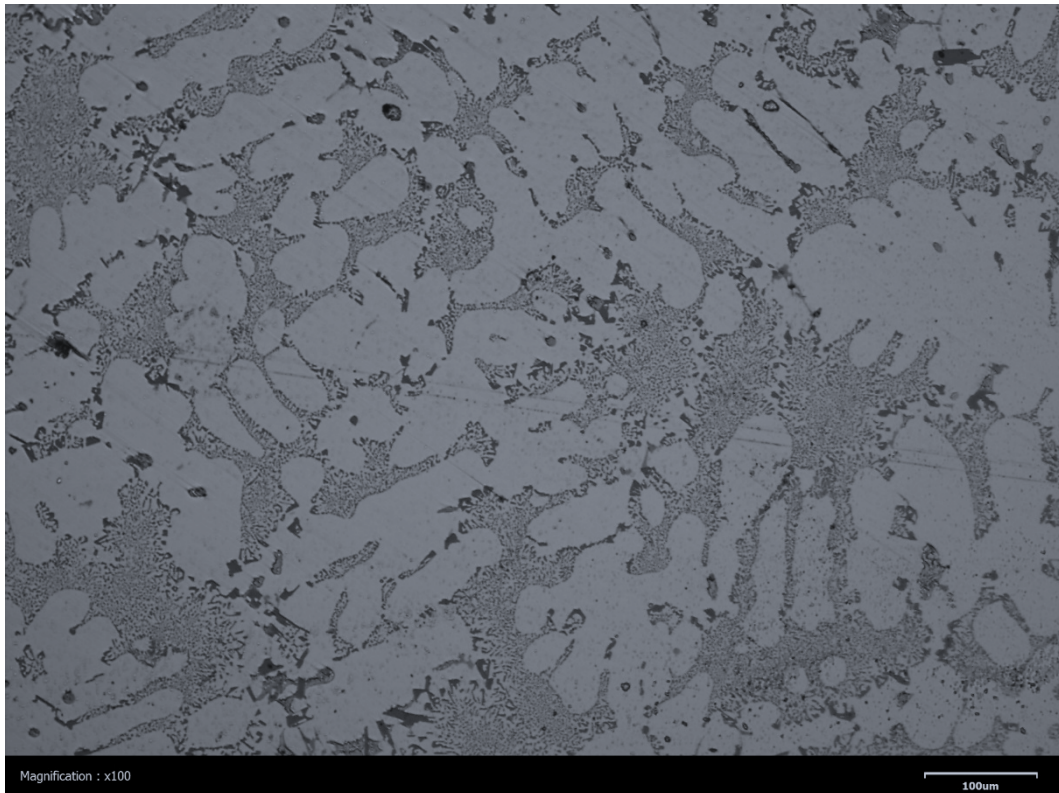


Figure 41 microstructure of A354, with 0.5% wt. Al-2Nb-B addition, taken at 40mm from the tip of the wedge mould, showing grain size.

5.2.2 Spectrographic analysis

Decreasing titanium levels with increased boron additions, and hold times may be caused by the formation of titanium boride particles. The excess boron may also form other particles such as MgB or AlB₂ particles, which have been proposed as nuclei themselves. These particles may also be influencing grain refinement, along with niobium particles. Further work could be carried out to determine if these suggestions are correct.

The sedimentation of other elements may mean that the niobium boron grain refiners are affecting the base chemistry of the alloys being treated. This is not a desirable characteristic, as it means additional alterations would be required, to bring the chemistry back into specification, through the introduction of other elements in purer forms. The chemistry of ingots may need to be adjusted to offset changes in chemistry caused by the grain refiners. This would be a major consideration to a foundry with established material supply.

The origin of this titanium which is present, is not from any grain refiner, but is already present in the alloy ingots, at a rate around 0.10 to 0.15% wt.

6.0 Conclusions

6.1 Effectiveness as a grain refiner in A356

The research has demonstrated that primary aluminium undercooling can be reduced with the addition of both the addition of Al-2Nb-2B and Al-2Nb-B master alloys. Reduced undercooling with the addition of these master alloys suggest that the second phase inclusions in these master alloys could be acting as heterogeneous nuclei. These enhanced nucleation rate in the melt led to formation of a refined primary grain structure. Reductions in eutectic undercooling were also detected in the experiments.

Effective reduction in primary and eutectic undercooling of A354, again at relatively low addition rates, which would be acceptable for prototype / niche volume casting production.

6.2 Effectiveness as a grain refiner in A354

The research has not demonstrated that primary aluminium undercooling can be reduced with the addition of Al-2Nb-B. This suggests lower barriers to nucleation are not the reason for a more refined primary grain structure. Reductions in eutectic undercooling were detected in the experiments.

Although the reduction in undercooling is not resulted, reductions in grain size were recorded in A356 even with moderate additions of Al-2Nb-B. At addition rates of <1.0% wt, the cost increase of manufacturing is acceptable for prototype and niche casting production, where material costs represent a lower % of total manufacturing cost.

6.3 Recommendations for future work

Further research is needed into the influence the grain refiners have on the overall chemistry of the alloys, and the effects of this. Given that it has been found to sediment titanium from the melts, new alloys may be designed without titanium content.

Further research should also be undertaken to establish the mechanism of how Al-2Nb-B reduces grain size in A356.

Appendix A – Microstructure samples

List of figures

Figure A - 1 Anodised microstructure of A356, taken at 10mm from the tip of the wedge mould, showing grain size.....	2
Figure A - 2 Anodised microstructure of A356, taken at 20mm from the tip of the wedge mould, showing grain size.....	2
Figure A - 3 Anodised microstructure of A356, taken at 30mm from the tip of the wedge mould, showing grain size.....	2
Figure A - 4 Anodised microstructure of A356, taken at 40mm from the tip of the wedge mould, showing grain size.....	3
Figure A - 5 Anodised microstructure of A356, taken at 50mm from the tip of the wedge mould, showing grain size.....	3
Figure A - 6 Anodised microstructure of A356, taken at 60mm from the tip of the wedge mould, showing grain size.....	4
Figure A - 7 Anodised microstructure of A356, taken at 70mm from the tip of the wedge mould, showing grain size.....	4
Figure A - 8 Anodised microstructure of A356, taken at 80mm from the tip of the wedge mould, showing grain size.....	5
Figure A - 9 Anodised microstructure of A356, taken at 90mm from the tip of the wedge mould, showing grain size.....	5
Figure A - 10 Anodised microstructure of A356, taken at 100mm from the tip of the wedge mould, showing grain size.....	6
Figure A - 11 Anodised microstructure of A356, with 0.1% wt. Al-5Ti-B addition, taken at 10mm from the tip of the wedge mould, showing grain size.	7
Figure A - 12 Anodised microstructure of A356, with 0.1% wt. Al-5Ti-B addition, taken at 20mm from the tip of the wedge mould, showing grain size.	7
Figure A - 13 Anodised microstructure of A356, with 0.1% wt. Al-5Ti-B addition, taken at 30mm from the tip of the wedge mould, showing grain size.	7
Figure A - 14 Anodised microstructure of A356, with 0.1% wt. Al-5Ti-B addition, taken at 40mm from the tip of the wedge mould, showing grain size.	8
Figure A - 15 Anodised microstructure of A356, with 0.1% wt. Al-5Ti-B addition, taken at 50mm from the tip of the wedge mould, showing grain size.	8
Figure A - 16 Anodised microstructure of A356, with 0.1% wt. Al-5Ti-B addition, taken at 60mm from the tip of the wedge mould, showing grain size.	8
Figure A - 17 Anodised microstructure of A356, with 0.1% wt. Al-5Ti-B addition, taken at 70mm from the tip of the wedge mould, showing grain size.	9
Figure A - 18 Anodised microstructure of A356, with 0.1% wt. Al-5Ti-B addition, taken at 80mm from the tip of the wedge mould, showing grain size.	9
Figure A - 19 Anodised microstructure of A356, with 0.1% wt. Al-5Ti-B addition, taken at 90mm from the tip of the wedge mould, showing grain size.	9
Figure A - 20 Anodised microstructure of A356, with 0.1% wt. Al-2Nb-B addition, taken at 10mm from the tip of the wedge mould, showing grain size.	10
Figure A - 21 Anodised microstructure of A356, with 0.1% wt. Al-2Nb-B addition, taken at 20mm from the tip of the wedge mould, showing grain size.	10
Figure A - 22 Anodised microstructure of A356, with 0.1% wt. Al-2Nb-B addition, taken at 30mm from the tip of the wedge mould, showing grain size.	10
Figure A - 23 Anodised microstructure of A356, with 0.1% wt. Al-2Nb-B addition, taken at 40mm from the tip of the wedge mould, showing grain size.	11
Figure A - 24 Anodised microstructure of A356, with 0.1% wt. Al-2Nb-B addition, taken at 50mm from the tip of the wedge mould, showing grain size.	11

A356

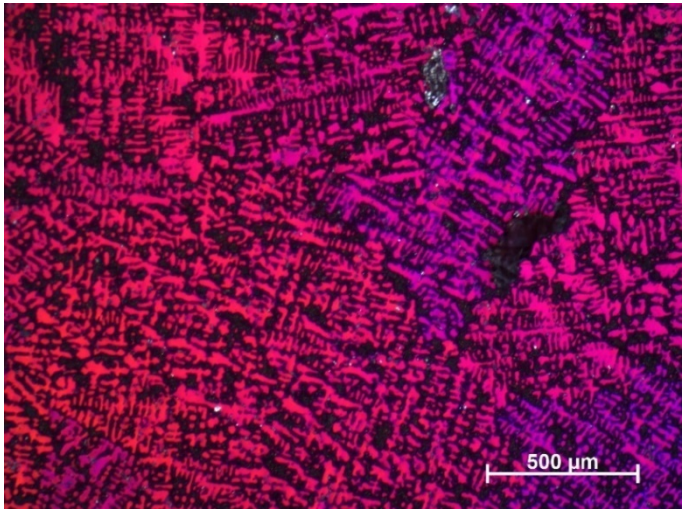


Figure A - 1 Anodised microstructure of A356, taken at 10mm from the tip of the wedge mould, showing grain size.

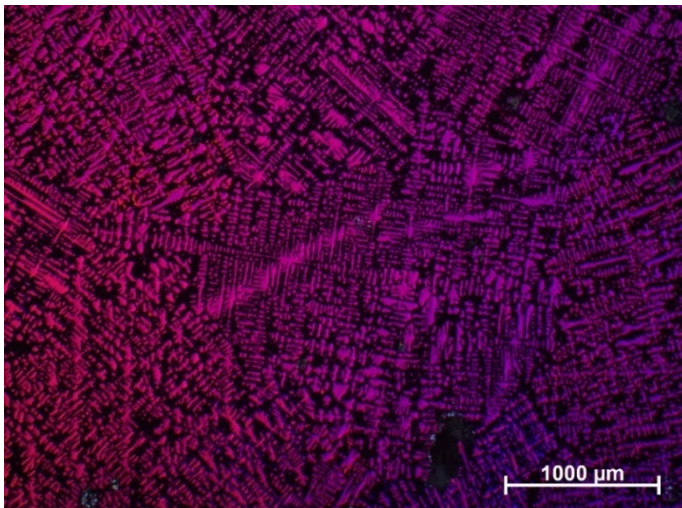


Figure A - 2 Anodised microstructure of A356, taken at 20mm from the tip of the wedge mould, showing grain size.

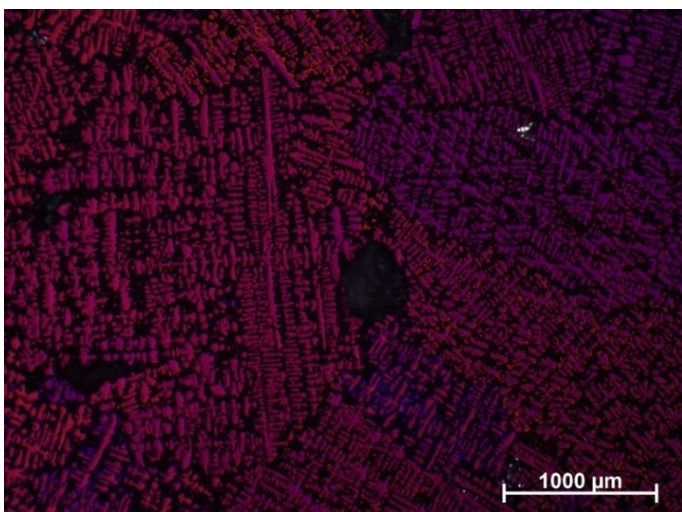


Figure A - 3 Anodised microstructure of A356, taken at 30mm from the tip of the wedge mould, showing grain size.

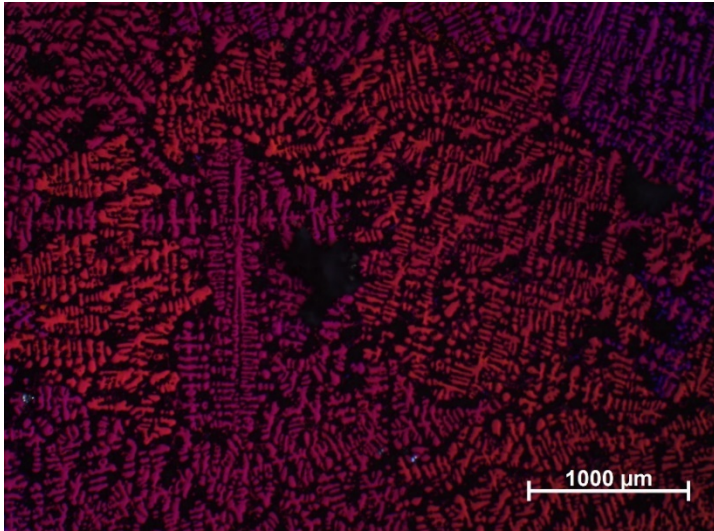


Figure A - 4 Anodised microstructure of A356, taken at 40mm from the tip of the wedge mould, showing grain size.

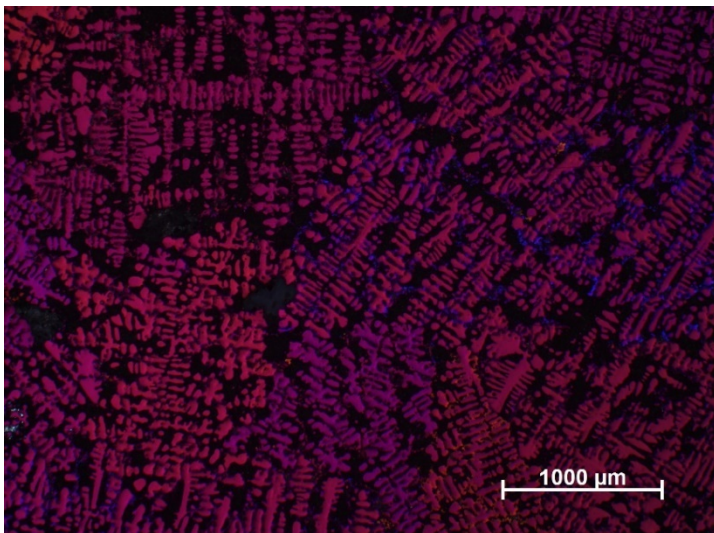


Figure A - 5 Anodised microstructure of A356, taken at 50mm from the tip of the wedge mould, showing grain size.

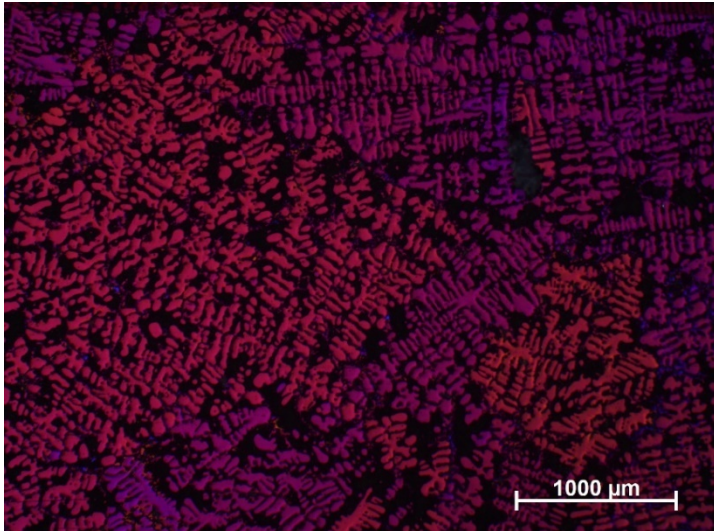


Figure A - 6 Anodised microstructure of A356, taken at 60mm from the tip of the wedge mould, showing grain size.

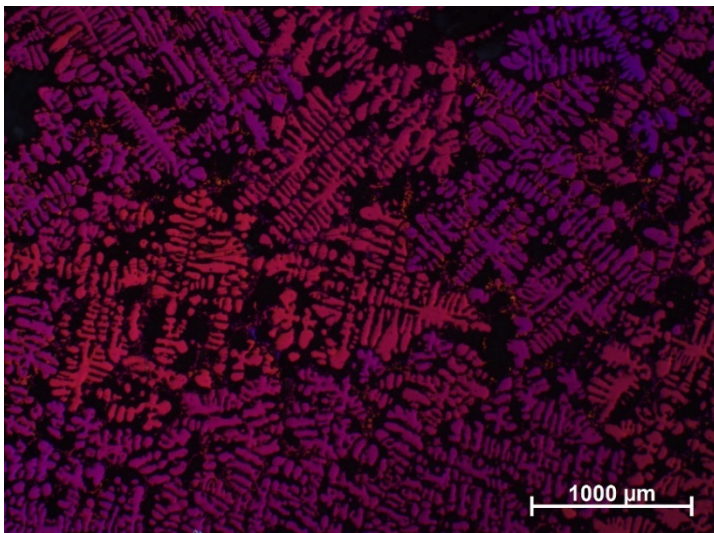


Figure A - 7 Anodised microstructure of A356, taken at 70mm from the tip of the wedge mould, showing grain size.

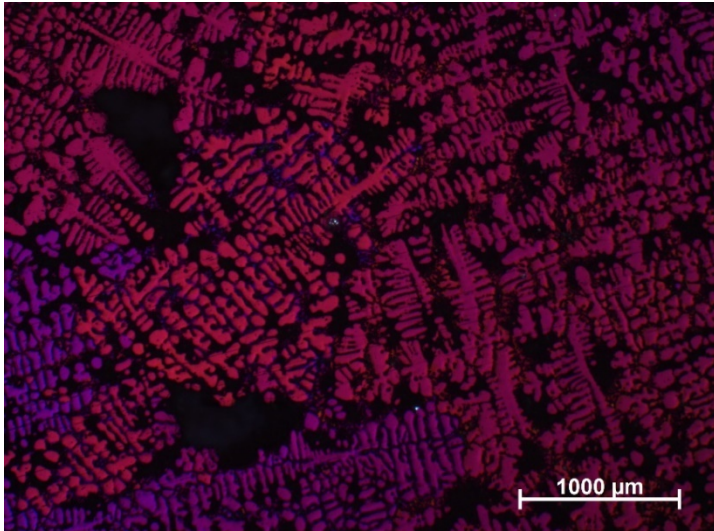


Figure A - 8 Anodised microstructure of A356, taken at 80mm from the tip of the wedge mould, showing grain size.

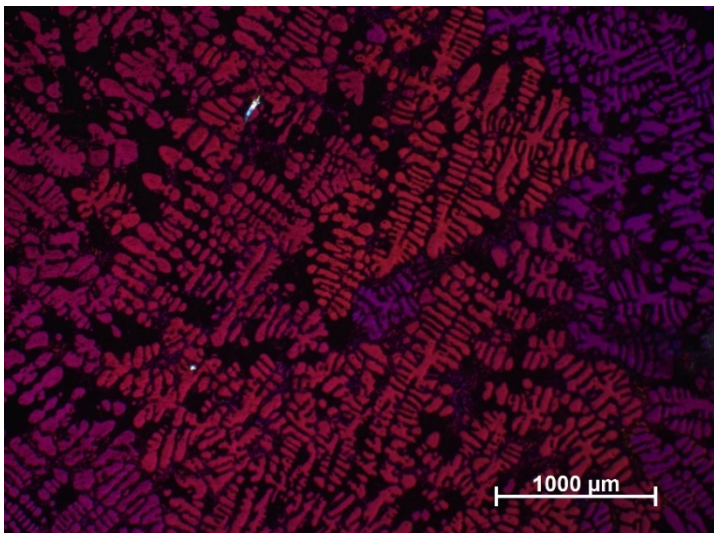


Figure A - 9 Anodised microstructure of A356, taken at 90mm from the tip of the wedge mould, showing grain size.

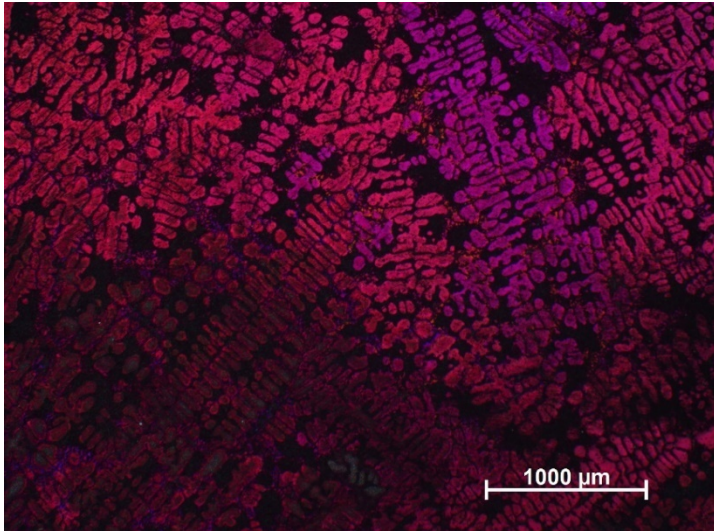


Figure A - 10 Anodised microstructure of A356, taken at 100mm from the tip of the wedge mould, showing grain size.

0.1% Al-5Ti-B

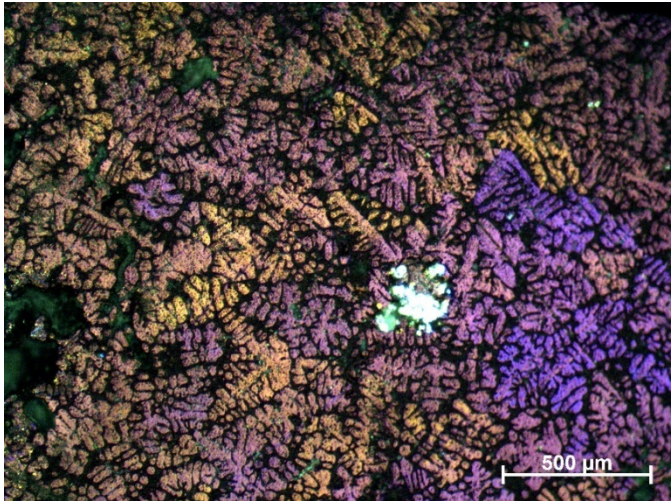


Figure A - 11 Anodised microstructure of A356, with 0.1% wt. Al-5Ti-B addition, taken at 10mm from the tip of the wedge mould, showing grain size.

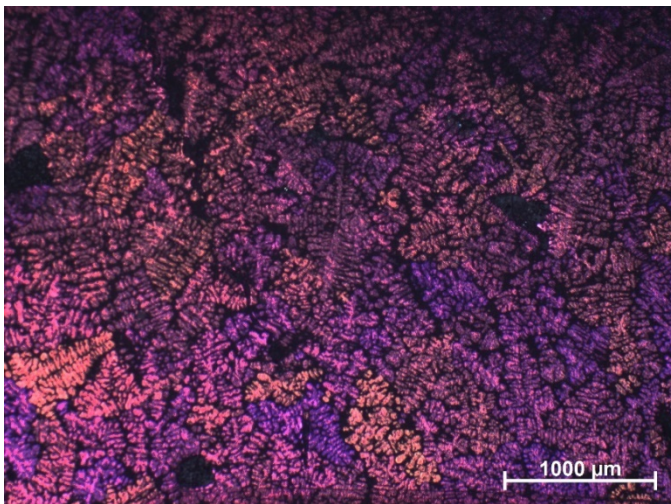


Figure A - 12 Anodised microstructure of A356, with 0.1% wt. Al-5Ti-B addition, taken at 20mm from the tip of the wedge mould, showing grain size.

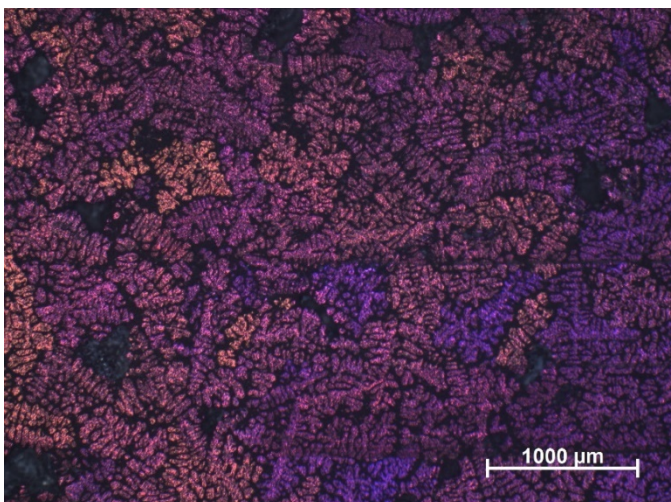


Figure A - 13 Anodised microstructure of A356, with 0.1% wt. Al-5Ti-B addition, taken at 30mm from the tip of the wedge mould, showing grain size.

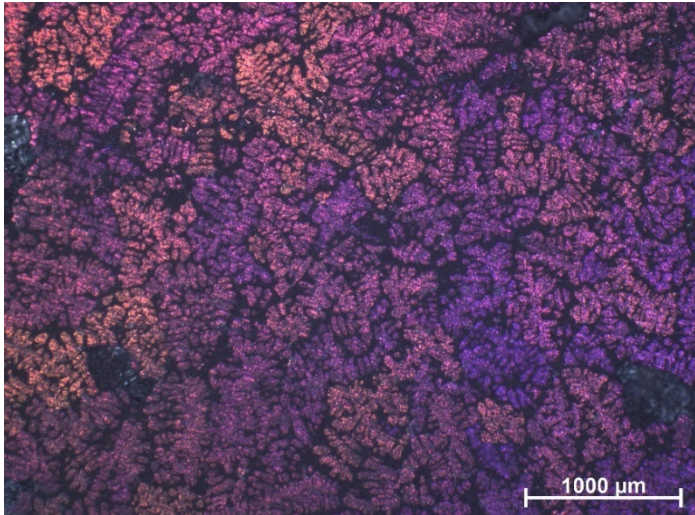


Figure A - 14 Anodised microstructure of A356, with 0.1% wt. Al-5Ti-B addition, taken at 40mm from the tip of the wedge mould, showing grain size.

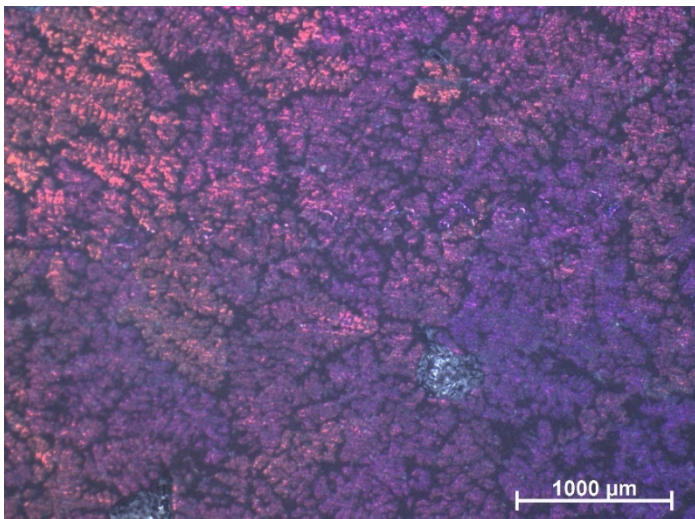


Figure A - 15 Anodised microstructure of A356, with 0.1% wt. Al-5Ti-B addition, taken at 50mm from the tip of the wedge mould, showing grain size.

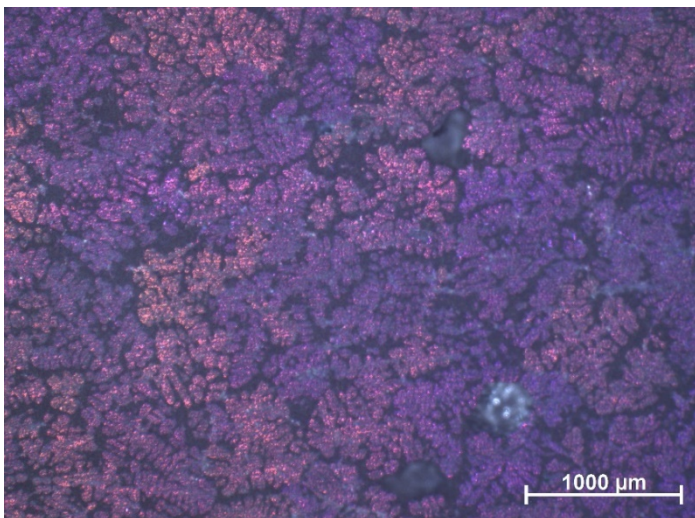


Figure A - 16 Anodised microstructure of A356, with 0.1% wt. Al-5Ti-B addition, taken at 60mm from the tip of the wedge mould, showing grain size.

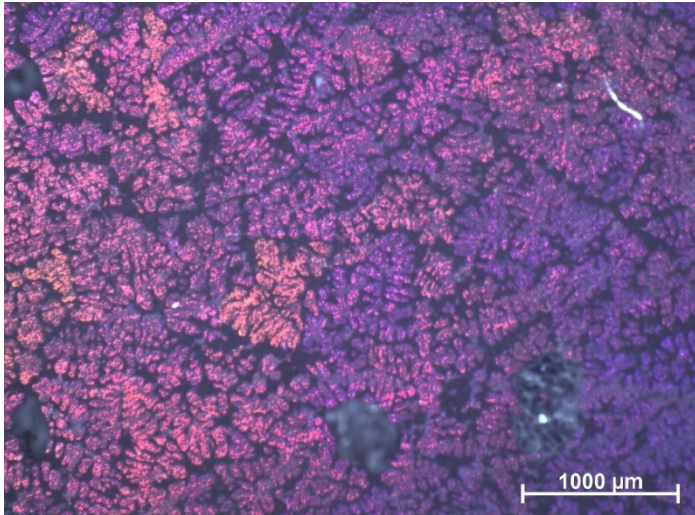


Figure A - 17 Anodised microstructure of A356, with 0.1% wt. Al-5Ti-B addition, taken at 70mm from the tip of the wedge mould, showing grain size.

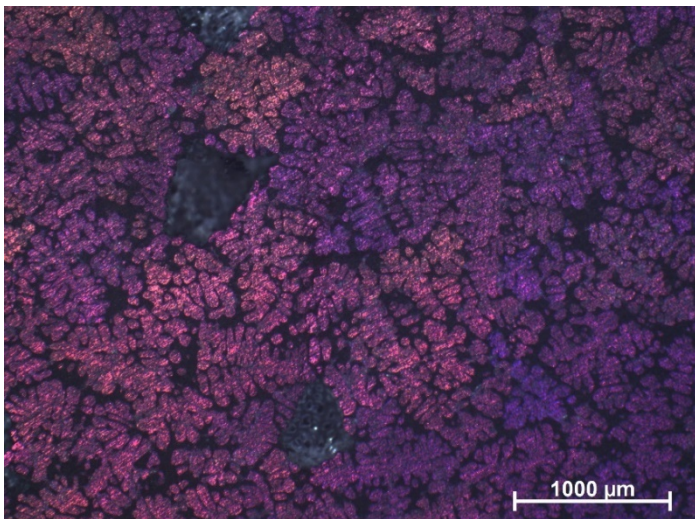


Figure A - 18 Anodised microstructure of A356, with 0.1% wt. Al-5Ti-B addition, taken at 80mm from the tip of the wedge mould, showing grain size.

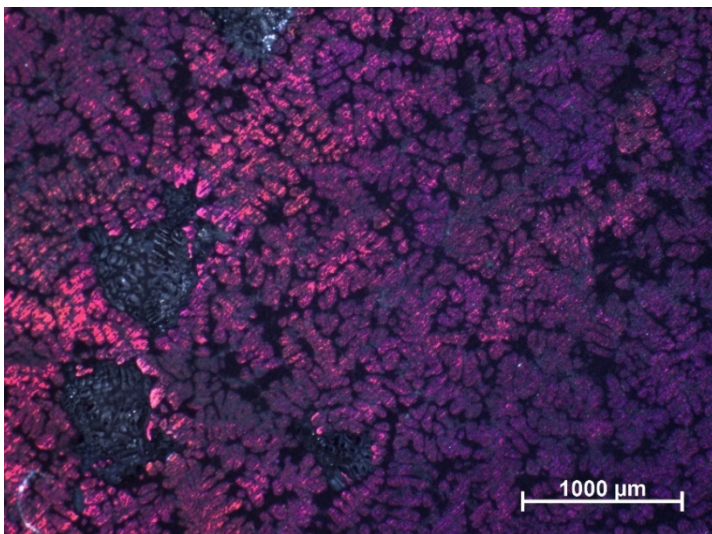


Figure A - 19 Anodised microstructure of A356, with 0.1% wt. Al-5Ti-B addition, taken at 90mm from the tip of the wedge mould, showing grain size.

0.1% Al-2Nb-B



Figure A - 20 Anodised microstructure of A356, with 0.1% wt. Al-2Nb-B addition, taken at 10mm from the tip of the wedge mould, showing grain size.

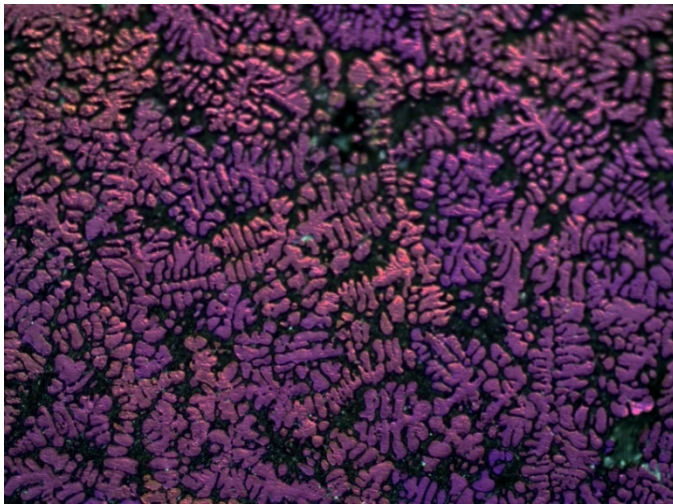


Figure A - 21 Anodised microstructure of A356, with 0.1% wt. Al-2Nb-B addition, taken at 20mm from the tip of the wedge mould, showing grain size.

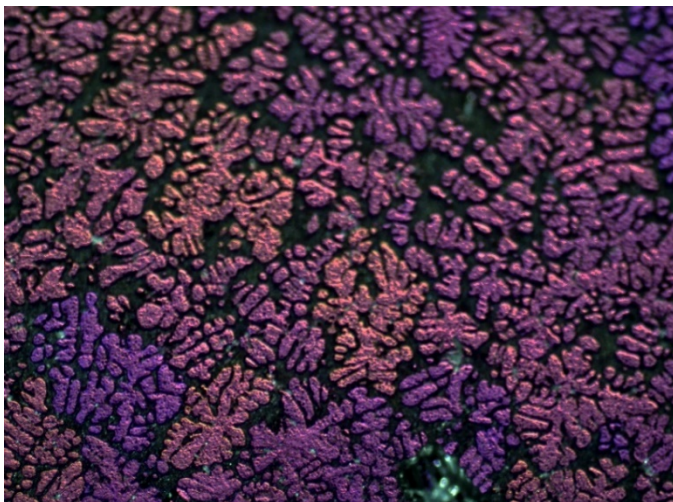


Figure A - 22 Anodised microstructure of A356, with 0.1% wt. Al-2Nb-B addition, taken at 30mm from the tip of the wedge mould, showing grain size.

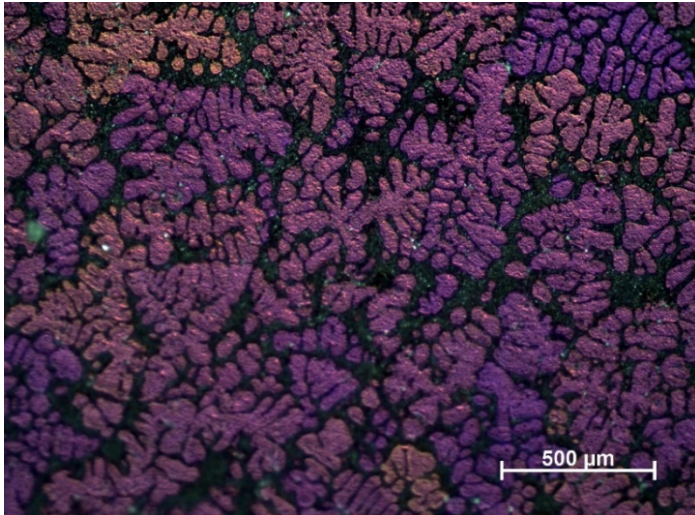


Figure A - 23 Anodised microstructure of A356, with 0.1% wt. Al-2Nb-B addition, taken at 40mm from the tip of the wedge mould, showing grain size.

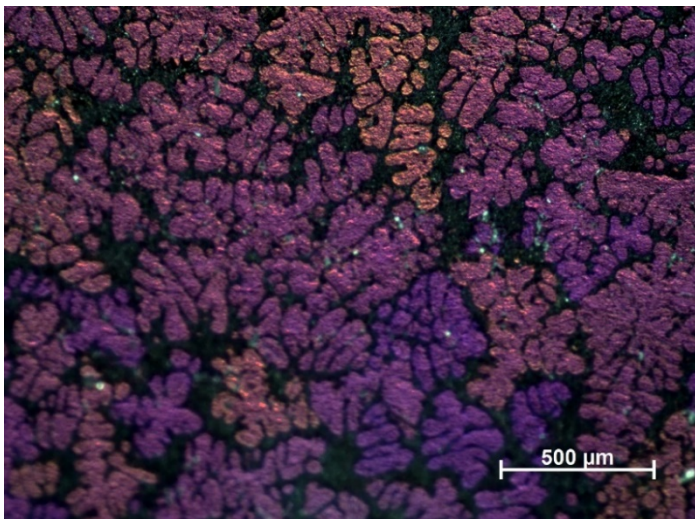


Figure A - 24 Anodised microstructure of A356, with 0.1% wt. Al-2Nb-B addition, taken at 50mm from the tip of the wedge mould, showing grain size.

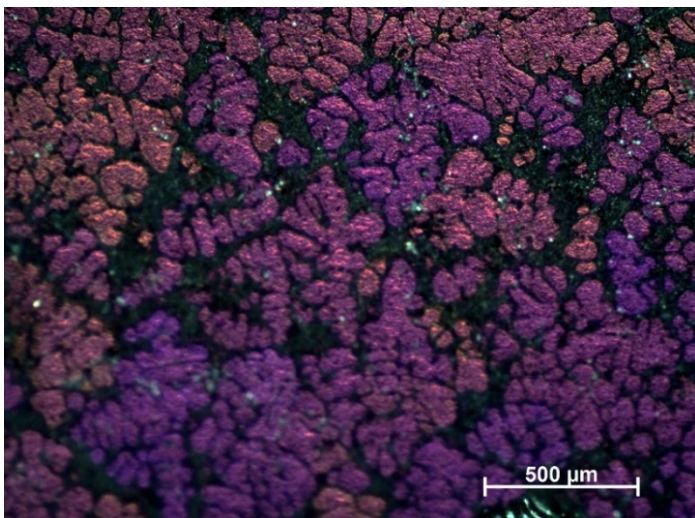


Figure A - 25 Anodised microstructure of A356, with 0.1% wt. Al-2Nb-B addition, taken at 60mm from the tip of the wedge mould, showing grain size.

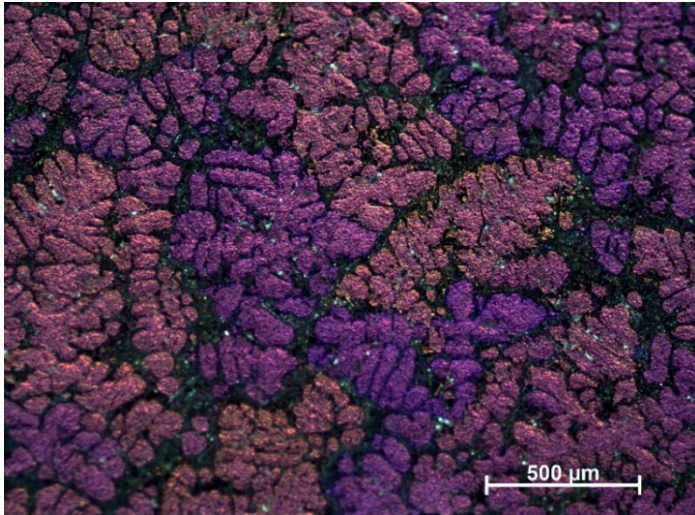


Figure A - 26 Anodised microstructure of A356, with 0.1% wt. Al-2Nb-B addition, taken at 70mm from the tip of the wedge mould, showing grain size.

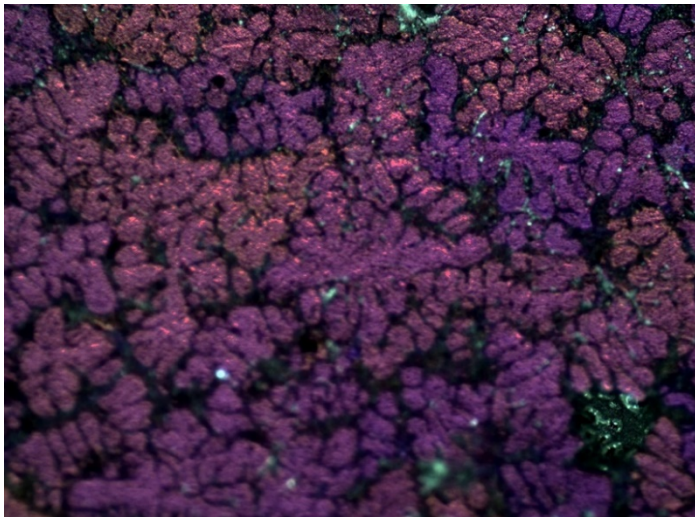


Figure A - 27 Anodised microstructure of A356, with 0.1% wt. Al-2Nb-B addition, taken at 80mm from the tip of the wedge mould, showing grain size.

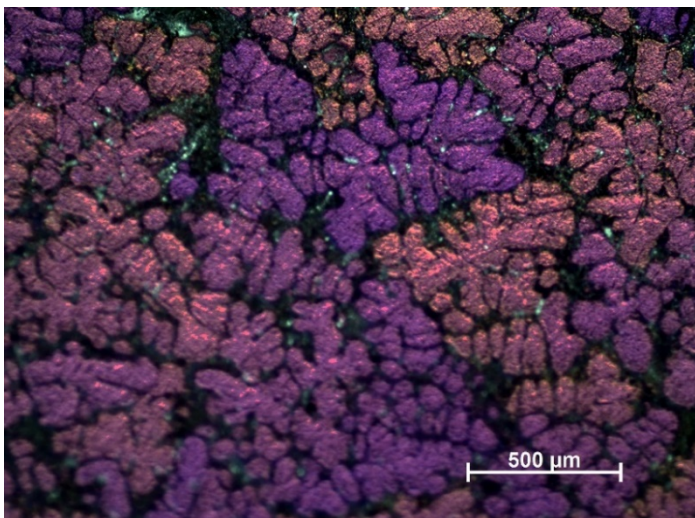


Figure A - 28 Anodised microstructure of A356, with 0.1% wt. Al-2Nb-B addition, taken at 90mm from the tip of the wedge mould, showing grain size.

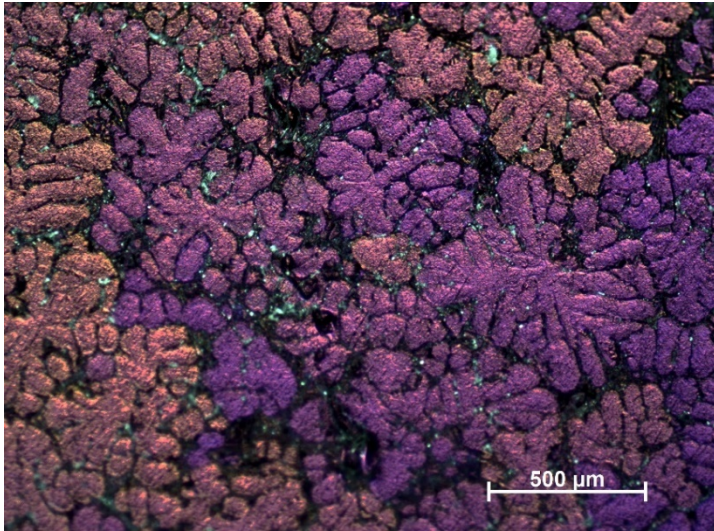


Figure A - 29 Anodised microstructure of A356, with 0.1% wt. Al-2Nb-B addition, taken at 100mm from the tip of the wedge mould, showing grain size.

A356 + 0.5% wt. Al-2Nb-B

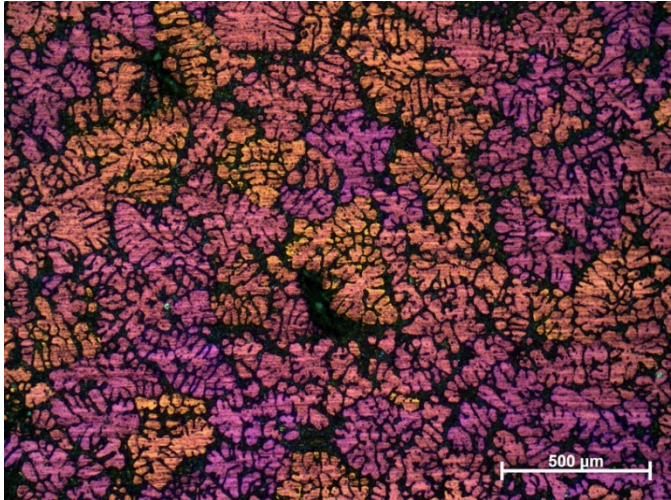


Figure A - 30 Anodised microstructure of A356, with 0.5% wt. Al-2Nb-B addition, taken at 10mm from the tip of the wedge mould, showing grain size.

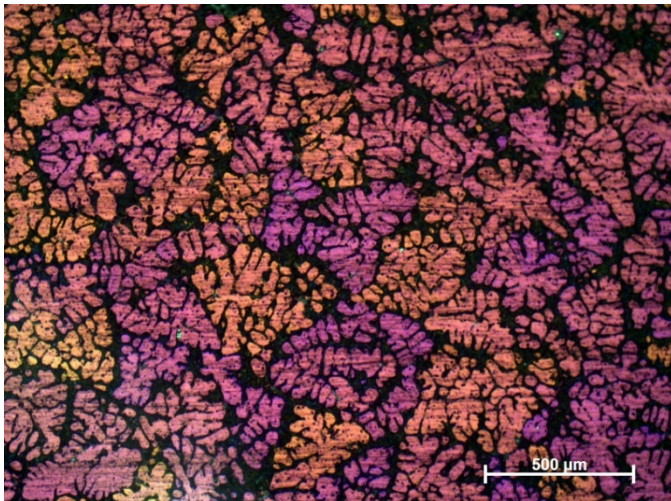


Figure A - 31 Anodised microstructure of A356, with 0.5% wt. Al-2Nb-B addition, taken at 20mm from the tip of the wedge mould, showing grain size.

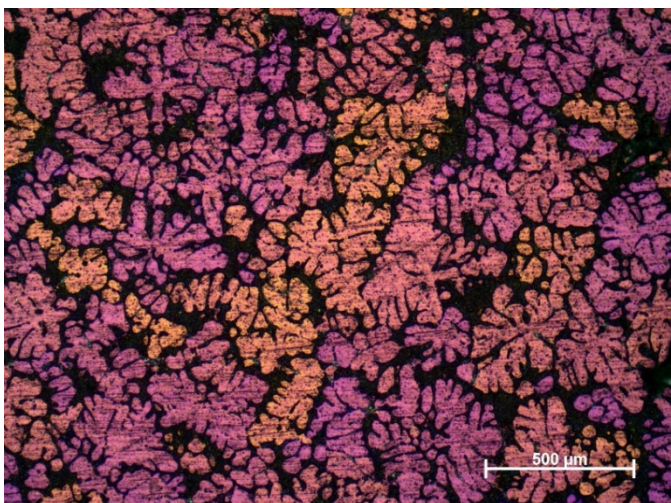


Figure A - 32 Anodised microstructure of A356, with 0.5% wt. Al-2Nb-B addition, taken at 30mm from the tip of the wedge mould, showing grain size.

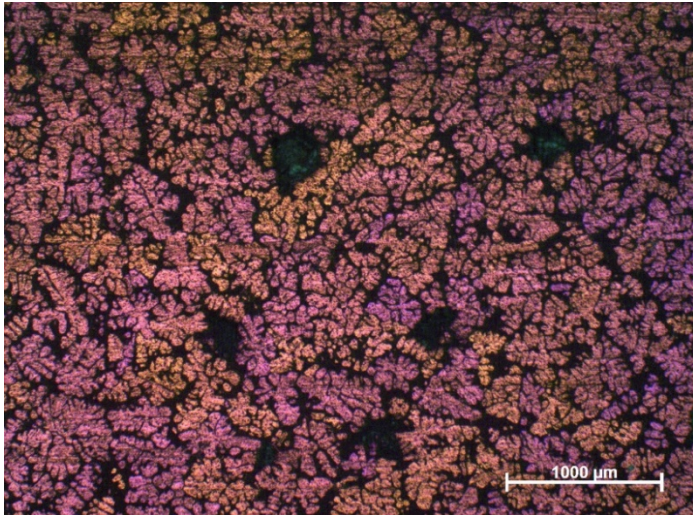


Figure A - 33 Anodised microstructure of A356, with 0.5% wt. Al-2Nb-B addition, taken at 40mm from the tip of the wedge mould, showing grain size.

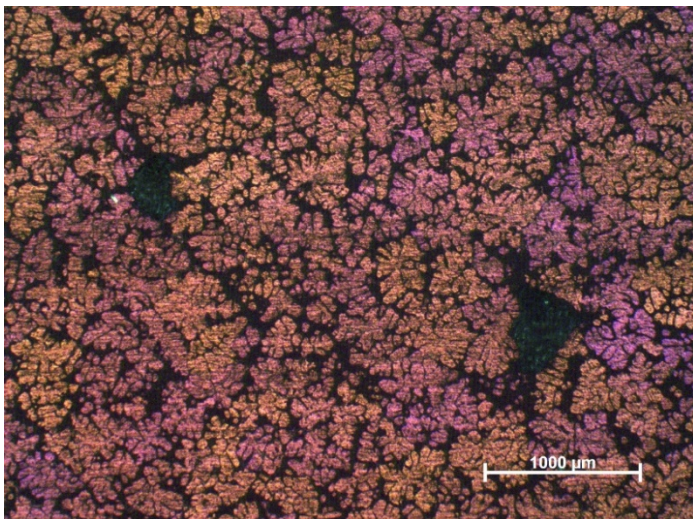


Figure A - 34 Anodised microstructure of A356, with 0.5% wt. Al-2Nb-B addition, taken at 50mm from the tip of the wedge mould, showing grain size.

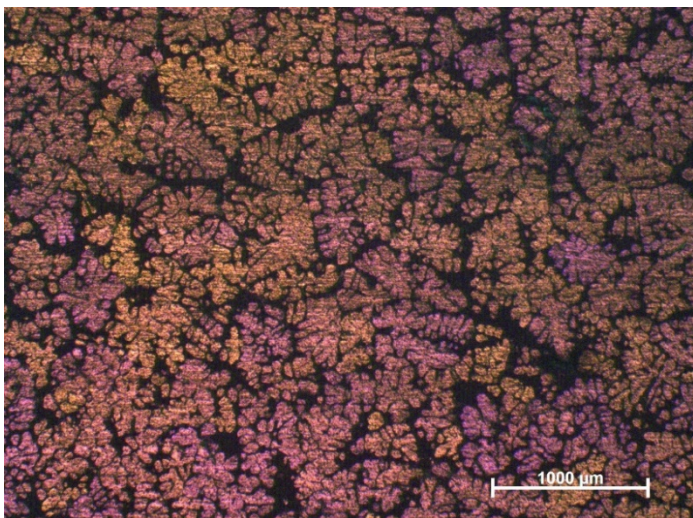


Figure A - 35 Anodised microstructure of A356, with 0.5% wt. Al-2Nb-B addition, taken at 60mm from the tip of the wedge mould, showing grain size.

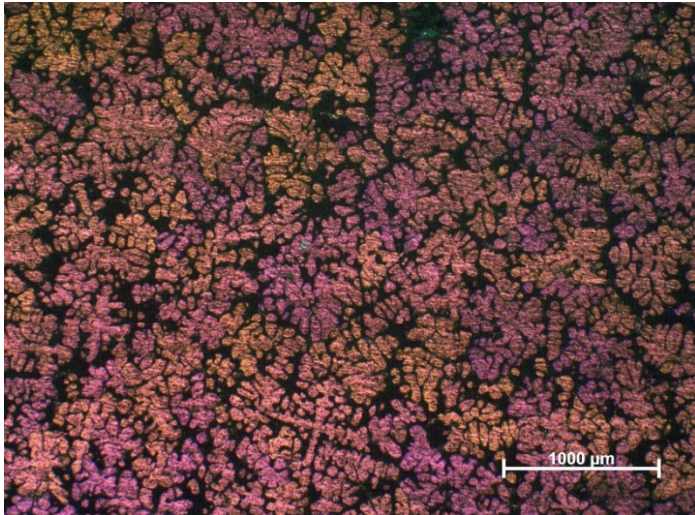


Figure A - 36 Anodised microstructure of A356, with 0.5% wt. Al-2Nb-B addition, taken at 70mm from the tip of the wedge mould, showing grain size.

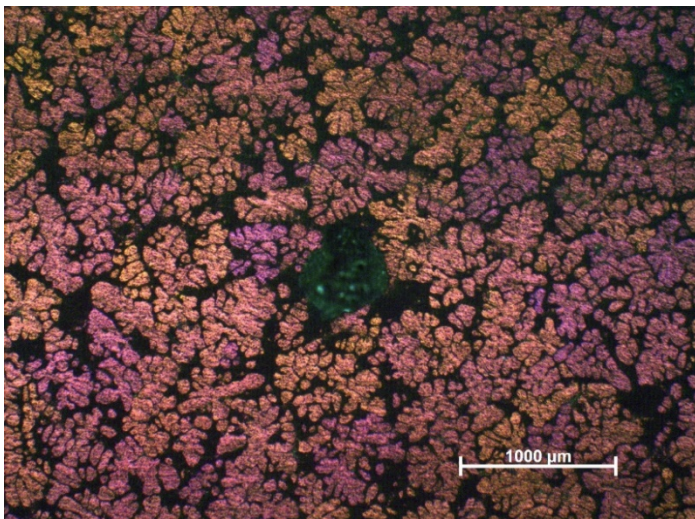


Figure A - 37 Anodised microstructure of A356, with 0.5% wt. Al-2Nb-B addition, taken at 80mm from the tip of the wedge mould, showing grain size.

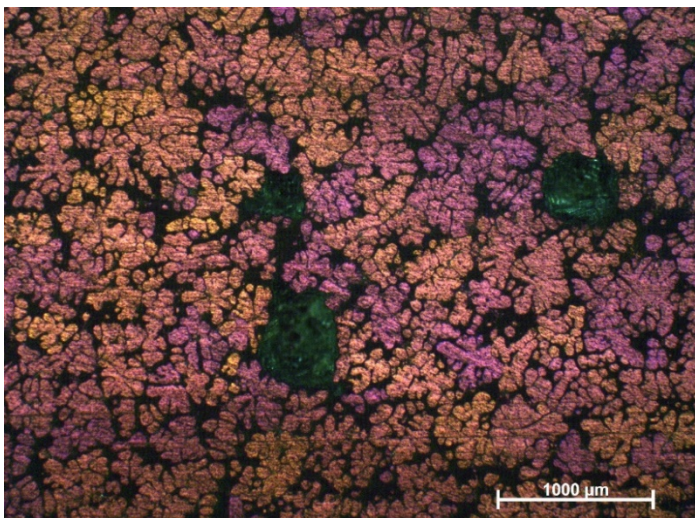


Figure A - 38 Anodised microstructure of A356, with 0.5% wt. Al-2Nb-B addition, taken at 90mm from the tip of the wedge mould, showing grain size.

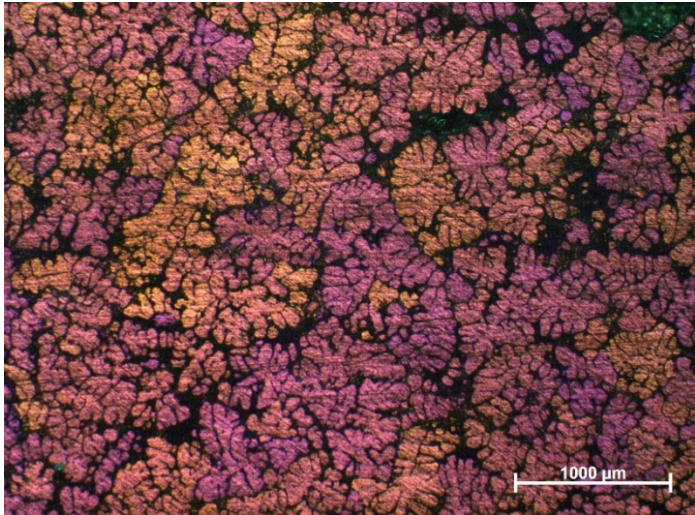


Figure A - 39 Anodised microstructure of A356, with 0.5% wt. Al-2Nb-B addition, taken at 100mm from the tip of the wedge mould, showing grain size.

A356 + 1.0% wt. Al-2Nb-B

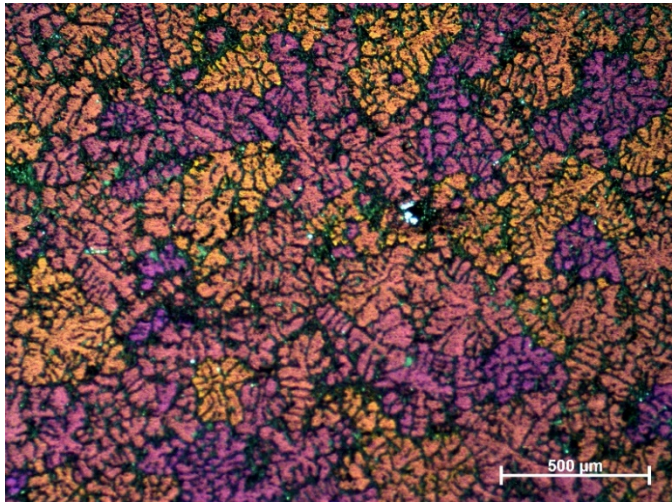


Figure A - 40 Anodised microstructure of A356, with 1.0% wt. Al-2Nb-B addition, taken at 10mm from the tip of the wedge mould, showing grain size.

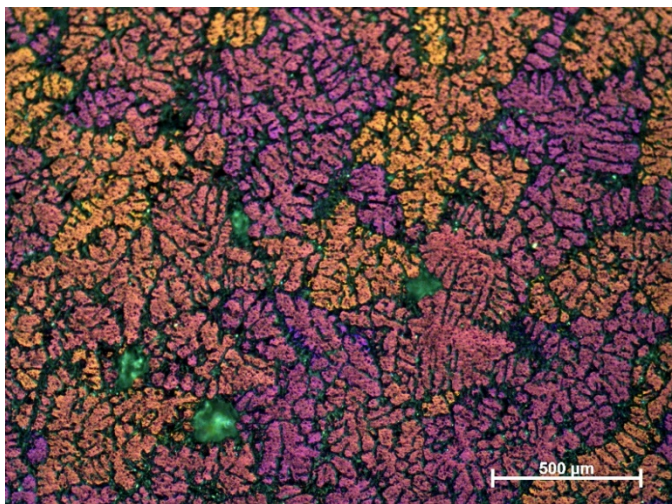


Figure A - 41 Anodised microstructure of A356, with 1.0% wt. Al-2Nb-B addition, taken at 20mm from the tip of the wedge mould, showing grain size.



Figure A - 42 Anodised microstructure of A356, with 1.0% wt. Al-2Nb-B addition, taken at 30mm from the tip of the wedge mould, showing grain size.

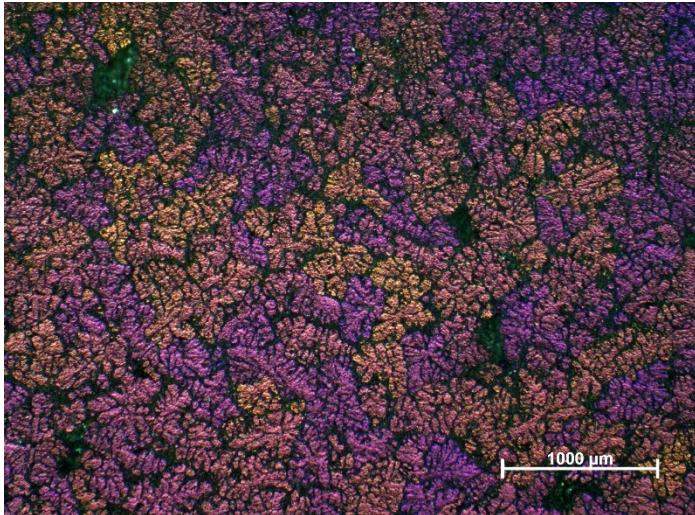


Figure A - 43 Anodised microstructure of A356, with 1.0% wt. Al-2Nb-B addition, taken at 40mm from the tip of the wedge mould, showing grain size.

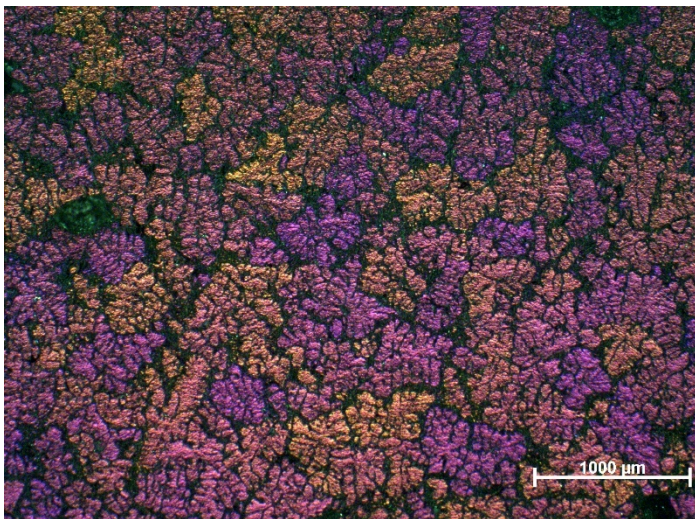


Figure A - 44 Anodised microstructure of A356, with 1.0% wt. Al-2Nb-B addition, taken at 50mm from the tip of the wedge mould, showing grain size.

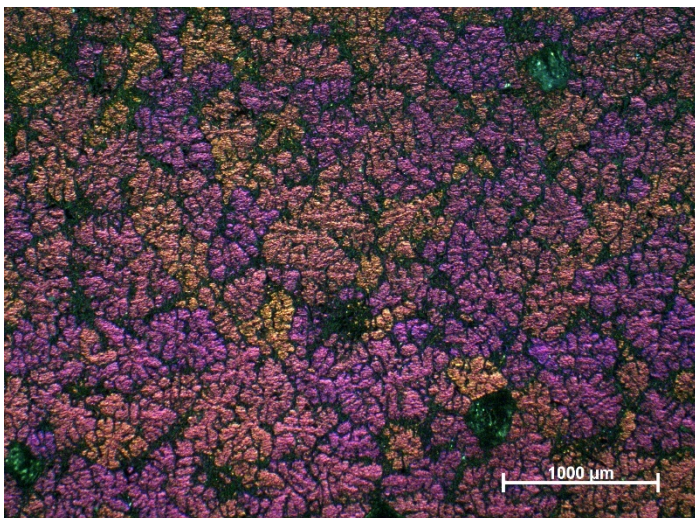


Figure A - 45 Anodised microstructure of A356, with 1.0% wt. Al-2Nb-B addition, taken at 60mm from the tip of the wedge mould, showing grain size.

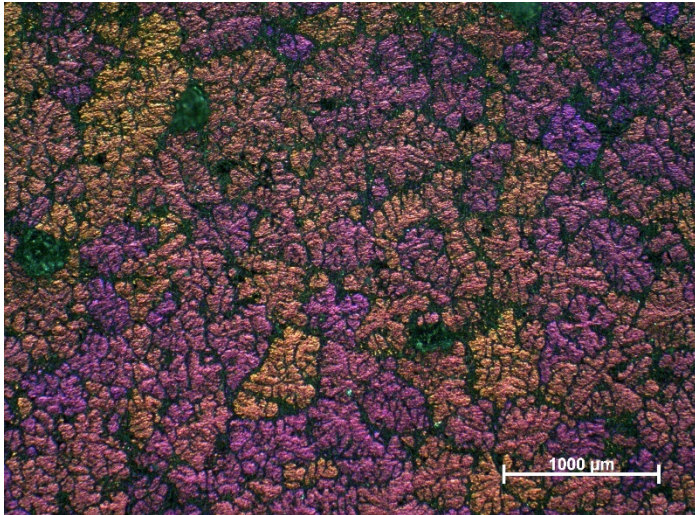


Figure A - 46 Anodised microstructure of A356, with 1.0% wt. Al-2Nb-B addition, taken at 70mm from the tip of the wedge mould, showing grain size.



Figure A - 47 Anodised microstructure of A356, with 1.0% wt. Al-2Nb-B addition, taken at 80mm from the tip of the wedge mould, showing grain size.

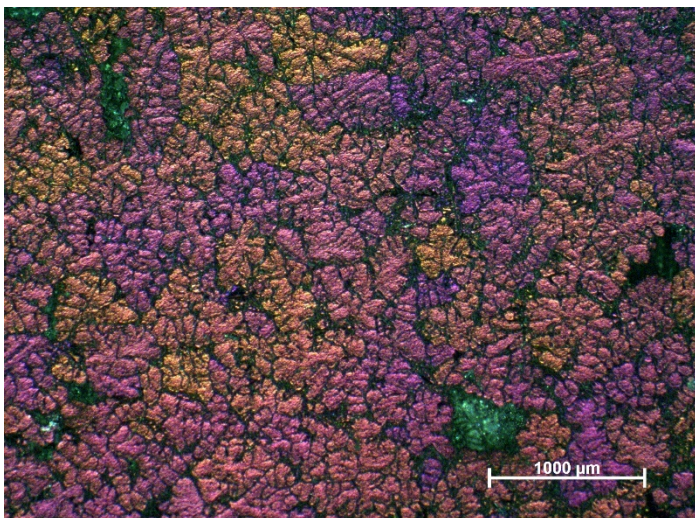


Figure A - 48 Anodised microstructure of A356, with 1.0% wt. Al-2Nb-B addition, taken at 90mm from the tip of the wedge mould, showing grain size.

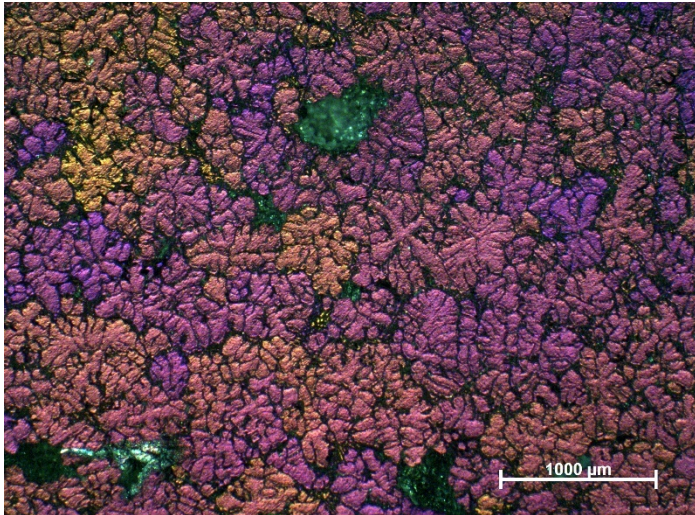


Figure A - 49 Anodised microstructure of A356, with 1.0% wt. Al-2Nb-B addition, taken at 100mm from the tip of the wedge mould, showing grain size.

